ON THE MECHANICS OF THE ROOT-SOIL SYSTEM

Thesis for the Degree of Ph. D.
MICHIGAN STATE UNIVERSITY
ANIVALDO PEDRO COBRA
1968



This is to certify that the

thesis entitled

On the Mechanics of the Root Soil-System

presented by

A. P. Cobra

has been accepted towards fulfillment of the requirements for

Ph.D. degree in Agricultural Engineering

Major professor

Date 5-14-6



AUL 711972 208

TON 1 1 1996

7

ABSTRACT

ON THE MECHANICS OF THE ROOT-SOIL SYSTEM

by Anivaldo Pedro Cobra

Several studies have been made to determine the uprooting force of crop plants. These studies do not,
however, contain any information related to the soil
characteristics and of the stress distribution and strength
of the root-soil composite.

A knowledge of the root-soil relationship would be of importance for the crop scientist, the soil scientist, and the agricultural engineer. It may become possible to determine the best positioning of soil in relation to the plants and to select strains to obtain better anchorage of the crop plants. Also, by learning about the interactive behavior of the root-soil composite, the prediction of failures of vegetated slopes and the endurance of vegetated linings of earth dams and canals can be further improved.

The objective of this work is to obtain background data for the study of root-soil relationships from an engineering standpoint.

For this study, sorghum was planted in the field in a loamy fine sand soil. When the plants had nearly reached their full size they were subjected to an uprooting force

		;
		â
		3

applied to the stems. Measurements of force and displacement at the base of the plant were made. The dry weight of stem samples and the stem bundle diameter at the base of the plant were measured. Soil moisture content, bulk density, and penetration values were determined. The weight, shape, and dimensions of the pulled out root-soil bulb and the remaining undisturbed crater were recorded.

In order to determine the stress and strain distribution and the strengthening effect of the root on the soil, underground and top surface failure patterns of the field plants were filmed for some tests.

Studies of the root system were made for plants grown in boxes in a greenhouse. Root angle and root length were determined by directly tracing the roots. These roots were sampled and tested for tensile strength. The measurements made at rupture were: force, strain, diameter, the distance from the attaching point to the fractured section and the position of the fracture with respect to the clamping jaws.

From the field experiments it was found that the maximum pulling force required to pull the plant was considerably greater than the weight of the bulb or the soil weight of the crater. The maximum pulling force was reasonably well correlated with the respective displacement at the base of the plant, the soil moisture content, the weight of the root-soil bulb, the dry weight of a 2-inch

sample of stems and the volume of the crater. Also a reasonable correlation was found between the displacement at the base of the plant and the depth of the crater.

From the studies of the root system it was found that the number and the length of roots varied with the angle measured from the soil surface. The greater number of roots and the longer roots were found at angles of 60 to 80 degrees.

The tensile tests showed that the strength of short roots was proportional to a linear dimension of the cross section, while that of long roots exhibited an additional proportionality to the square of the same dimension. In general, the further away from the attaching point of the root the tension specimens were taken, the weaker these specimens were found to be. Finally, short roots exhibited lower average strength than long roots. This difference in strength is probably due to biological differences in the two types of root.

The observations of failure patterns showed that the underground rupture of the root-soil composite started at the centerline of the plant at the bottom of the future crater, when the pulling force was close to its maximum value. The failure surface developed from the centerline laterally outward to a polar angle of about 60 degrees and slightly concave upward. Then it assumed the shape of a typical Rankine pattern, up to the soil surface. The

soil surface failure cracks indicated that the least strength of the composite is in the direction perpendicular to a plane containing the centerline of the plant. The maximum strength of the root-soil composite was found to be in the direction of the roots, or in a polar-spherical direction.

An attempt was made to develop constitutive equations which would enable the evaluation of the strengthening effect of roots on the soil, in terms of a strengthening factor.

Approved

Major Professor

Approved

Department Chairman

ON THE MECHANICS OF THE ROOT-SOIL SYSTEM

Ву

Anivaldo Pedro Cobra

A THESIS

Submitted to
Michigan State University
in partial fulfillment of the requirements
for the degree of

DOCTOR OF PHILOSOPHY

Department of Agricultural Engineering

1968

10-24-68

ACKNOWLEDGMENT

I express my gratitude to Dr. Sverker P. E. Persson for his advice and assistance given during this work.

Acknowledgment also goes to the "Escola Superior de Agricultura Luiz de Queiroz " University of Sao Paulo, Brazil and to The Rockefeller Foundation which provided for my stay in this country.

I would also like to thank Mr. Glenn Bowditch, of the University of New South Wales, Australia, for his assistance in the preparation of equipment and the carrying out of experiments.

To my wife and five children I am deeply grateful.

TABLE OF CONTENTS

ACKNO	WLEDGN	MENTS													Page
	OF FIG			•	•	•	•	•	•	•	•	•	•	•	ii
LIST (•	•	•	•	•	•	•	•		•	•	iv
CHAPTE	ER		•	•	•	•	•	•	•	•	•	•	•	•	viii
1.	INT	RODUC	rion												
2.	THE	UPRO	OTIN	ਮੂਜ ਹ)RCF	•	•	•	•	•	•	•		•	1
							•	•	•	•	•	•		•	4
		Revi Fiel Resu	.u. ri		מכווויו	~ ~ ~	~ ~ T	∃qu	ipm	ent		•		•	4 6 16
3.	THE	ROOT	SYSI	EM,	DES	SCRI	PTI	ON	AN	D S	TRE	NG	עם		47
		Desc	ript	ion	οf	tho	D.								4 /
	3.2	Proc	edur	rat e fi	ure or T	·)eta	· nm i		•		•	•			47
	3.3	2016	ユドレロ	OI	ROC	TC				•	•	•			51 56
4.	STRE	SS DIS	STRI	BUT]	ON	•	•	•			•	•	•		81
	4.1 4.2		'у о1	f th	e M	echa	ania	Cs	of	the	•	•	•		81
	4.3	Root- Obser	201	LSy	stei	m.			•	•	•	•	•		84
5.	RECOM	IMENDA								•	•	•	•		120
-						URT	'HEH	ł W	ORK	•	•	•	•		143
6.		RY OF	RES	ULT:	S.	•	•		•	•			•		145
REFERENC	CES.	• •	•	•		•	•		•	•	•		•		147

LIST OF FIGURES

Figure		Page
2.2.1	A general view of pulling device and measuring instrument	9
2.2.2	Typical arrangement of the load cell, traction jaws, and spike of the displacement bar with LVDT	9
2.2.3	Typical penetration curve (from experiment number 10)	12
2.3.1	Typical shape and dimensions of a pulled out root-soil bulb (load centrally applied)	17
2.3.2	The effect of force misalignment or non- verticality of stems as affecting the final shape of the root-soil bulb	18
2.3.3	(A), (B), and (C) Crater profiles from tests 21-26	20
2.3.4	Typical force versus displacement curve for an integral plant	27
2.3.5	Typical force versus displacement curve for a sectioned plant	29
2.3.6	Maximum pulling force versus soil moisture content	32
2.3.7	Maximum pulling force versus displacement at base of plant	33
2.3.8	Maximum pulling force versus weight of root-soil bulb plus weight of jaws	34
2.3.9	Maximum pulling force versus average diameter of stems at base of plant	36
2.3.10	Maximum pulling force versus dry weight of a 2-inch sample of stems	37
2.3.11	Displacement at base of plant versus average diameter of stem bundle at the base of the plant	39

Figure		Page
2.3.12	Weight of root-soil bulb plus weight of jaws versus soil bulk density	40
2.3.13	Maximum pulling force versus volume of crater given in pounds of water and cubic feet	42
2.3.14	Volume of crater in pounds of water and cubic feet versus soil moisture content.	44
2.3.15	Volume of crater in pounds of water and cubic feet versus weight of root-soil bulb plus weight of jaws	46
3.2.1	Diagram showing how the dimensions and root angle were obtained by direct tracing the roots	53
3.3.1	Typical force vs deformation curves from root tensile tests	59
3.3.2	Root angle vs root original length, with transition zone included	62
3.3.3	Diameter of fracture vs root original length	64
3.3.4	Force vs diameter of fracture	66
3.3.5	Stress vs. diameter of fracture	67
3.3.6	$F/\pi d$ vs diameter of fracture for short roots	69
3.3.7	F/πd vs diameter of fracture for long roots	70
3.3.8	$F/\pi d$ vs root original length	73
3.3.9	Modulus vs root original length	75
3.3.10	Diameter of fracture vs dipoint	77
3.3.11	Force vs dipoint	78
3.3.12	$F/\pi d$ vs dipoint	79
4.2.1	Free body diagram of root embedded in the soil	88
4.2.2	Axial tangential stress (τ) versus displacement (j)	94

Figure		Page
4.2.3	Residual force (F,), displacement (j) and the axial tangential stress (τ) as functions of the radial coordinate (ρ).	96
4.2.4	The displacement at failure surface is maximum for $\theta = 0$, and minimum for $\theta = \pi/2$	107
4.2.5	The static system of the soil composite .	110
4.2.6	Equilibrium diagram: $\Sigma F_z = 0$	112
4.2.7	Isostrength curves $\sigma_R = \text{constant}$	115
4.2.8	The strengthening effect of roots on failure surface	118
4.3.1	Sectioned wall at zero load	122
4.3.2	Failure occurred first at the centerline .	122
4.3.3	Rankine pattern is well outlined here	124
4.3.4	Tertiary crack and tension crack at soil surface are outlined	124
4.3.5	Tension crack and tertiary crack at soil surface is now quite visible	125
4.3.6	Observe the compression zone and an unfractured root which did not attain the effective length	125
4.3.7	Forces acting on the root-soil bulb	127
4.3.8	The disruption of the bulb is outlined based on surface tension crack	129
4.3.9	A close-up of the compression zone	129
4.3.10	Final stage of rupture prior to bulb disruption	130
4.3.11	A close up of root in the process of reaching the effective length	130
4.3.12	Observe that the roots are all fractured at the failure surface	132
4.3.13	Underground failure with x-y recorder in the filming, at zero load	133
4.3.14	x-y recorder in the field of filming	133

Figure		Page
4.3.15	Crack appeared at .85 of F max (F = 247 lbs)	134
4.3.16	Crack pattern at .97 of Fmax	134
4.3.18	Pulling force vs displacement curve of the specimen illustrated by figures 4.2.13 to 17 and 19	135
4.3.17	Crack pattern when force has declined to .70 of F_{max}	136
4.3.19	Note bulb disruption about the compression plane, in final stage of rupture	136
4.3.20	Shows the symmetry of the cracks in the initial stage of rupture	138
4.3.21	Shows that symmetry persisted until the final stage of rupture	138
4.3.22	The disruption of the bulb leads to an asymmetric appearance	139
4.3.23	No symmetry can be visualized by observing the pulled out bulb	139
4.3.24	Soil surface cracks	140

LIST OF TABLES

Table		Page
2.1	Major soil characteristics	6
2.2	Variables measured in the field experiments	14
3.1	Results of tensile tests and direct tracing of short roots	57
3.2	Results of tensile tests and direct tracing of long roots	58
3.3	Rupture strength parameter F/Nd in pounds per inch	7 ^L

1. INTRODUCTION

During the growth of a crop it is important that the stability of the aerial part of the plants be maintained in order to secure a full development of the product and to allow an efficient performance of the machinery involved in the production process.

The stability of a plant in the field is affected not only by the weight of the plant itself, but also by such horizontal forces as wind load (or similar horizontal loads). Under such loads, the plant sometimes becomes unstable and lodging occurs. This lodging may be due either to failure of the anchoring system or to failure of the aerial part. There is no standard definition for lodging; but it seems to be commonplace in works appearing after Hall (1934) to consider as "lodged" any plant leaning more than 45° from the vertical, including both root lodging and stalk breakage.

A knowledge of the strength relationships between root and soil is necessary in order to interpret the factors affecting the underground failure of the plant. These relationships are very complex due to the nature of the materials involved. Therefore, for an engineering approach of the problem it was decided that a simple type of loading, such as an uprooting force, would permit a

preliminary assessment of the important parameters for plant anchoring.

The objective of this research is to find background data to study the strength relationships between soil and root using as an example sudangrass (Sorghum vulgare var. Sudanense, Hitch.), subjected to an uprooting force. The ultimate goal, however, is to detect the important parameters regulating the strength of the root-soil composite, so that they can be assessed and used to predict failure of the root-soil system of other crops of economical importance, such as sugar cane or corn.

The original intention was to study these relationships for sugar cane. However, due to ecological difficulties presented to the growth of sugar cane in this area,
it was decided that the work could be done with sorghum,
because of its similarity in the root system, and the size
of the plant which would facilitate the experiments.

To fulfill the objectives, sorghum plants were planted in field conditions and subjected to a vertical pull. A continuous record of force versus displacement at the base of the plant were made. Soil and plant characteristics were determined as a basis for further correlations.

The establishment of the mechanical relationships between root and soil may become important in the ascertainment of factors which contribute to the full

development of a crop. This knowledge can be used in many phases involved in the process of crop improvement and production.

It will enable the breeder to select varieties whose root configuration will be adequate to perform the desired anchoring function, or a configuration that will offer a high resistance to uprooting. This statement is also applicable to the selection of grasses used to line canals, slopes, etc.

It will indicate to the agronomist and soil scientist how to position and shape the soil at the soil surface to impart a better anchorage to the plant. This will allow a more advantageous use of certain varieties. Resistance to wind forces could be ascertained and crop lodging could be prevented or minimized by providing better mechanical anchorage.

In the design of harvesting equipment it will furnish relations that will allow the determination of the magnitude and mode of the uprooting force. In the cases where small plants are taken out of the ground to be re-planted, critical force values can be determined as to least affect the root system.

2. THE UPROOTING FORCE

2.1 Review of Literature

Holbert and Koehler (1924) working with corn found a relationship between root anchorage and lodging, such that when the mean pulling resistance of a group of plants decreased, the percentage of leaning plants increased (plants leaning 30° or more). Also it was determined that for plants of good strain (which exhibited greater pulling resistance) the number of main and lateral roots was higher than that presented by plants susceptible to disease.

Wilson (1930) reported that in the absence of brace roots corn lodged badly. However, the secondary roots and plant height were not related to lodging. In the field, the diameter of the stem of the lowest internode showed no relation with lodging.

Hall (1934), working with corn under natural rainfall conditions found that in most cases the force required
to pull the plant from the soil was negatively correlated
to lodging. A similar relationship was found for force
and disease. He also reported that no relationship existed
between lodging and ear height, cross section or ear weight.
Hall used a mechanical device for obtaining the force
required to pull the stalks over to an angle of 45°,
keeping the stalk rigid from the first internode to the

point of attachment of the load, by fastening the stalk to a piece of wood.

Dillewijn (1952) reported that it is generally recognized that lodging exerts a harmful effect on sugar yield of sugar cane, but exact figures as to the losses involved are scarce. For pot experiments made by Borden, an average loss of sugar of 25 per cent was reported to be due to poorer juice quality of lodged plants. He also reported that according to Honig lodging is associated with starch formation in the concave side of the stem.

Newman et al. (1952) reported that stalk breakage caused more loss of corn and reduction of quality than root lodging. It was reported that root lodging generally occurred only before the corn is ripe and if the ground is soft.

Nelson (1958), in his work with field corn reported that

"significant relationships were shown between lodging and the mechanical force needed to break the standing stalk or the third internode, the diameter of the third internode, the height of the ear, and the yield of grain. The best single measurement for determining the lodging potential was the force needed to break the third internode. In combination, the best two measurements were ear height and the force needed to break the standing stalk."

Nelson also used mechanical devices to record the force required to pull the stalks over to an angle of 45° and the force to break the stalk at the third internode.

In the works reported here there has been no consideration given to root distribution as affected by factors such as soil bulk density, availability of nutrients and water, and seasonal variations. When an uprooting force was applied, no effect of soil moisture content was specifically determined, no measure of soil strength given, nor was root strength determined.

2.2 Field Procedure and Equipment

The field experiments were made in a plot of the Soil Science experimental farm of Michigan State University, on a loamy fine sand soil. Some of the major characteristics of the soil can be seen in Table 2.1.

TABLE 2.1--Major soil characteristics.

Soil:	Spinksloamy	fine sand	
Mechanical Analy	sis**	Donaitu	2.62
0 .1	3 0 C #	Density	2.02
fine gravel	1.36%	Bulk density	1.51*
coarse sand	3.66%	Total porosity (air pyc.)	39.90%*
medium sand	7.73%	• •	
fine sand	50.30%	Non-cap.porosity (air pyc.)	10.00%*
very fine sa	and 20.63%	Upper plast.limit	19.90%
·		Lower plast.limit	; -
silt and cl	ay 16.32%	Moisture equiv.	15.80%
	M.C.	at 60 cm tension	20.40%

^{*}Corresponding values.

^{**}Silt and clay content was calculated by subtraction.

On June 15, 1967, after the field had been plowed and harrowed, three to five seeds of sorghum per hill were manually planted in hills spaced five feet between rows and four feet in the row. This spacing was expected to avoid major interferences of root systems.

A starting fertilization on the basis of 12.5 lb. of nitrogen per acre was applied. After the plants reached a height of 12-15 inches, a side dressing was applied with 100 lb. of nitrogen, 25 lb. of P_2O_5 and 75 lb. of K_2O per acre.

On July 5 the experimental plot was cultivated between rows with a front-mounted cultivator and handhoed in the rows. On August 5 a second cultivation was made similar to the first. After September 15 a mower was used whenever needed to control weeds and to minimize disturbance to the soil. Nevertheless, it was noticed during the experiments that weed roots were present, in some cases interfering with the results, as was apparent in one of the sectioned plants.

For the pulling experiments a pulling device was built and instrumented. The pulling device consisted of a 12 V dc compound electric motor (3800 rpm) with a worm-gear box for speed reduction. A screw, attached to the gear box output shaft drove a nut welded inside a square tube. This vertically driven tube was prevented from rotating and guided by a square opening in the outer housing tube. The

displacement rate obtained was approximately 2 to 2.4 inches per minute, respectively for loaded and unloaded conditions. The housing tube supported the whole device and was loosely bolted to a tripod. Footings were provided for the tripod to minimize sinkage of the system. 2.2.1 and 2.2.2 show respectively a general view of the pulling device and a closeup giving the typical placement of load cell, traction jaws and displacement bar with the linear variable differential transformer (LVDT). pulling force was applied to the plant by two traction jaws made of L-shaped steel bars with metal lath welded to their inner faces. The addition of this metal lath imparted no major injury to the stem. The pressure against the stems was produced by equally tightening the wing nuts holding the two bars together. No slip problem was experienced provided the wing nuts were adequately tightened.

The tripod was located over the plant with the telescoping tube aligned with the center of the plant. A load cell was connected between the traction jaws and the telescoping tube including a universal joint to eliminate side pull. The force was measured using a Daytronic 250 lb. load cell with a 300 C/61 transducer-plugin amplifier combination.



Figure 2.2.2. Typical arrangement of the load cell, traction jaws, and spike of the displacement bar with LVDT.



Figure 2.2.1. A general view of pulling device and measuring instrument.

An aluminum bar with a hinged spike in one end was used to sense the lifting of the base of the plant. The spike was pushed into the base of the plant. The displacement was measured by a Schaevitz HR 2000 LVDT (± 1 inch linear range), located at midpoint of the bar. The output was demodulated and amplified by a Daytronic 300 C transducer amplifier with a modified type 60 plug-in unit.

A 750 watt, 60 Hz generator was used to provide power for the equipment in the field. Adequate grounding was provided to minimize noise.

A force versus displacement curve was recorded from the two transducer amplifier outputs on a Moseley Autograf x-y recorder, model 135. Figures 2.3.4 and 2.3.5 in Section 2.3.4 show typical force vs. displacement graphs for integral and sectioned pullings, respectively.

The diameter of the plant stem bundle in its natural state was measured at its base before pulling. Then the stems were cut at 20 inches above the soil surface and a stem sample two inches long was collected for later drying and weighing. The traction jaws were then attached to the stems in such a way to cause minimum disturbance to the plant.

Soil moisture content, bulk density and penetrometer readings were determined for most of the pullings. One undisturbed soil sample and two or three penetrometer readings were taken for each test, at a radius of about 20 inches from the plant.

The penetrometer readings were made with a recording penetrometer with a probe area of 0.5 square inch. Peak values were obtained at a depth of about 5 inches. A typical penetration diagram is given in Figure 2.2.3. Difficulties were encountered in obtaining penetration readings in some stony spots. A plow sole was detected at a depth of approximately 8 inches whose effects will be commented on later.

Observations as to shape and dimensions of the root-soil bulbs were made after they had been pulled, with the intention of using their shape as representative of the failure surface and their dimensions as possible parameters to be compared with the pulling force. Average values of the dimensions are given in Figure 2.3.1.

When pulling the plant, observations were made as to the development of surface cracks. This was facilitated by "powdering" the area around the plant with industrial plaster. The development of these cracks was filmed during some tests. A series of photographs from the film are shown in Section 4.3, where the cracks are described as they took place.

The development of the failure surface below the soil surface was also observed and filmed for some experiments (called sectioned tests). For these tests two

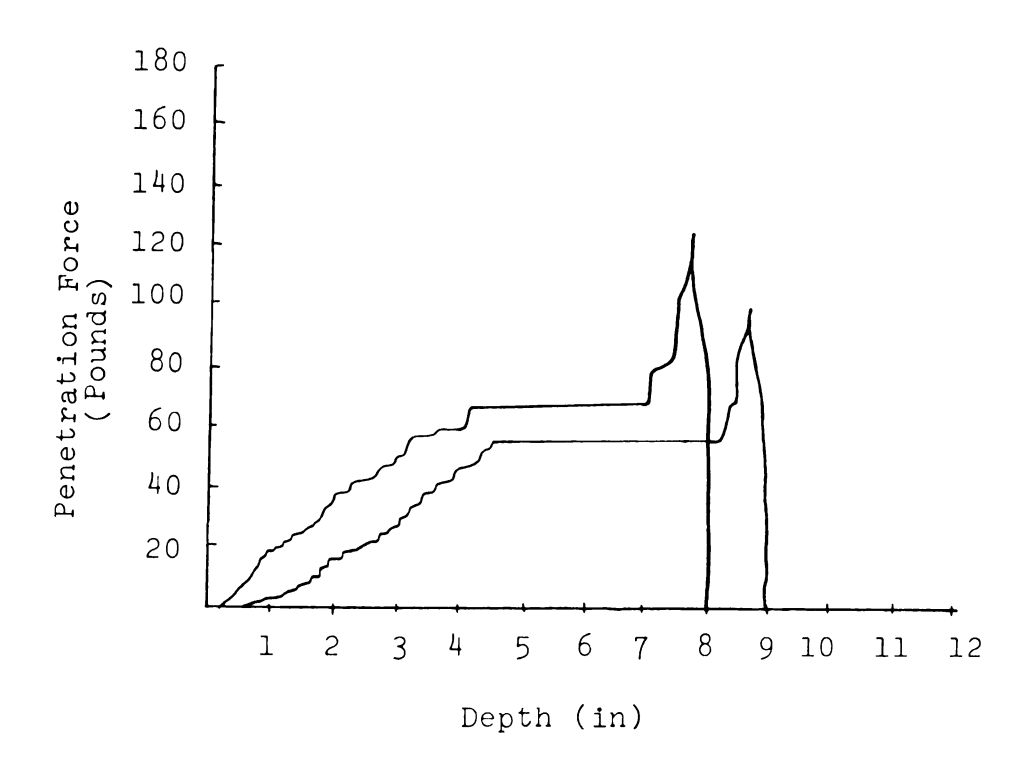


Figure 2.2.3--Typical penetration curve(from experiment number10).

sectors of 90° each, meeting at the center of the plant were opened symmetrically in the soil. The sides of the sectors were first cut with a trowel and then carefully the rest of the soil was removed. The depth of these sectioned walls at plant center was always greater than 10 inches to avoid a possible effect of the bottom of the section upon the failure surface. Following a smoothingup of the sectioned wall, a grid pattern was applied to it by powdering industrial plaster through a grid with 0.75 inch mesh. To allow filming of the trace of the failure surface, a shallow trench was made perpendicular to the sectioned wall to be filmed. The failure surface development could then be observed and filmed. A series of photographs showing the shape and location of the failure surface with respect to the plant are given in Section 4.3. Some of the filming was done with the x-y recorder in the field of view to allow a comparison between development of cracks and the magnitude of the pulling force. Thus, two types of pulling tests were made, namely: sectioned, which has just been described, and integral where no sectors had been cut in the ground. Table 2.2 shows the data obtained in the field for all integral and sectioned tests.

As the experiment developed it was noticed that if no extraneous roots or other materials were present, a distinct undisturbed crater surface could be found by carefully removing the disturbed soil of the crater after the bulb had been removed. This was done and the crater

TABLE 2.2--Variables measured in the field experiments.

f Depth of Crater at ce Center (in)	11.111111111111111111111111111111111111
Diameter of Crater at Soil Surface (in)	1 1 1 1 1 1 1 1 1 1 1 1 1 1 1 1 1 1 1
Volume of Crater (1b of H ₂ 0)	97.65.000 1 1 1 1 1 1 1 1 1 1 1 1 1 1 1 1 1 1
Penetro- meter Reading (1b)	00000000000000000000000000000000000000
Plameter of Stem at Base of Plant (In)	1 1 1 1 1 1 1 1 1 1 1 1 1 1 1 1 1 1 1
Welght of Fully + Jak + (15)	೯೯೬ ರತ್ತು ಅತ್ಯಾತ್ರವಾಗಿ ಕೆ. ಈ ಚಿತ್ರವಾಗಿ ಕೆ. ಈ ಚ ಹೊಗ್ಗಳ ಅತ್ಯಾಪ್ತಿಗೆ ಈ ಚಿತ್ರಗಳ ಅತ್ಯಾಪ್ತಿಗಳ ಪ್ರತಿಗಳ ಅಭಿವರ್ಧ ಅಪ್ಪುಗಳ ಹೊಗ್ಗಳ ಪ್ರವರ್ಧ ಪ್ರತಿಗಳ ಪ್ರತಿಗಳ ಪ್ರತಿಗಳ ಪ್ರತಿಗ ಹೊಗ್ಗಳ ಆಗ್ರಾಮ ಕೆ. ಈ ಚಿತ್ರವಾಗಿ ಕ
Dry Welfit of Stem Sample (grams)	
Dry Bulk Density (grams/ cm3)	
Soll Moisture Content (%)	
Displac. at (Fmax) (in)	
Maximum Force (F max)	33 25 25 25 25 25 25 25 25 25 25 25 25 25
Experiment Number	2000 - 0 0 0 0 0 0 0 0 0 0 0 0 0 0 0 0 0

*Experiment numbers with -S indicate sectioned tests. **Welght of Jaw = 6.7 lbs.

profile, volume, diameter at soil surface and depth at the center were measured using the following order and procedure:

A.--Crater profile and depth at center: the disturbed soil was removed and a pantograph was used to reproduce (trace) the crater profile (N-S, E-W). A diagram with height and dimensions are given in Figure 2.3.3;

B.--Crater diameter: three measurements were made (N-S, E-W, NW-SE) for each of nine experiments, and the average used as a representative value of crater diameter:

C.--Crater volume: the crater was lined with a thin sheet of plastic. The weight of water required to fill the volume displaced by the root-soil mass was determined.

The values for crater volume, average diameter and depth are given in Table 2.2.

An attempt was made to estimate the amount of roots remaining in the soil below the crater, but all the methods which were considered seemed unreliable.

In order to ascertain the performance of the pulling device and the instrumentation, several trial tests were made in the field. These tests are numbered from 1 thru 9 in Table 2.2. The first preliminary experiments on integral plants were carried out on October 7, in order to observe what other variables should be measured besides pulling force, displacement at base of plant, soil moisture content

and bulk density, weight of dry stem and weight of the bulb. Experiments number 7 and 8 were performed with sectioned plants on October 8, to verify the symmetry response of the root-soil system with respect to pulling force. Experiments number 10 to 20 were performed on October 14, and other variables such as diameter of stem bundle at base of plant, penetrometer reading and shape and dimensions of the pulled bulb were collected. For these experiments a series of randomly located integral and sectioned plants were pulled in order to further ascertain the symmetry response. During these experiments the importance of the crater parameters was noticed and some preliminary observations were made. On October 25, experiments 21 to 26 were made in order to observe and determine parameters of the crater. On October 27, the first snowfall took place in the region, resulting in stem breakage, thus preventing further tests.

2.3 Results and Discussion

2.3.1 Root-Soil Bulb

From the observations made of the conformation and dimensions of the root-soil bulbs that were pulled up with the plants, it was possible to reproduce a diagram that is shown in Figure 2.3.1. The values in the diagram represent averages of three measurements for each dimension for five bulbs of integral plants. In Figure 2.3.1,

the line ch indicates a circular conical band consistently showing the greatest number of roots projecting out of the root-soil bulb. Though the angle < cah could not be determined accurately, its value as calculated varied from 18 to 32 degrees with an average of 28 degrees. However, the shape and dimensions of the pulled out root-soil bulb was considerably altered during the detachment from the soil. This was chiefly due to the tension cracks developed in the soil surface and the falling-off of the soil sustained by the root mesh during the pulling action. This matter will be elaborated on in Section 4.3.

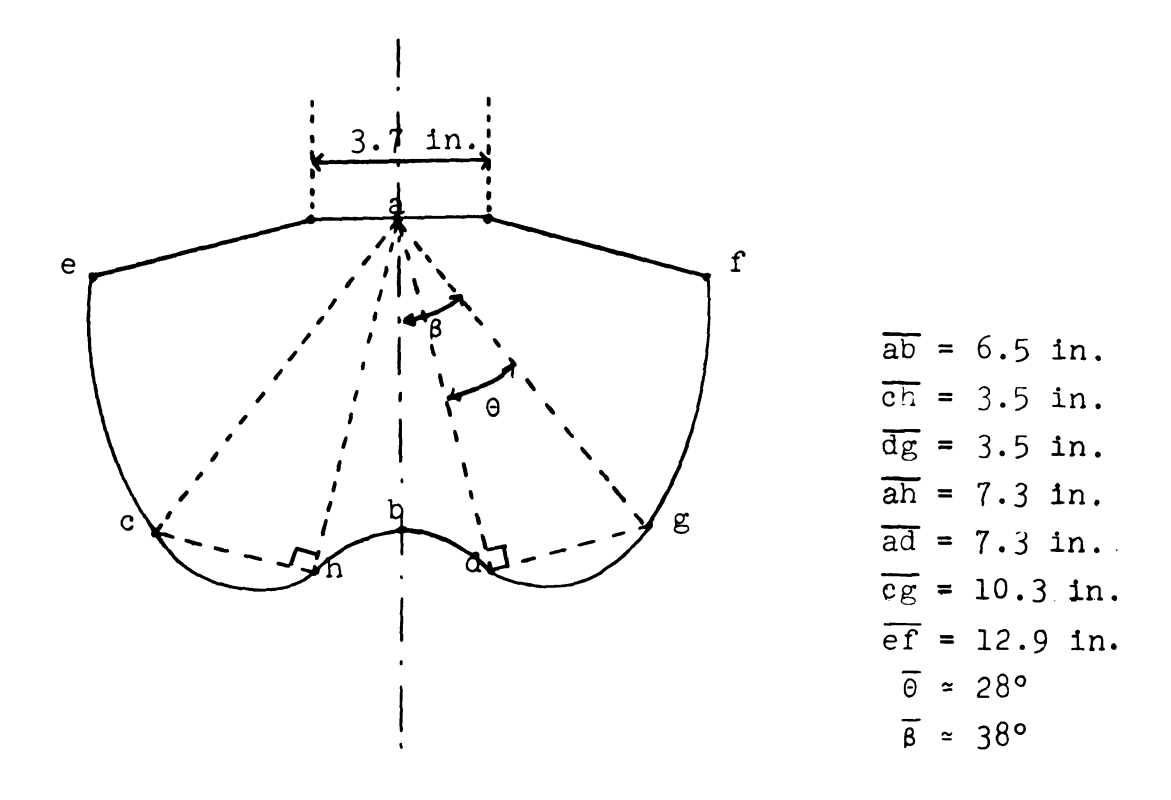


Figure 2.3.1--Typical shape and dimensions of a pulled out root-soil bulb (load centrally applied).

In some cases it was found that the bulb was unsymmetrical. The main source of this seemed to be a misalignment of the pulling force on the plant caused by the positioning of the tripod. After this was first observed the operation was more carefully performed. Nevertheless, in some plants it was noticed that the stems for some reason did not grow perpendicularly to the soil surface. Whenever a misalignment took place, some difficulties were experienced in measuring the displacement at the base of the plant. This was due to a bending moment introduced at that point, which caused a slight movement lengthwise of the aluminum bar used to sense the displace-The movement of the bar affected the positioning of the LVDT thus somewhat affecting the measurement. effect of this bending moment was noticeable in the final shape of the bulb. A diagram based on these observations is given in Figure 2.3.2. If the diagram of Figure 2.3.2 is compared with that of Figure 2.3.1, this effect is quite

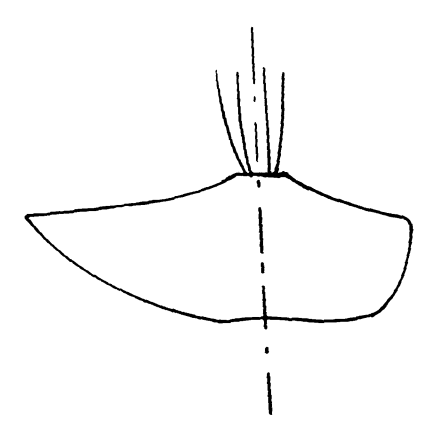


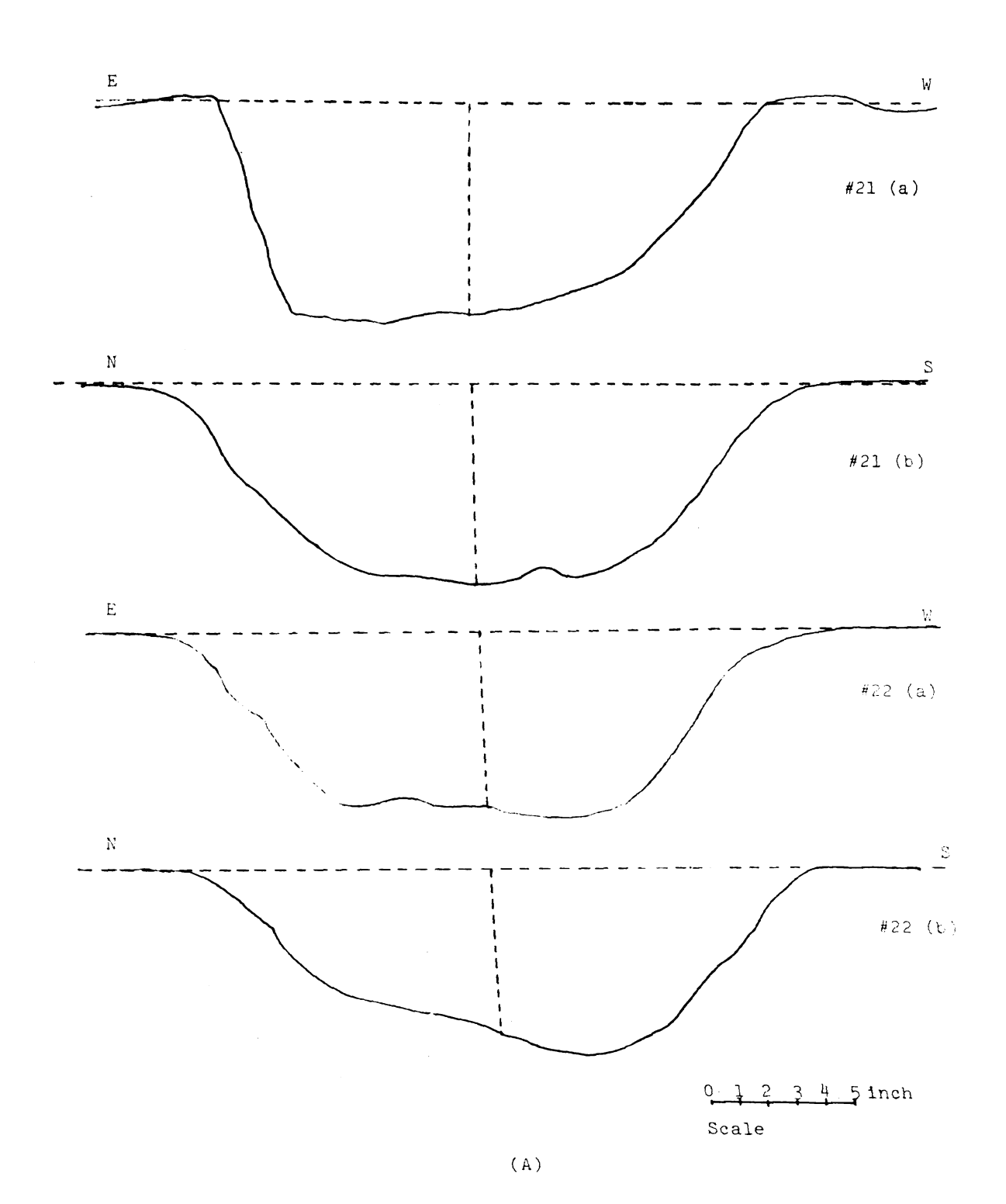
Figure 2.3.2--The effect of force misalignment or non-verticality of stems as affecting the final shape of the root-soil bulb.

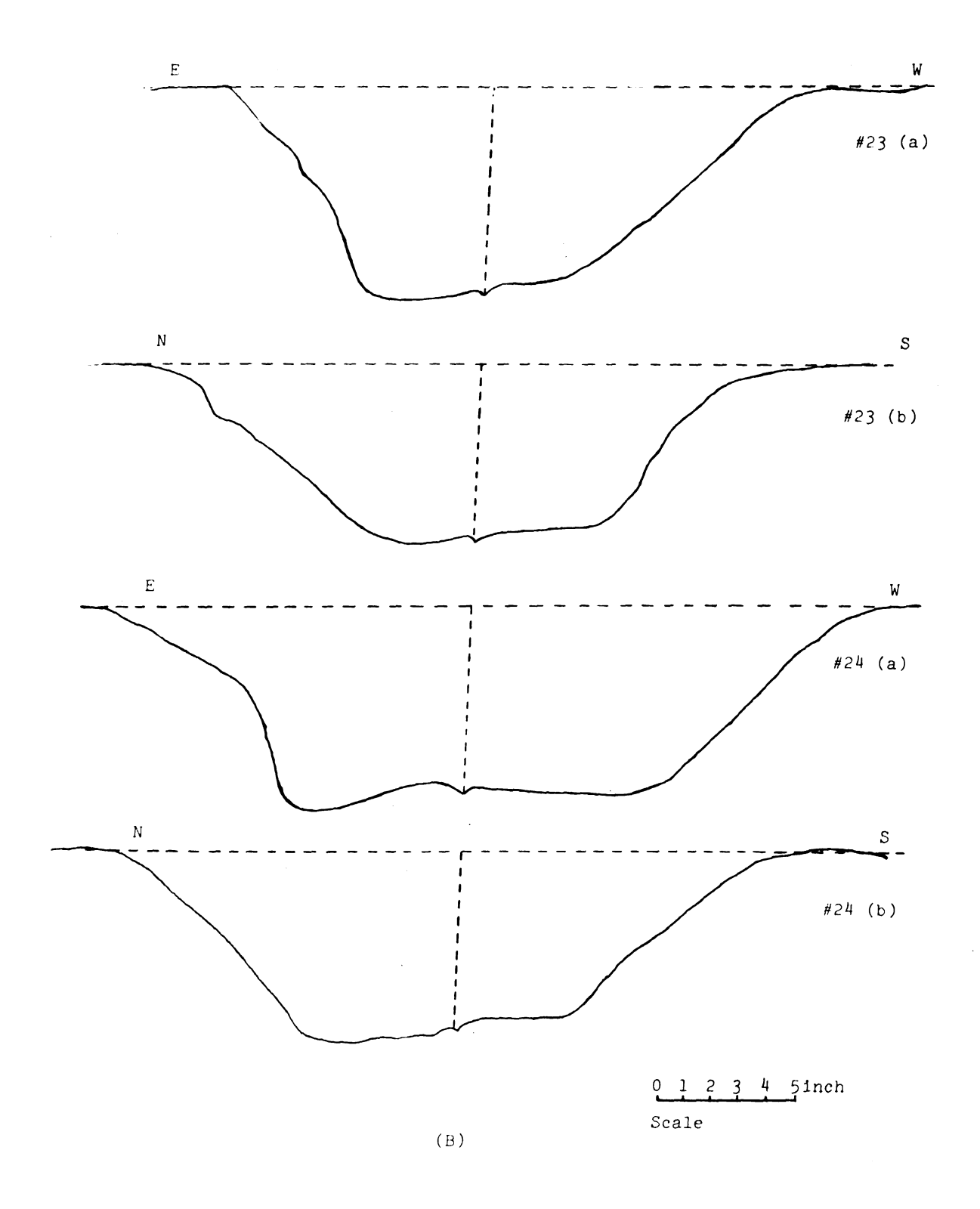
evident. As it might be expected, the shape of the crater also became altered. This was quite evident as observed for experiments 26 and 23 where the effect can be seen through the profiles given in Figure 2.3.3.

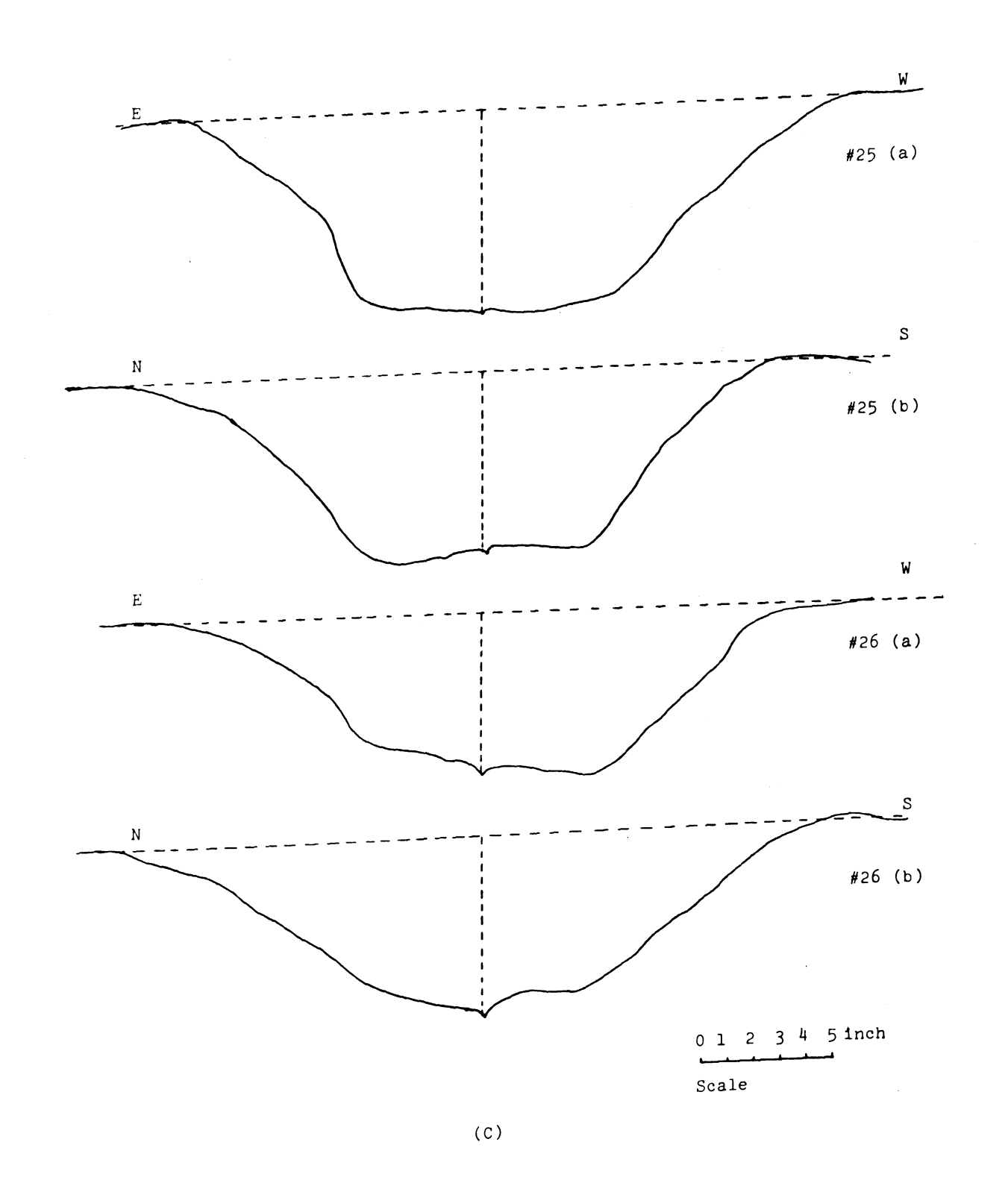
2.3.2 The Crater

As earlier mentioned the crater was defined as the hole in the ground after all disturbed soil had been removed. Observations of crater profile and depth were graphically made for experiments 21 to 26. These can be seen in the diagrams of Figures 2.3.3 (A), (B), and (C). The center of the crater, as shown in these figures corresponds to the vertical line through the center of the plant, as it was located prior to pulling. The depth of the crater was measured to the line representing the surrounding surface of the soil. The difference in height that two profiles of the same crater might present, is mainly due to the unevenness of the soil surface close to the crater. In these figures it can be noticed that at least one of the profiles of each crater presents a similar configuration with the others. Despite careful finger-tracing of the bottom of the crater when removing the disturbed soil, difficulties were encountered in some cases in distinguishing clearly the undisturbed surface. According to the observations, the factors causing these

Figure 2.3.3--(A), (B), and (C)--Crater profiles from tests 21-26. Broken lines indicate the soil surface and the vertical axis of the plant.







difficulties were: mesh of extraneous roots (weeds); in some tests, the high moisture of the soil which interfered with the feel of the undisturbed surface; the effect of secondary failure surfaces which remained adhered to the bottom of the crater strongly enough to be felt as a part of it. This latter effect will be better understood when the failure patterns are described in Section 4.3.

In general, the non-homogeneity of the root-soil system affected the tracing of the crater bottom, and consequently that of the failure surface.

2.3.3 Effect of Sectioning

In Table 2.2 the experiment numbers followed by a -S indicate tests with sectioned plants. For the cases of experiments 7 and 8, they were the first trials with sectioned plants and since the sides of the sectors were not cut as to meet at the center of the plant, their results should be considered with reservations.

A statistical analysis was made to find out whether the mean value of maximum force for sectioned plants was equal to one-half that of the integral plants. For this analysis the maximum force values from the following experiments, reduced by the weight of the jaws (6.7 lb), were used: 11, 12, 14, 16, 18 and 20 for sectioned plants (X_s) and 10, 13, 15, 17, 19 and 21 for integral (X_i) . The number of observations per group was: $n_s = n_i = n = 6$.

The basic hypothesis $\mu_s = \frac{1}{2}\mu_i$ was to be tested at a significance level of 0.05.

An F-test was used to compare the variances of the samples under the hypothesis $\sigma_s^2 = \sigma_i^2$. The value of F was:

$$F = \frac{s_{s}^{2}}{s_{i}^{2}} = 14.53$$

A comparison to F (.025, 5, 5) = 7.15 implied that one could be 95% confident that the variances were different. (A more appropriate hypothesis had probably been $\sigma_s^2 = \frac{1}{4}\sigma_1^2$.) Therefore the approximate t-test to be used to compare the sample means was

$$t' = \frac{\overline{X}_{s} - \frac{1}{2}\overline{X}_{i}}{\sum_{s=1}^{2} + (.25) S_{i}^{2}} = 1.592.$$

The critical value t (.05, 5) = 2.571 indicated that there was little evidence that the mean value of the maximum force for sectioned plants was not equal to one-half the mean value of the maximum force for integral plants. This justified our assumption of undisturbed response of the root-soil system with respect to the value of the maximum pulling force for sectioned plants.

A similar analysis was made for the weight of the root-soil bulb of sectioned plants, as compared to

one-half of that of the integral plants. Since in this case the variances of the sample means were regarded equal by an F test, an exact t test was used, considering:

$$V(\overline{X}_{s} - \frac{1}{2}\overline{X}_{1}) = V(\overline{X}_{s}) + \frac{1}{4}V(\overline{X}_{1}) \text{ and}$$

$$V(\overline{X}_{s}) = V(\overline{X}_{1}), \text{ then}$$

$$V(\overline{X}_{s} - \frac{1}{2}\overline{X}_{1}) = 1.25 \sigma_{\overline{X}}^{2}$$

where $\sigma \frac{2}{x}$ is a variance common to both means. Thus,

$$t = \frac{\overline{X}_{s} - \frac{1}{2}\overline{X}_{i}}{(2)(1.25)S^{2}} \quad \text{and} \quad S^{2} = \frac{SS_{s} + SS_{i}}{n_{s} + n_{i} - 2}$$

$$t = 0.0567$$
 and $t (.05, 10) = 2.228$

which indicates that there is little evidence that the mean value of the weight of the root-soil bulb for sectioned plants differs from one-half that of the integral plants.

An analysis of the displacement at maximum pulling force showed that there was no evidence of a difference between sectioned and integral plants.

2.3.4 Force and Displacement

The graph of force versus displacement in Figure 2.3.4 shows that for integral plants a fairly linear



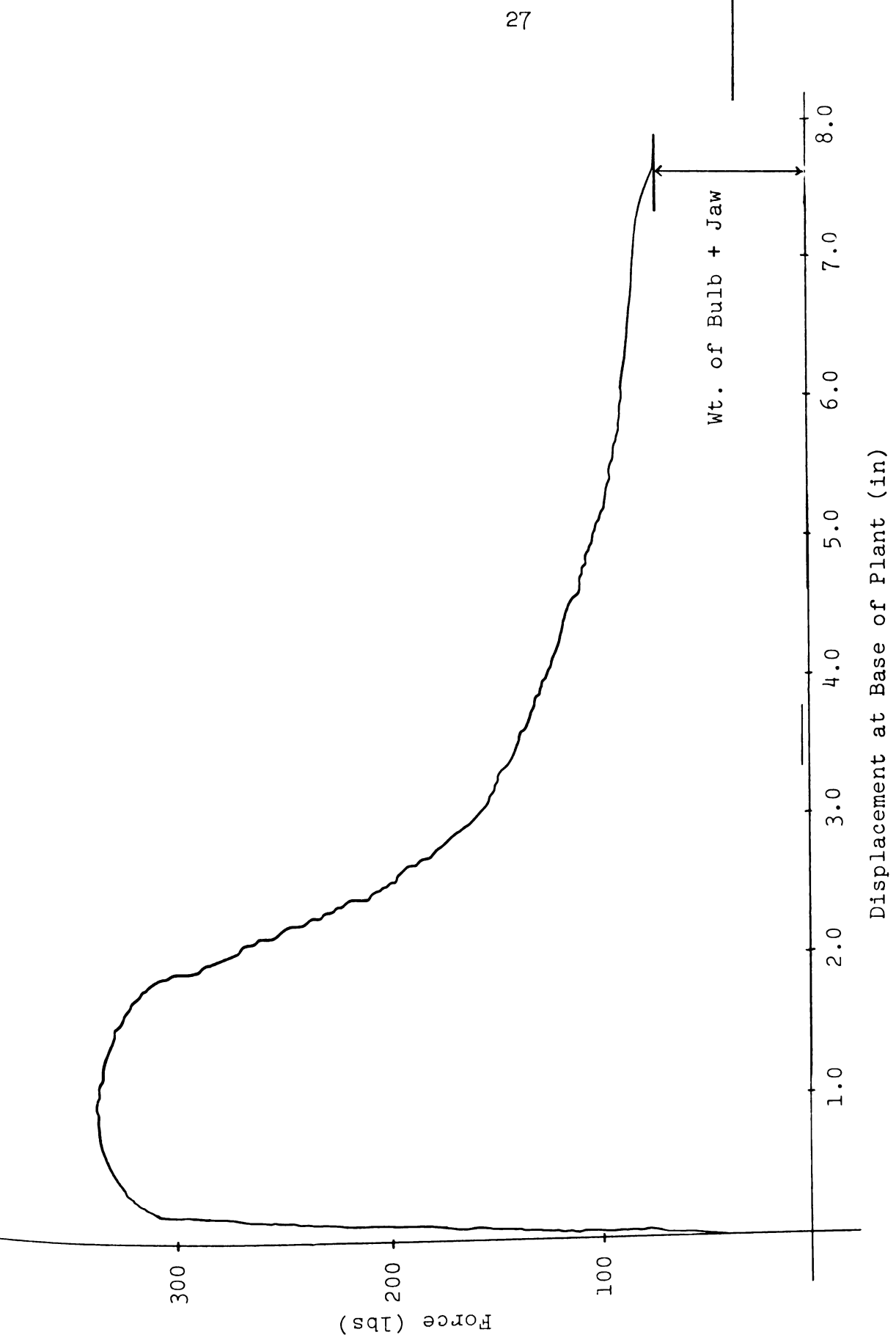


Figure 2.3.4--Typical force versus displacement curve for an integral plant.

relationship applies up to a point close to the maximum Beyond this assumed straight line, the system begins to yield with an increase in the rate of displacement, resulting in a curved shape of the graph. Around the point of the maximum force the curved path of the graph is characterized by sudden jumps of the recording pen, which suggest the successive breaking of roots. During the tests this jerk of the recording pen would take place accompanied by an audible breaking sound coming from the ground. The successive, instead of simultaneous breaking, of roots will be explained later in Section 4.3 with reference to the effective root length. In some cases these sudden jumps are more noticeable as can be seen in Figure 2.3.5 for a sectioned plant. As to the initial section of this curve, it is also seen that the curved shape became more evident with sectioned plants. Also, by comparing the straight line portions with the values of the maximum forces of the two typical curves, it is seen that the proportional limit is smaller for sectioned plants. A reasonable explanation of this effect may be found by considering the viscoelastic nature of the soil and that of the roots. The interaction between soil and root under the natural geometry seems to lead the behavior of the composite to a "quasi-elastic" response and to a closer value of the maximum force, which can be seen from the curve of the integral plants. It

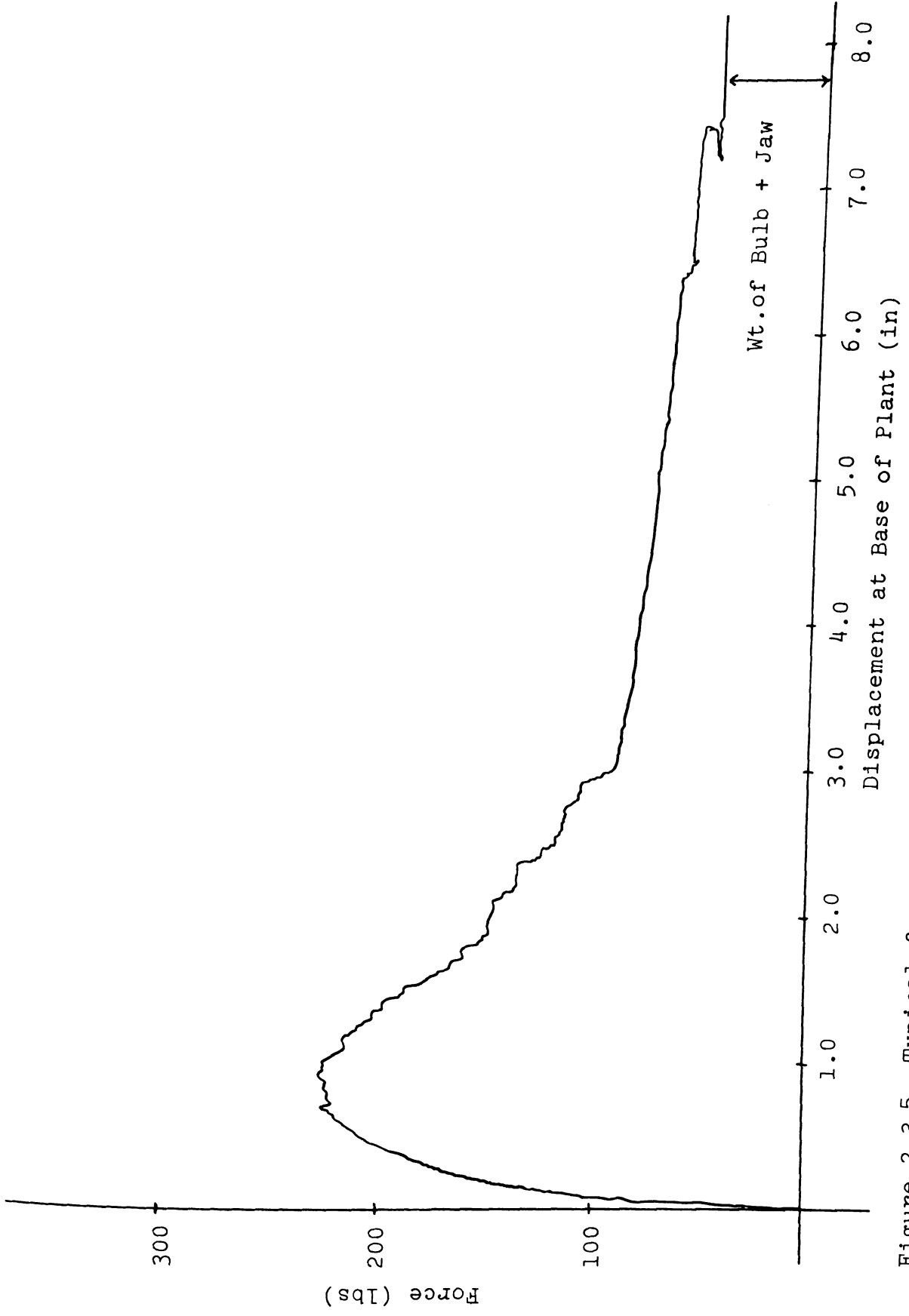


Figure 2.3.5--Typical force versus displacement curve for a sectioned plant.

seems that by cutting the sectors this "quasi-elastic" behavior of the composite is considerably reduced.

At the end of the test the curves indicate only the weight of the bulb plus that of the jaws. Typical values are shown in Figures 2.3.4 and 2.3.5.

Simple correlation and regression analysis were made using Michigan Agricultural Experiment Station (1967) Stat Series Routines. The correlated variables which presented a significant partial correlation coefficient, were plotted. The pertinent partial correlation coefficient and regression equation obtained are given at respective graphs. In addition, certain variables were plotted despite a rather low partial correlation coefficient, to give an idea of the variations experienced.

Two sets of tests from the data given in Table 2.2 were analyzed separately as follows: experiments number 10, 13, 15, 17, 19, and 21 to 26, were used for the analysis of all the variables listed, except crater values; the analysis of the data of experiments 21 to 26 included also the crater parameters, and these results and discussion will be presented later in this section. As mentioned earlier tests 1 thru 9 were preliminary tests. Their values were not statistically analyzed.

A plot of force* versus soil moisture content is shown in Figure 2.3.6. A large variation is apparent and no specific conclusion can be drawn from the plot. It is noticed, however, there is a tendency to a decrease in the value of the force with increasing soil moisture content.

Very low partial correlation coefficients were found for force or displacement with respect ot penetrometer reading. The same was true for displacement or penetration value versus soil moisture content.

The force was found to be positively related to displacement, weight of bulb, dry weight of a 2-inch sample of stems and diameter of stem bundle at the base of the plant.

The maximum force versus corresponding displacement are shown in Figure 2.3.7. This behavior was expected, if the root system size is taken into account. However, the partial correlation coefficient was rather low for this relationship.

Figure 2.3.8 shows a plot of force versus weight of root-soil bulb. During the experiments it was noticed that the shape and the dimensions of the bulb

^{*}Further use of the terms force and displacement (in this chapter) will mean the maximum pulling force and the respective displacement at the base of the plant, unless otherwise stated.

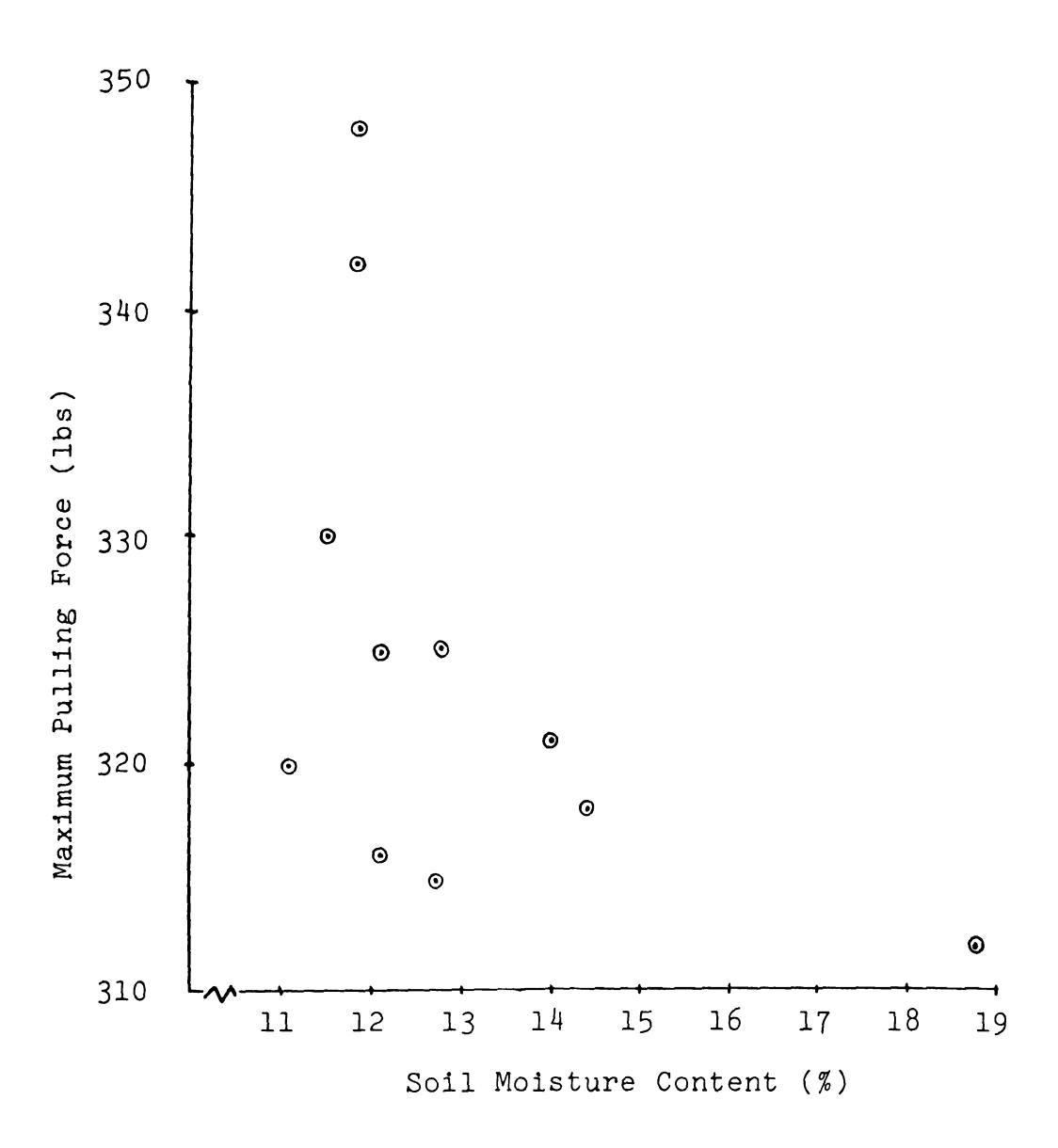


Figure 2.3.6--Maximum pulling force versus soil moisture content.

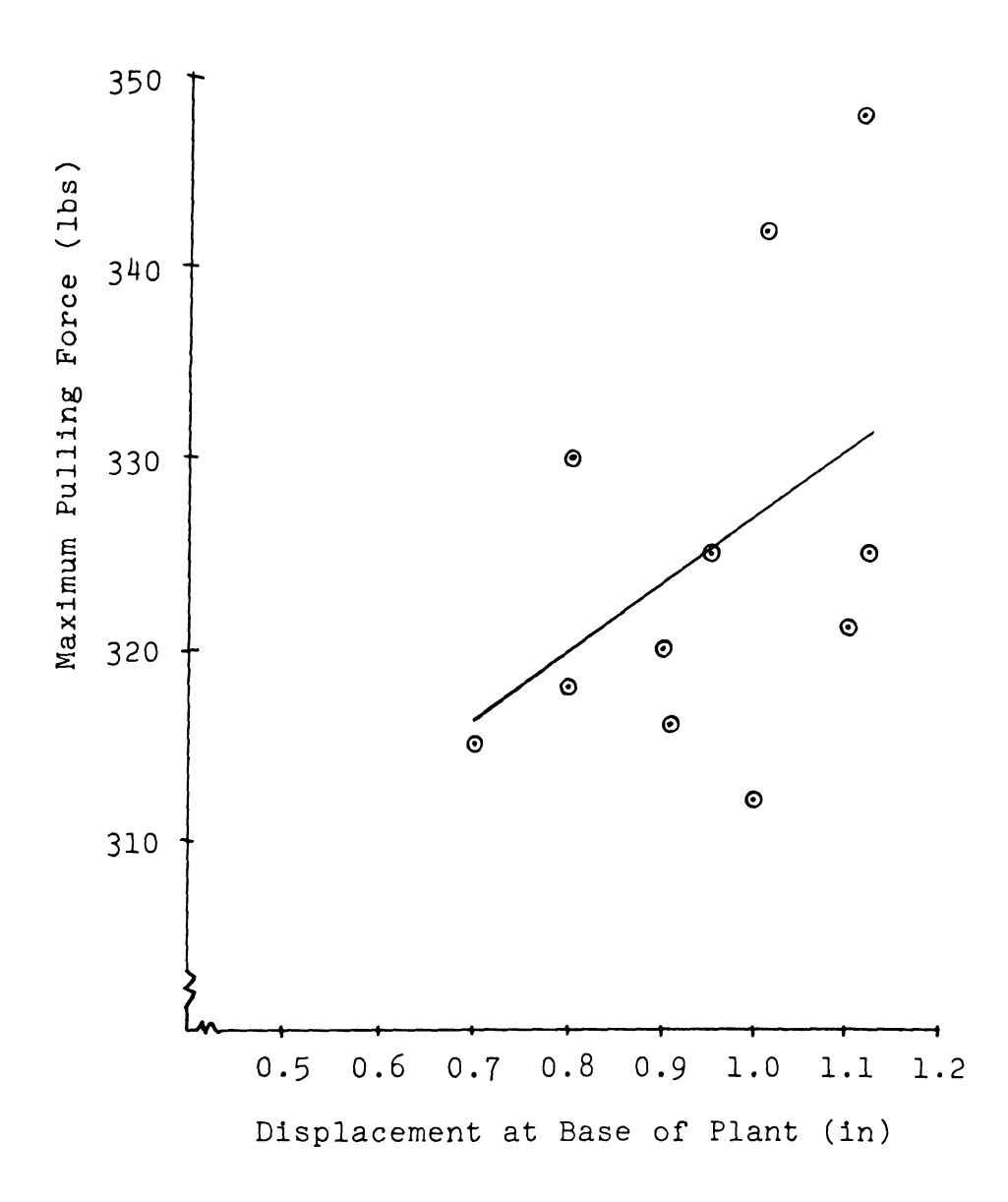


Figure 2.3.7--Maximum pulling force versus displacement at base of plant. Regression equation: Y = 291 + 36 X; pcc = .450.

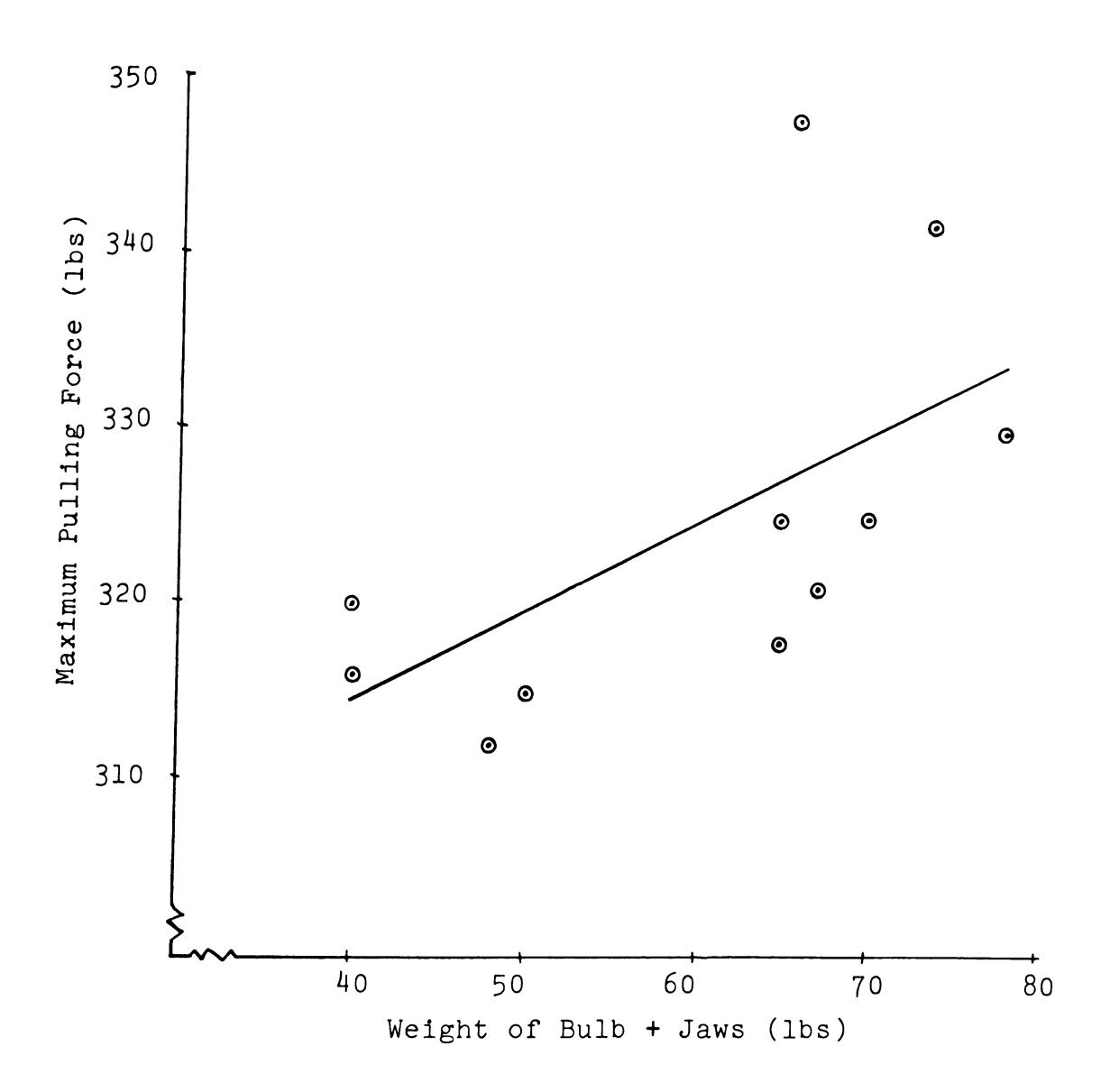


Figure 2.3.8--Maximum pulling force versus weight of rootsoil bulb plus weight of jaws. Regression equation: Y = 293 + .52 X; pcc = .611.

did not represent that of the underground failure surface as was assumed in the beginning of this section. However, the analysis of the data shows that the force is reasonably correlated with the weight of the bulb. This suggests that the weight of the root-soil bulb is to some extent representative of the root development, despite the detachment of soil which takes place during the pulling process. The large constant term and the low ratio indicate that the pulling force is mainly determined by other factors than the bulb weight.

A positive relationship was found for the force as compared with the diameter of the stem bundle at the base of the plant. A plot of this relationship, the regression equation and partial correlation coefficient are given in Figure 2.3.9. Again the large constant term indicates only a partial influence of plant size or a nonlinear relationship. The diameter of the stem bundle and the dry weight of a 2-inch sample of stems were expected to indicate the size of the plant. A plot and the partial correlation coefficient of force versus dry weight of 2-inch of stems are shown in Figure 2.3.10.

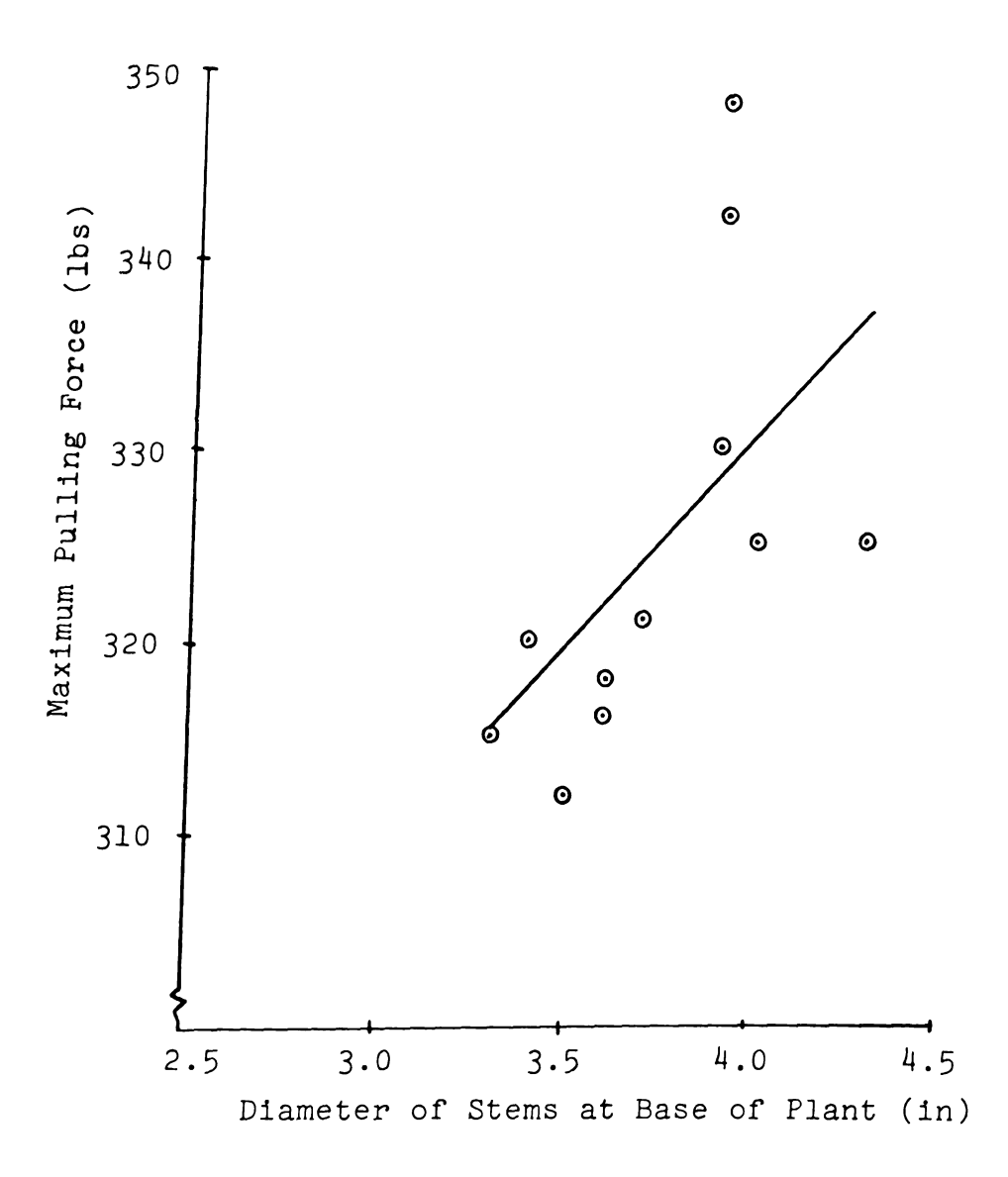


Figure 2.3.9--Maximum pulling force versus average diameter of stems at base of plant. Regression equation: Y = 243 + 22 X; pcc = .564.

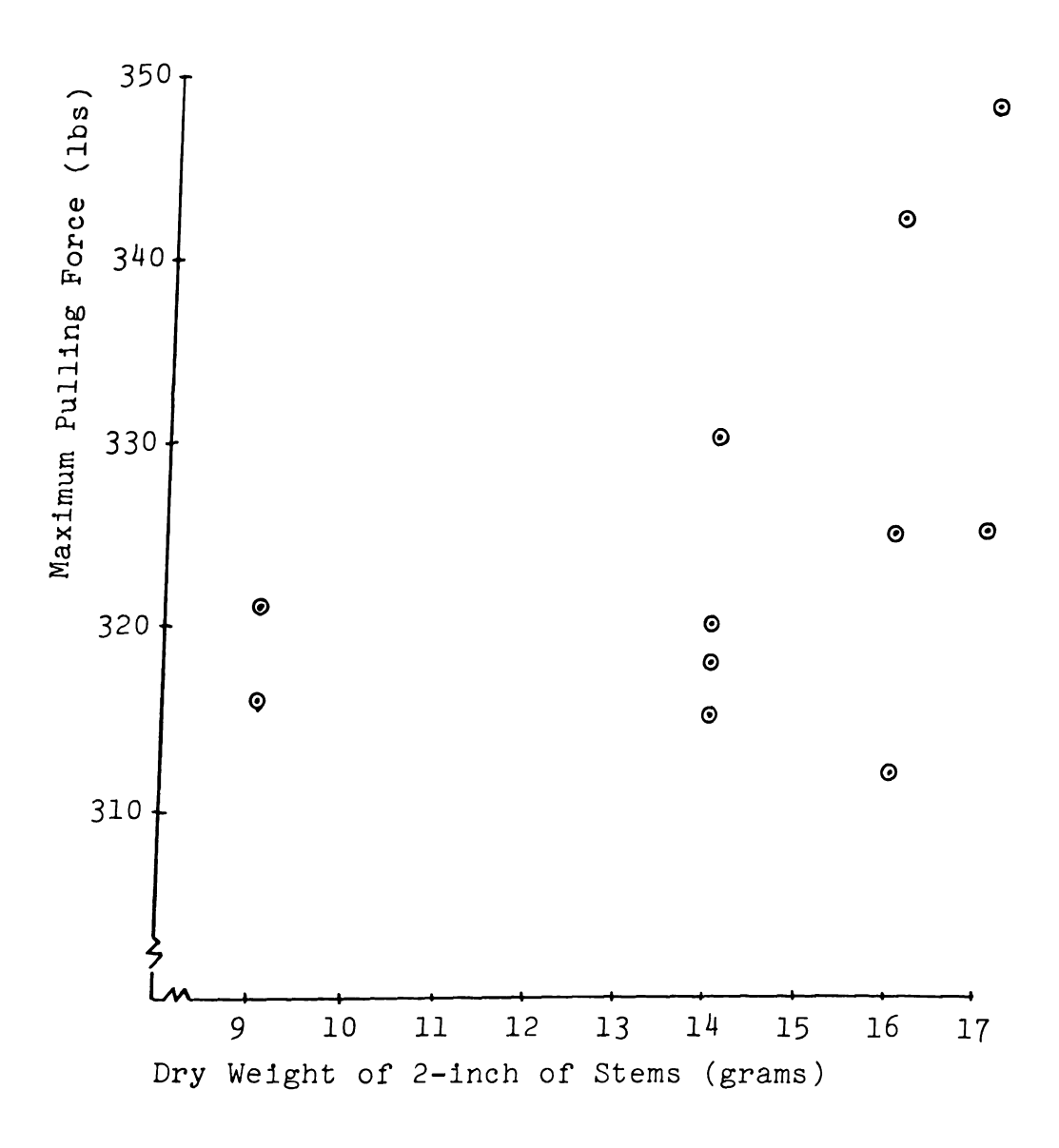


Figure 2.3.10--Maximum pulling force versus dry weight of a 2-inch sample of stems. pcc = .446.

As to displacement and diameter of stem bundle at the base of the plant, a plot and partial correlation coefficient is given in Figure 2.3.11. Part of the variation shown by the plotting may be attributed to a misalignment of the pulling force and consequent movement of the displacement sensing bar, as previously mentioned.

The effect of soil bulk density upon the weight of the bulb can be seen in Figure 2.3.12. An increase in soil bulk density caused a decrease in the weight of bulb. Although the change in bulk density was small and not artificially induced, this fact may suggest some impeding effect of the soil bulk density upon the root and plant development. Other reasons for the relationship also probably exist, as will be mentioned in Section 3.1.

A partial correlation coefficient of -.412 was determined for the weight of 2-inch samples of stems versus the diameter of the stem bundle at the base of the plant. This suggests the possibility of the latter to be used as a parameter of plant size, since it is a rather simple measurement.

Since bulb size did not seem to be the main factor influencing the force, crater size was determined in the last set of experiments. In order to detect how the crater depth, diameter and volume behaved with respect to other variables, a correlation and a regression analysis were made for experiments 21 to 26, including the crater measurements.

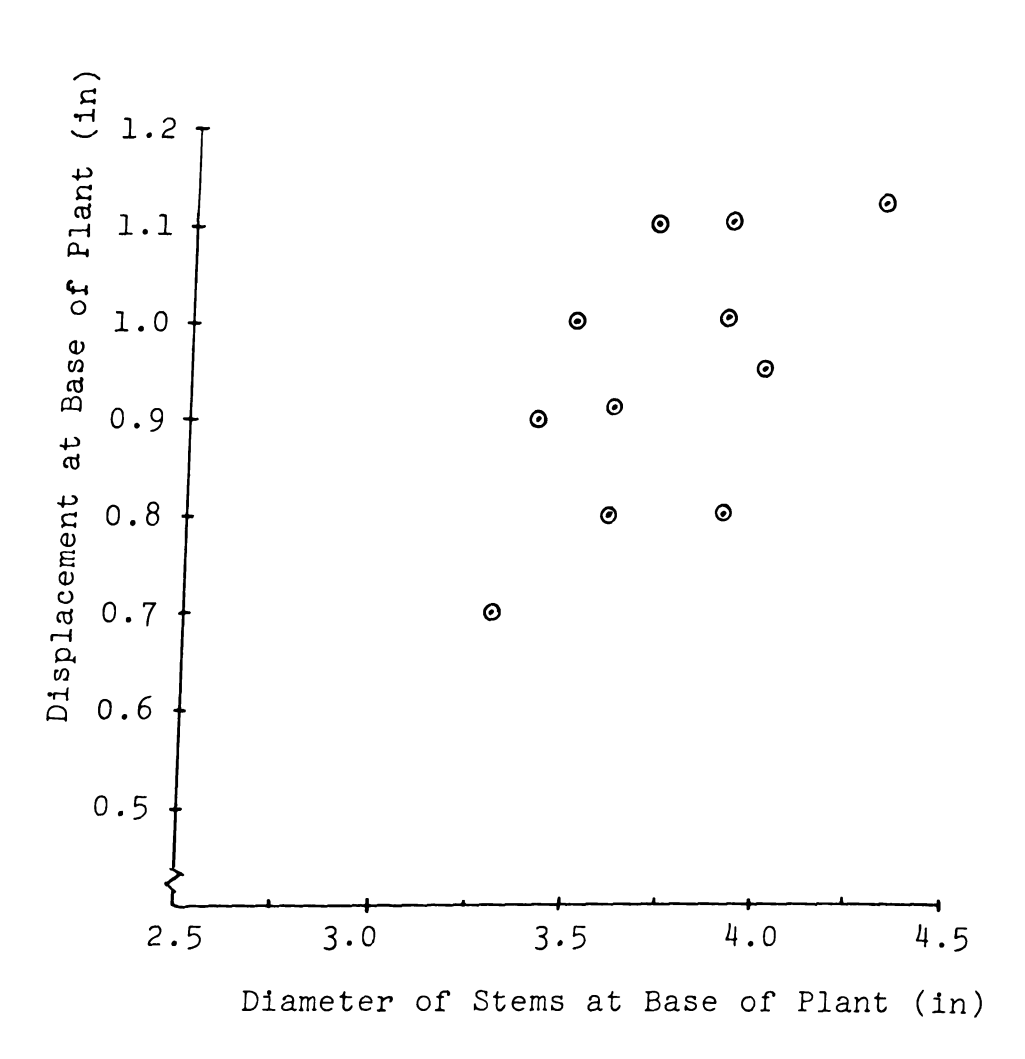


Figure 2.3.11--Displacement at base of plant versus average diameter of stem bundle at the base of the plant. pcc = .597.

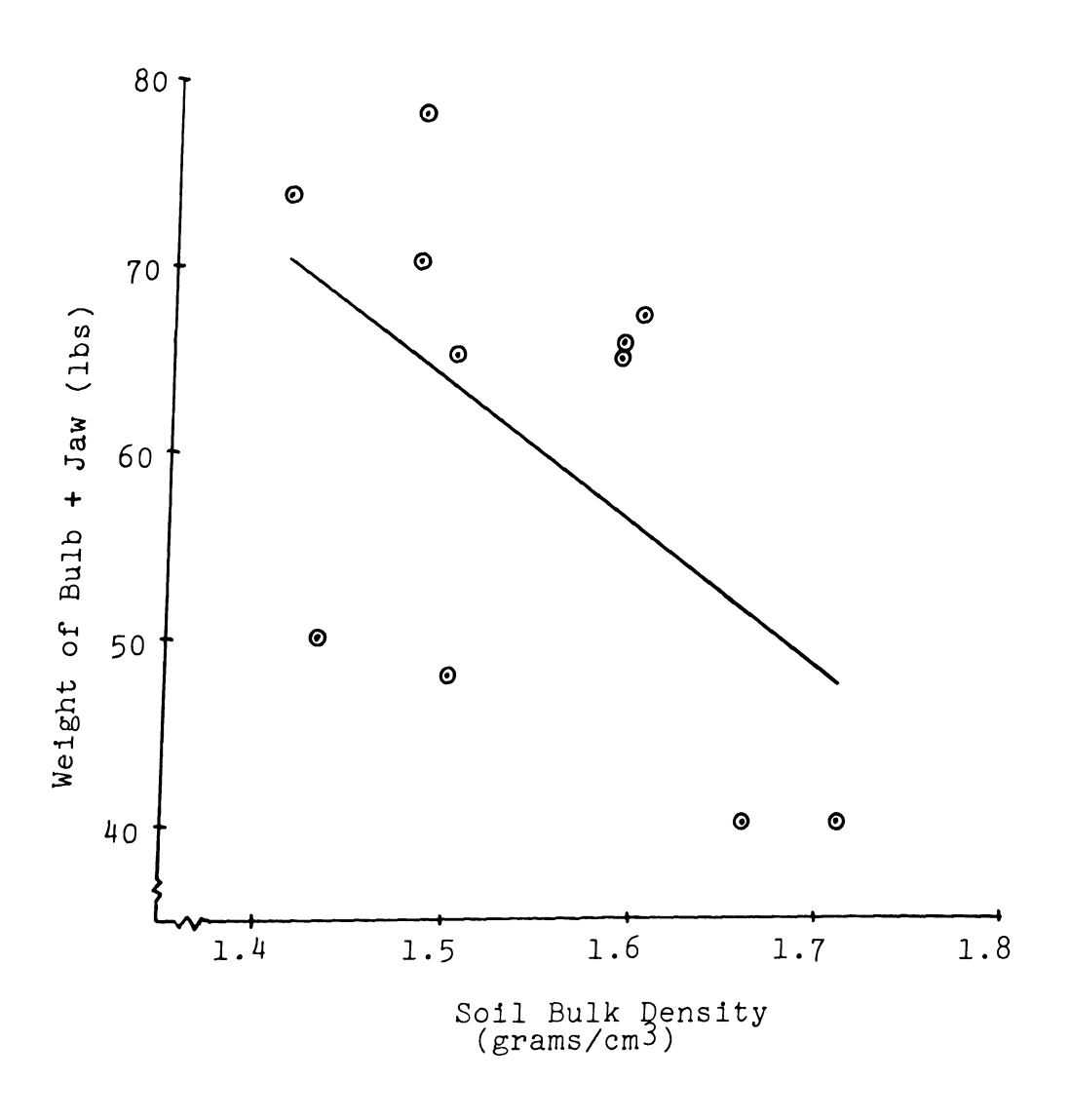


Figure 2.3.12--Weight of root-soil bulb plus weight of jaws versus soil bulk density. Regression equation: Y = 177 - 76 X; pcc =-.543.

A partial correlation coefficient of 0.735 was found for force versus crater volume. A plot and regression equation are given in Figure 2.3.13. From the regression equation it is seen that the tendency is to have an increase in maximum force as the volume of the crater increases. The increase is less than the increase in crater soil weight but there is a large constant term. The total soil weight in the crater is considerably less than the maximum pulling force. This indicates that soil weight is not a main part of the pulling force, and that root strength, tension and shear stress in the soil contribute to the anchoring of the plant. The reasons for the increase in the force may be due to an interaction with the soil moisture content, which is discussed later, or there may be a variation in the development of the root system of the plant.

It is reasonable to assume that a larger root system would require a higher force, if other variables remain constant. In Figure 2.3.8, which is a plot of force versus weight of bulb, it was seen that the force increased as the weight of bulb increased. If it is assumed that the weight of the bulb is an indicative parameter of the root system size, it seems reasonable to attribute the relationship between force and crater volume as found in Figure 2.3.13 to a larger root system of the plant. Bulb weight and crater volume were clearly correlated as shown later in Figure 2.3.15.

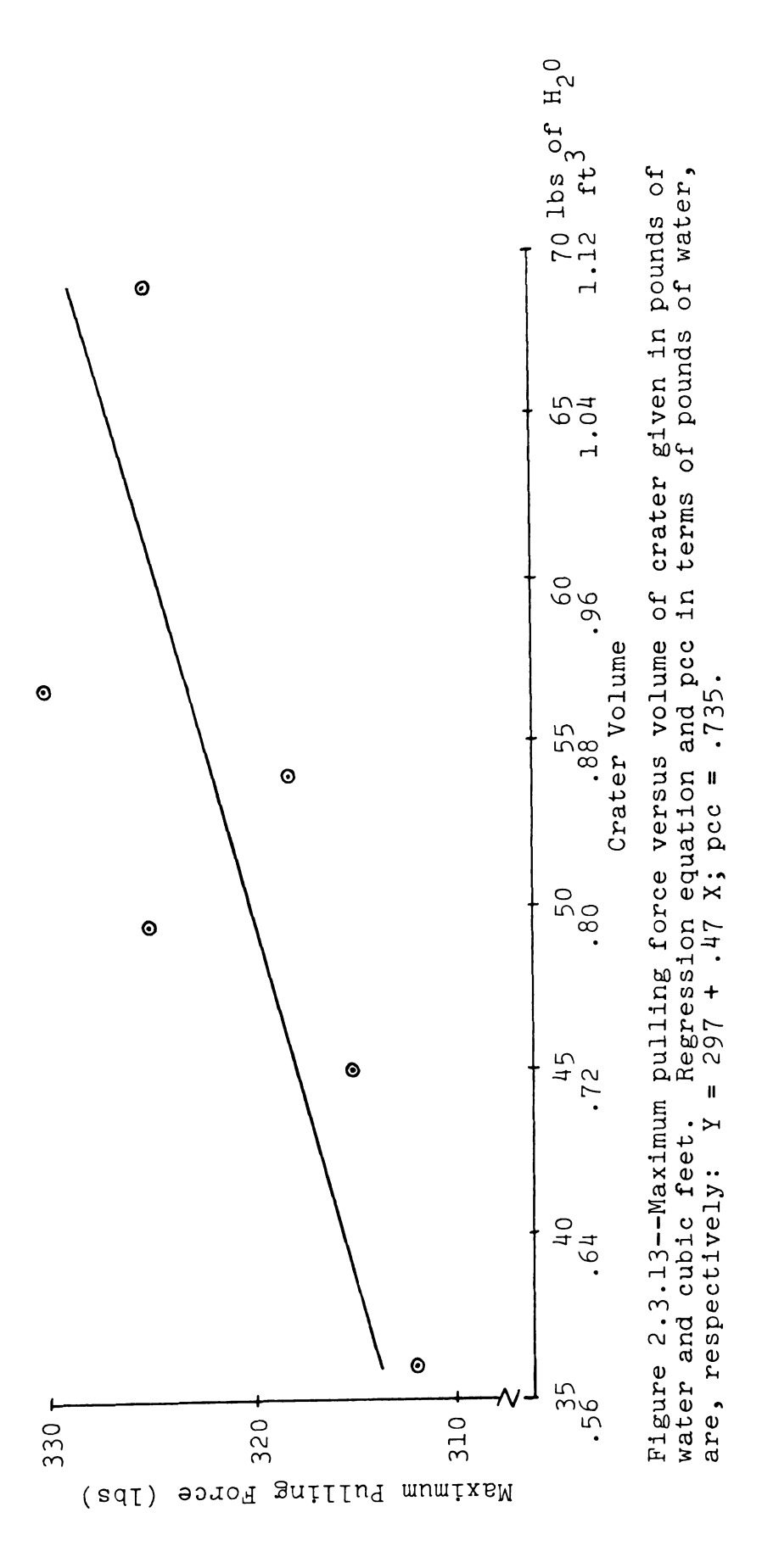


Figure 2.3.14 shows a plot of crater volume versus soil moisture content. The variations are of such magnitude that no conclusions can be drawn with regard to this relationship. It seems reasonable to visualize a tendency of decreasing crater volume with increasing soil moisture content.

A possible relationship which was not contradicted by the experiment might be found considering the tensile strength of the soil and its adherence to the roots. Considering the roots as a reinforcing medium adhered to the soil, the bonding force between them is likely to decrease with an increase in the soil water content. In a fully saturated soil mass, the pulling force would be limited to that of sliding the roots out of the medium. No root failure would be likely to occur if the tensile strength of the roots were greater than that imposed by the respective sliding force. Theoretically, a soil in such a state would leave a very small crater volume since it is reasonable to assume that when the adherence is zero the roots could be pulled out with a minimum disturbance of the soil. As the moisture content of the soil decreases, the root-soil adherence increases and so does the resisting sliding force between the root and soil. If the soil moisture is decreased beyond a certain value where the bonding force between all the roots and the soil is equal to or larger than the pulling force, the system is likely to fail at a

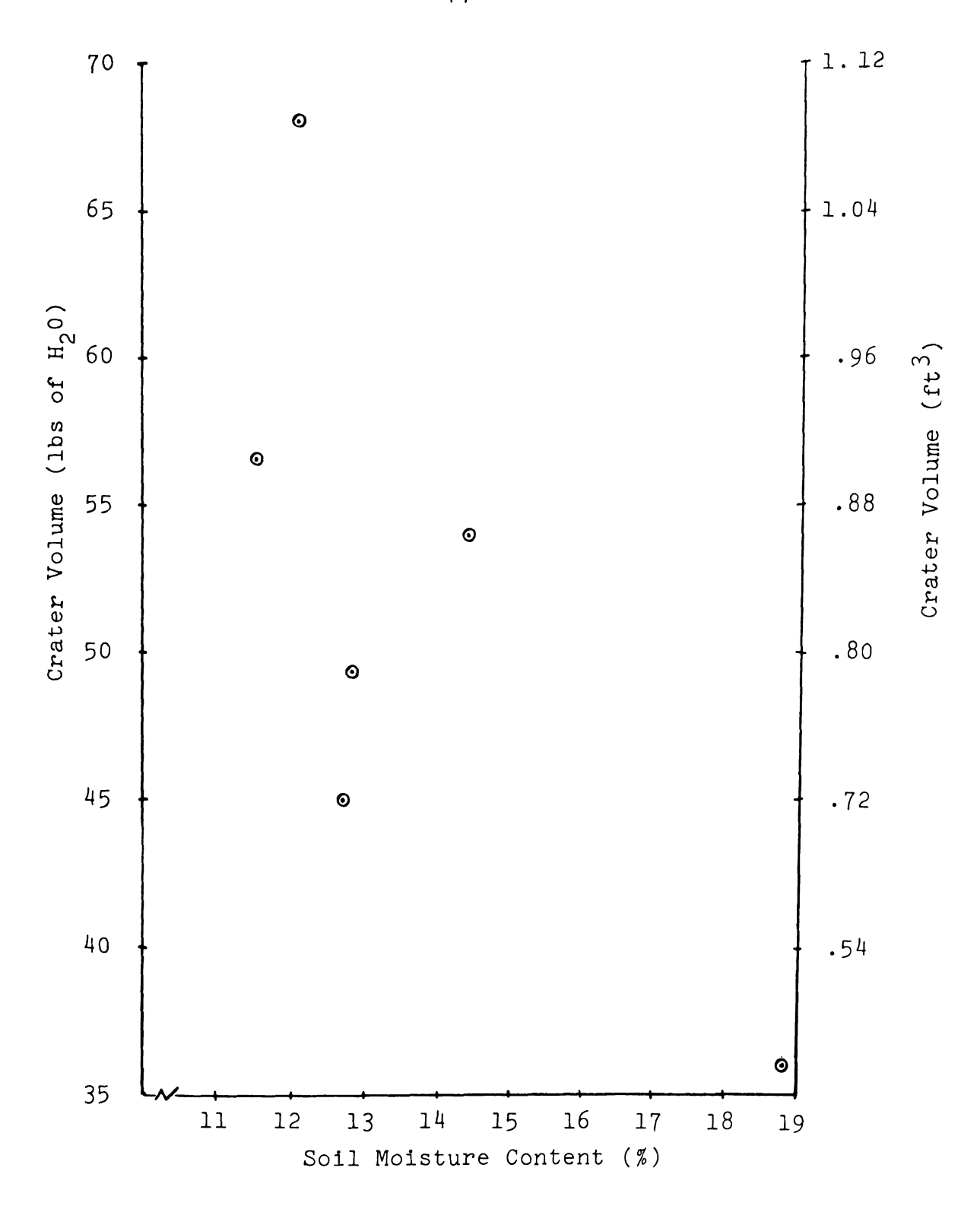


Figure 2.3.14--Volume of crater in pounds of water and cubic feet versus soil moisture content.

surface where its tensile strength equals that imposed by the pulling force as transmitted through the roots to the soil inside the failure surface. Thus, the volume of the crater will be dictated by this failure surface and, within limits, the greater the adherence between root and soil, the larger will be the crater volume expected to become, because:

- A. The better the bonding between root and soil, the more efficient the reinforcing effect;
- B. The better the reinforcing effect, the failure is likely to occur deeper because the
 reinforcement at the crown is quite substantial and tends to decrease with depth;
- C. The deeper the failure (the crater depth) the larger the volume of the crater, if the profile maintains a reasonably constant shape as was shown earlier in this section.

The weight of the bulb showed a positive correlation with the volume of the crater. Figure 2.3.15 shows a plot, regression equation and partial correlation coefficient. The low constant value and the high correlation coefficient suggest that the bulb weight may be considered a good indicator of crater volume.

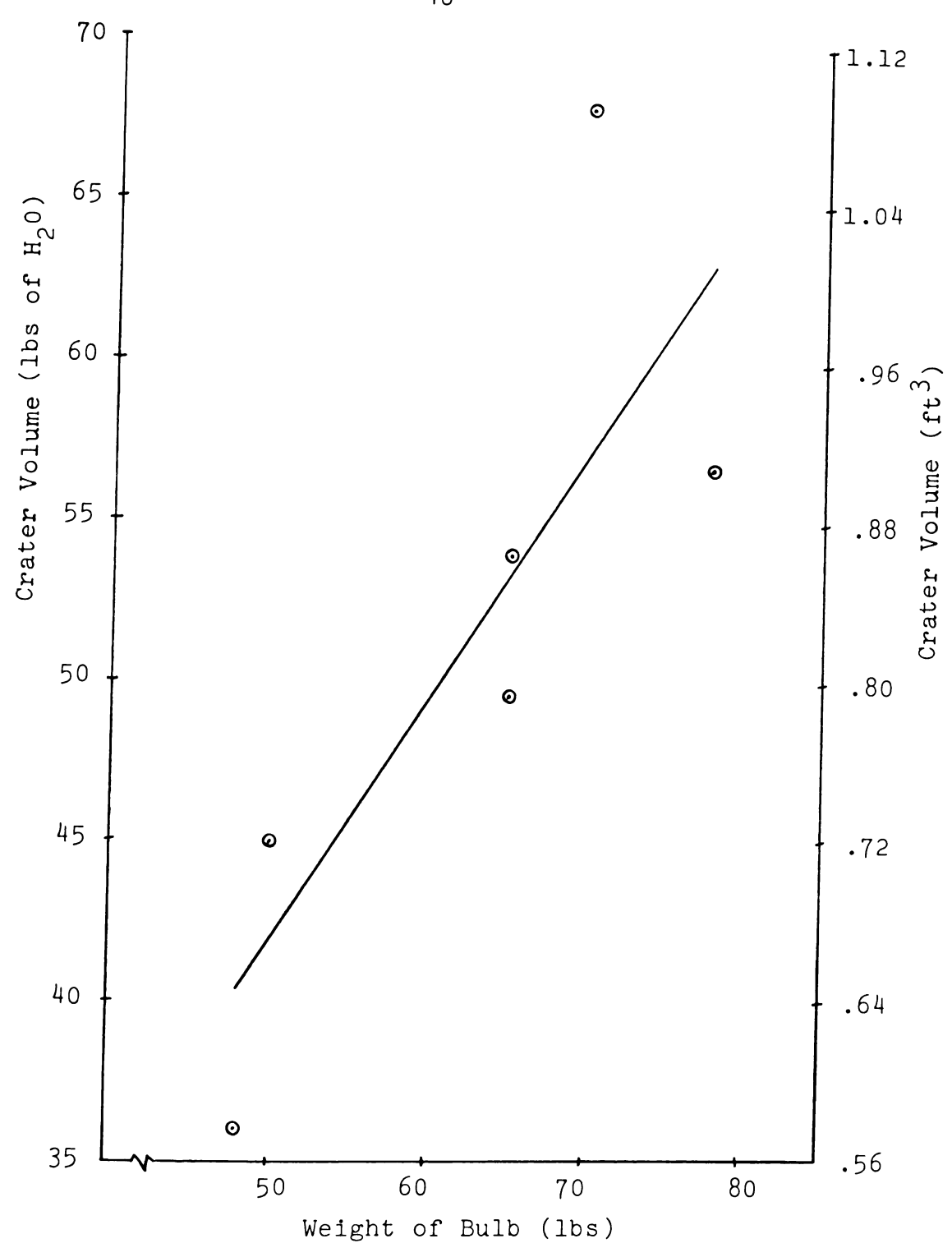


Figure 2.3.15--Volume of crater in pounds of water and cubic feet versus weight of root-soil bulb plus weight of jaws. Regression equation and pcc in terms of pounds of water are, respectively: Y = 4.0 + .76 X; pcc = .809.

3. THE ROOT SYSTEM, DESCRIPTION AND STRENGTH

3.1 Description of the Root System in the Literature

It is clear from the literature that the study of the root system has been neglected in favor of that of the aerial part. The reason is probably the difficulties encountered with this type of research. The root system is hidden in the soil mass which is characterized as a heterogeneous medium, represented by stones and hard pan, differences in soil moisture, in soil structure, and in chemical composition. Therefore, great variations in root development have to be expected since the roots are exposed to these heterogeneous and ever-changing conditions of growth. This fact also explains to a great extent the contradictory results found in experiments performed in this area of study.

Weaver (1926) states that "roots have a form and structure remarkedly well adapted to perform their function of anchorage; and of absorption, conduction and storage of water, nutrients, and elaborated foods." This was demonstrated by experiments with corn in soils of very similar physical and chemical composition. The crops were grown under different amounts of irrigation and root development

and distribution were markedly different. In the fully irrigated soil, where both water and nutrients were plentiful, the roots were almost all in the upper one foot and nearly parallel with the surface soil. In fact the bulk of them was in the surface 6 inches of soil. As to the root habits of sorghum, Weaver summarizes that

"though varying somewhat in the different varieties, is very similar to that of corn. The roots are finer and more fibrous, and often have twice as many branches as those of corn in a similar stage of development. The early superficial rooting habit is marked, plants only in the 6- to 8-leaf stage having a lateral spread of 3 feet, with a network of roots extending even to the soil surface, although the entire root system may be confined to the surface 1.6 feet of soil. Later in the development, the roots penetrate the deeper soils, working levels of 3 to 4 feet being common and maximum depths of 4.5 to 6 feet frequent."

References such as that of Miller (1916) still constitute a very good source of quantitative information for the study of the root system. Data are given as to the extent of the root system in four stages of growth, number of secondary roots per unit of length of primary roots, and soil moisture content and depth of root penetration. Photographs presented by Miller on his work with sorghum showed that a large portion of the roots were distributed in a conically shaped area, symmetrical about the plant vertical axis. This was observed when the plants were at the 13th week of growth, maturing seed, and at a height of about 5 feet. Under these conditions most roots reached 3 to 4 feet to the side and 5 to 6 feet below the plant center.

Dillewijn (1952) reports on investigations done in sugar cane. Lee et al. found that in irrigated cane, generally more than 50 per cent of the roots (by weight) occurred in the topmost 8 inches of soil, and this percentage decreased markedly in the deeper layers. The vertical distribution of roots changed with the age of the plants, and the percentage of roots at different levels attained a maximum at 4 months after planting. Kamerling worked with roots in soils with poor physical characteristics. In such soil, the root tip was often damaged resulting in the formation of lateral roots. When the tips of the latter also became damaged, they too started to Thus the roots in a compacted soil remained relabranch. tively short and much-branched as compared to longer and little-branched in a physically good soil.

The mechanical properties of the soil influence those of the root-soil composite in two ways: directly as an element of the composite, and indirectly by its influence on the root system development. It is clear from the review of literature related to physicochemical properties of soil affecting root growth that an interaction of soil density, particle shape and size distribution, aeration and moisture content are major factors influencing the mechanical impedance and growth characteristics of roots. This was particularly evident for seedling roots, in works of Gill and Miller (1956), Wiersum (1957) and Tackett and Pearson (1964), and for adult roots in works of Bertrand

and Kohnke (1957) and Scott and Erickson (1964). Wiersum states that,

"Attention is drawn to the fact that it is usually difficult to be certain of the importance of mechanical resistance in the field, in account of the close similarity of its effect with those of excess water and insufficient aeration."

Gill and Bolt (1955), reporting on Pfeffer's studies of the root growth pressures, state that due to the "plastic" properties of the root its path through the soil will generally be along the line of least resistance. Roo (1966) states that the absence of any significant root growth in and through the plow pan is caused not by insufficient aeration but by mechanical obstruction to the roots. Letey et al. (1961) working with snap dragons found support for the idea that the effect of aeration is dependent on the stage of plant growth. Stoltzy et al. (1961) established a range of oxygen diffusion rates at which root initiation was reduced or stopped. Williamson (1964) working with grain sorghum, soybeans, cabbage, sweet corn, and dwarf field corn, found that under extremely poor aeration the yields of those crops were reduced by 25, 35, 40, 65 and 75 per cent, respectively.

Spencer (1940) made a comparative study of the seasonal development of the corn root system of hybrids and inbred lines. He reports that marked differences were noted among the strains in regard to number, dry weight, and total length of main roots of the crown root

system. The single-cross hybrids exceeded the inbred lines in dry weight of roots, dry weight of tops, diameter of main roots, length of roots, resistance to vertical pull, diameter of culm and plant height. Within all strains the force required to pull a corn plant from the ground was most closely correlated with dry weight of the crown roots. However, it was not made clear whether this dry weight of crown roots was obtained from the pulled bulb or from the whole root system. It was also stated that no data were available to test the differences in seasonal root development as a criterion of the ability of a plant to resist lodging, but the problem was considered of sufficient importance to deserve further study.

Pavlychenko (1937) published a good review of literature of the methods used in the study of root systems. In addition to his own soil-block washing method, he described eleven different ways used by previous investigators. It seems, however, that the direct tracing of roots is the method which yields the most consistent results.

3.2 Procedure for Determining Tensile Strength of Roots

On June 22, 1967, sorghum seeds were planted in three wooden boxes with dimensions 48 inches long, 24 inches wide, and 18 inches deep, filled with soil from the experimental plot. Two hills with 3 to 5 seeds per

hill were planted on the center line of each box, and were located about 15 inches from the ends.

These boxes were left outdoors and the plants received the same fertilization schedule used for field plants, plus additional nitrogen equivalent to the starting dosage, since they presented symptoms of nitrogen deficiency. Nevertheless their development was subnormal, and of the original six plants only three survived. On October 20 the boxes were transferred to the greenhouse and at the time tests were made only one plant had recovered, but it still did not present an aerial development similar to that of the majority of the field plants.

On December 22 root samples were collected according to the following procedure. Two sectors A and B of 30° angle each were marked on the soil surface. The sides of sector A were cut with a trowel, and two thin sheets of metal were placed in the cuts. The roots in this sector were directly traced by use of brushes and small hooks, and values such as angle formed with the surface line, original length and the quarter of the sector angle in which the roots were positioned were

determined for each root. The roots were not classified as main or secondary roots for this tracing. They were viewed as elements of a given root system which had a reinforcing action upon the soil. The root angle was calculated from measurements obtained according to Figure 3.2.1.

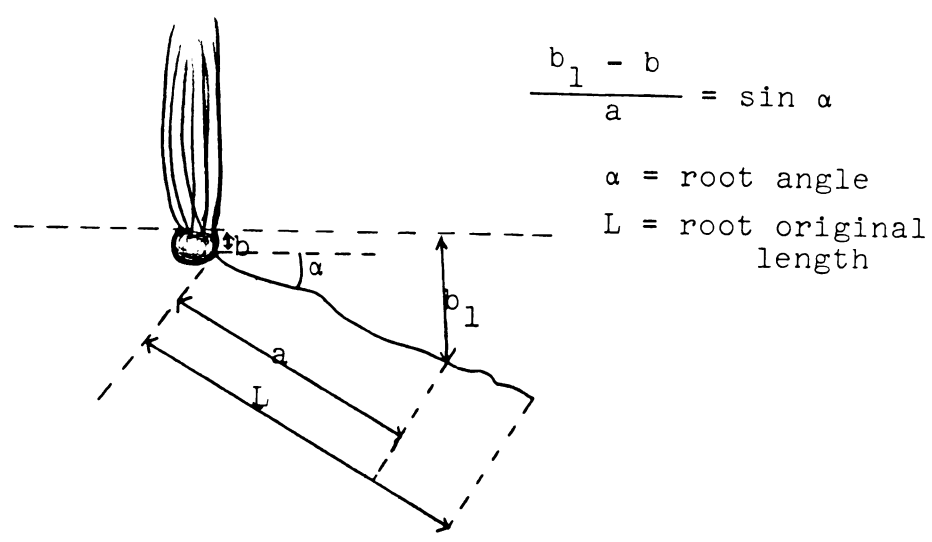


Figure 3.2.1—Diagram showing how the dimensions and root angle were obtained by direct tracing the roots.

It was later realized that little meaning could be attributed to the quarter-location in the sector, since many roots were developed so tortuously that they entered all four quarters of the sector. The roots were then cut loose at the point where they were attached to the crown ("the attaching point"), and numbered in the order they were found. This same procedure was used in collecting root samples for sector B. Roots numbered from 1 to 9 were sampled in sector A and 10 to 26 in sector B. Some

support roots of very short length were considered vertical (90° angle), despite a slight inclination of some of them.

The roots thus numbered and positioned were taken to the laboratory in boxes covered with soil to avoid drying. Within 6 to 7 hours they were tested for tensile strength in an Instron testing machine, model TM, using a tension-compression load cell model DR.

Trial tests using other roots were previously made to determine the pressure of the traction jaws which would cause a minimum of stress concentration. Tests were made both with and without cushioning material. These tests, however, did not furnish consistent results, but they indicated that the pressure should have a value of 10 to 15 psi as a minimum value to avoid slipping with a bare jaw.

The sample roots were consistently positioned in the center of the traction jaws and in such a way that the end toward the plant center was always held by the top jaw. The velocity of the cross head of the Instron testing machine was 2 inches per minute, which was about the same as that given by the pulling device in the field. The gage length was one inch for most of the tests, being changed to 0.7 inch for roots of original length smaller than 2 inches. More than one specimen was tested for the same root whenever the original length permitted such a procedure. Based on this characteristic the roots were called "long roots" or "short roots."

A force versus deformation graph was recorded up to the rupture point. The velocity of the recording paper was also 2.0 inches per minute in order to record actual deformation of the specimen (Figure 3.3.1).

The diameter of the fractured roots were measured at the section of rupture using a Bausch and Lomb stereomicroscope and a scale graduated in hundredths of an inch. Measurements were also made of the distance from the attaching point (see above) to the section of rupture. This distance was called "dipoint."

Record was kept of the point where the fracture occurred as related to the traction jaws. A rupture at the bottom jaw was coded "B" and one at the top jaw "T". Similarly if the position of the fracture occurred at the midpoint from the jaws, it was coded "C"; and if at a certain distance from the jaws, e.g., .l inch "B" or "T". The number of roots breaking at the bottom jaw was very large. This fact was expected since the root tissue is made of younger cells at the greater distances from the attaching point.

For long roots the first specimen closest to the attaching point was coded, e.g., as 20-1, the second as 20-2 and so forth as presented in Table 3.2. The dipoint was also measured at the end of the test for each root, by assembling all the specimens tested into the whole root, and taking measurements from the attaching

point to the respective sections of rupture. The third specimen of root 19 was discarded because of bruises.

obtained for the study of the root system, for the short and the long roots respectively. The data in Table 3.2 are more useful for studying the variations within one root, as indicated by the changes of characteristics as functions of the dipoint. The values in Table 3.1 plus the values of the first specimens in Table 3.2 are most useful for comparisons between roots.

3.3 Results and Discussion

The data were analyzed to obtain a partial correlation coefficient for the variables of interest and a regression equation. This was respectively done by a BASTAT and a LEAST SQUARES routine programmed for the computer of Michigan State University by Michigan Agricultural Experiment Station (1967). Roots number 6, 10 and 14 in Table 3.1 were not tested since they were too short to be clamped by the traction jaws.

A typical force and deformation curve as obtained from the Instron recorder is given in Figure 3.3.1. For this root and most of the others, it was evident in the force versus deformation curve that a straight line portion

13.8

11.4

38.3

28.7

14.0 8.0 14.5 23.8 10.2

14.2 16.3 9.0 31.1

F/#d (1b/1n) Modulus (F/Ae) (ps1) 11300 3100 12500 16500 14000 20800 15800 19000 3000 2500 8800 24000 8000 13200 Stress (F/A) (ps1) 1140 1120 2970 810 2090 3330 5070 3800 1120 430 1670 2400 1600 (1n²). 96100 000080 00138 .00015 .00196 .00503 .00031 .00442 96000 .00050 00018 .00071 .00071 00125 Area (A) Diameter of
Fracture
(d)
(in) .030 .050 .080 .030 040. .020 .015 .030 .050 .075 .035 040 .025 .015 Dipoint (in) 1.0 1.5 1.4 2.3 2.3 2.1 2.3 7.0 1.3 1.7 1.2 , ı ı Rest Original Length (1) 1.0 2.0 1.9 5.0 1.0 3.0 0.4 2.5 7.5 3.5 5., Acot Angle (a) (degrees) 36 90 90 90 66 90 67 72 90 06 05 Strain (c) .20 60. .18 .20 .16 .32 .14 Position of Fracture Plane in. B 20 20 20 20 æ B E ۲. Rupture Force (F) 4.10 06.0 4.10 0.87 0.50 3.60 2.70 2.20 1.90 1.60 3.00 . ı Root Number 9 3 3 5 10 œ 13 18

TABLE 3.1--Results of tensile tests and direct tracing of short roots.

F/md (lb/in) Modulus (F/A_E) (ps1) 22800 30900 30900 112200 12800 22800 22800 11600 22800 22800 22800 22800 15900 15900 15900 15000 15000 15000 Stress (F/A) (ps1) (1n²) 00071 00542 00542 00071 00071 00071 00071 00071 00071 00071 00071 00071 00071 00071 00031 Area (A) Llameter of Fracture (d) Lipoint (in) CAON COORTECTION CONTRACTOR Uritinal Length of Foot (I) (In) hoot Angle (a) (degrees) Strain (E) Position of Fracture Flane 1 B B Rupture Force (F) Root Number

IABLE 3.2--Results of tensile tests and direct tracing of long roots.

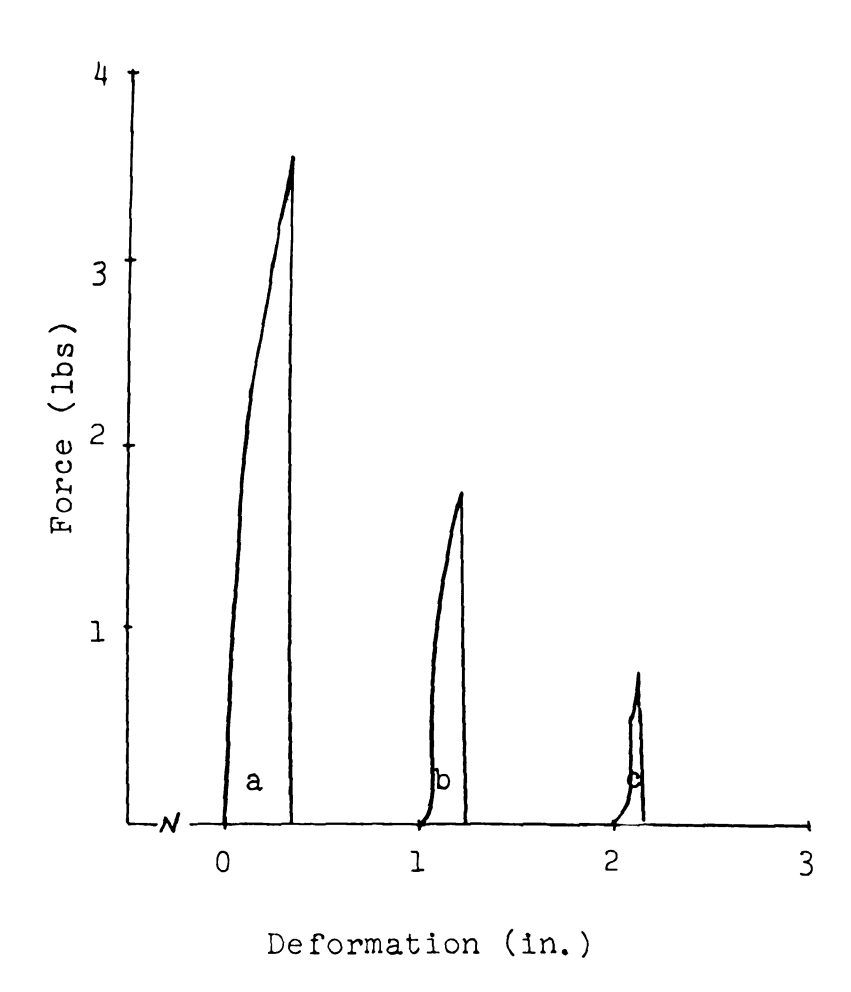


Figure 3.3.1—Typical force vs deformation curves from root tensile tests: a) root number 15; b) root number 7.2, and c) root number 25.

consistently appeared up to a value of .4 to .6 of the force of rupture, indicating a Hookean behavior. Once past the linear limit the rate of increase in deformation is larger until the point of failure is reached, without an evident bio-yielding point. A rather brittle failure took place which indicates a possible behavior of the material, or suggests the occurrence of stress concentrations at the jaws.

The values for strain were obtained from the force versus deformation curves by measuring the deformation at the point of rupture and dividing this value by the gage length. Since the root presents a natural tortuosity, its real initial length was greater than the gage length established by the jaws. This introduced an inaccuracy in the measurement of strain since it is calculated from the gage length established by the testing machine. Therefore, the values calculated for strain are likely to be higher than the real values if the root had been naturally straight at the beginning of the testing. This effect is more evident for roots of larger diameter in which the force required for this straightening up of the root affects the initial shape of the force-deformation curve. The ratio between this idle displacement due to root tortuosity and the displacement at rupture, varied from .1 to .5, respectively for roots of smaller and larger diameter.

The region of the root attachment to the plant was a transition zone of stems and roots. This zone was estimated

to be a semi-sphere with a radius of 1.5 to 2.5 inches and centered at the intersection between plant centerline and soil surface. A plot of root angle vs. length is given in Figure 3.3.2. If the two sectors A and B are added it can be seen that most of the roots were found at an angle ranging from 30 to 80 degrees from the surface line. The greatest number of roots were located at an angle from 60 to 80 degrees. This indicates a reasonable qualitative agreement with the photographic evidence given by Miller from his study of other varieties of sorghum.

The area of rupture was calculated from the diameter measured at the section of rupture, assuming a circular cross section. The stress was calculated as the ratio of the force of rupture to this area. The strength of the root at the point of rupture, which was called "modulus," was calculated as the ratio of the stress to the strain at rupture point.

Average diameter and standard deviation were calculated for short and long roots and the values are, respectively:

5	Short Root (in)	Long Root (in)
Diameter	0.038	0.0239
Standard Deviation	0.020	0.0073

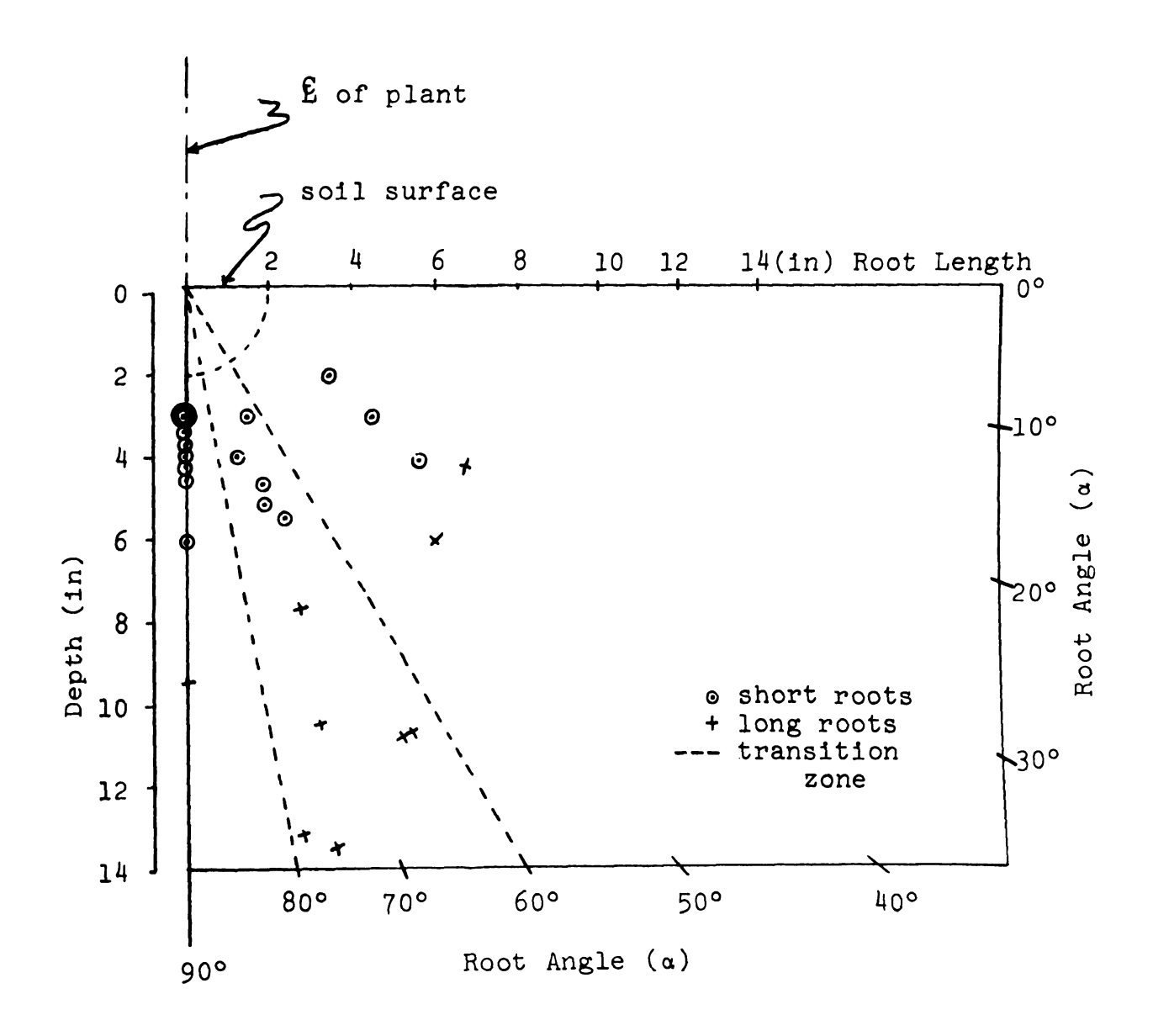


Figure 3.3.2--Root angle vs root original length, with transition zone included.

The rather high value for the standard deviation of short roots may be attributed to the comparatively small number of observations and to the fact that among these short roots there were in reality two different types of roots, one of them being similar to the long roots. The other was the bracing roots, which have a larger diameter, are more aqueous and less fibrous, as was noticed during the experiments. This was confirmed by further studies of the types of roots and by literature. Weaver (1926) reports work done by Eyick, with a Folger variety of sorghum, in which it was found to have a great resemblance of the root system with that of corn, "although the fibrous growth of roots near the surface was much less prominent." From Figure 3.3.2 it is seen that the less fibrous roots are located in the topmost 4 inches of soil.

Figure 3.3.3 shows a plot of the diameter of fracture for the first specimen (the base diameter) vs. root original length. This plot, and all the others involving root original length were made with the respective values found in Table 3.1 and those of the first specimens of long roots from Table 3.2. It is seen that the spread of values in base diameter for short roots was much larger than that of long roots. This explains the

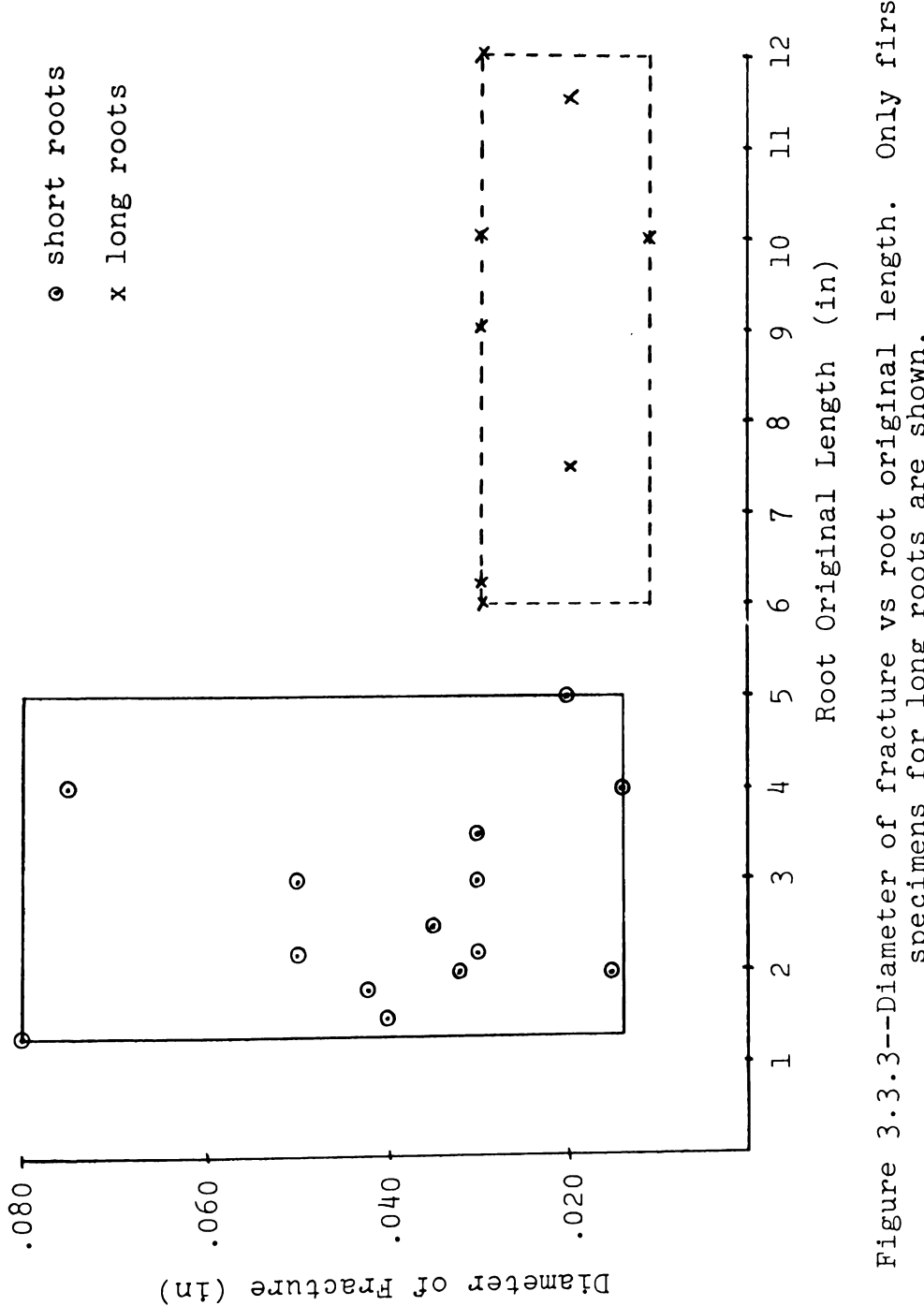


Figure 3.3.3--Diameter of fracture vs root original length. Only first specimens for long roots are shown.

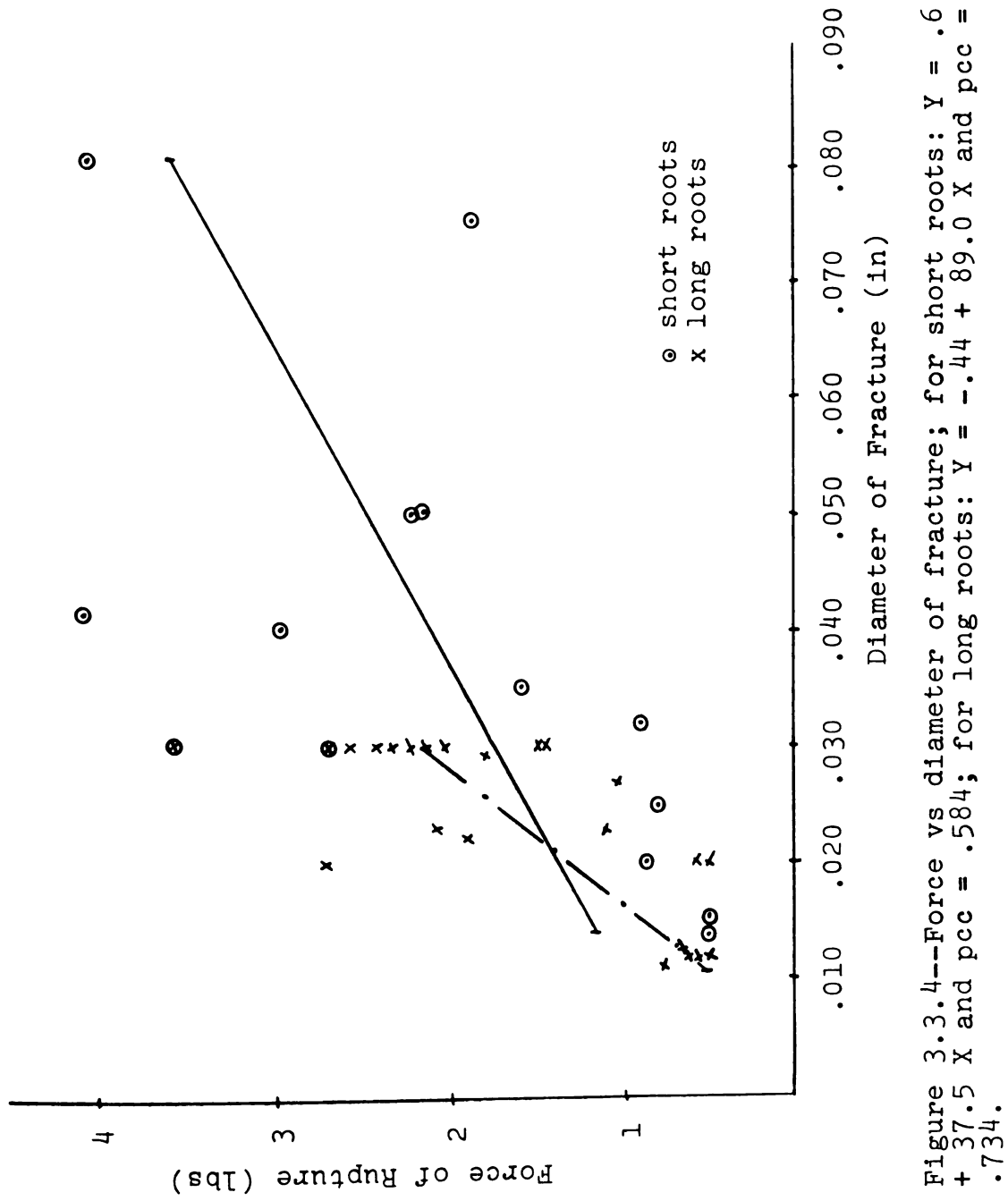
rather high standard deviation found for short roots. It suggests also that in the study of root strength at least two types of roots have to be considered.

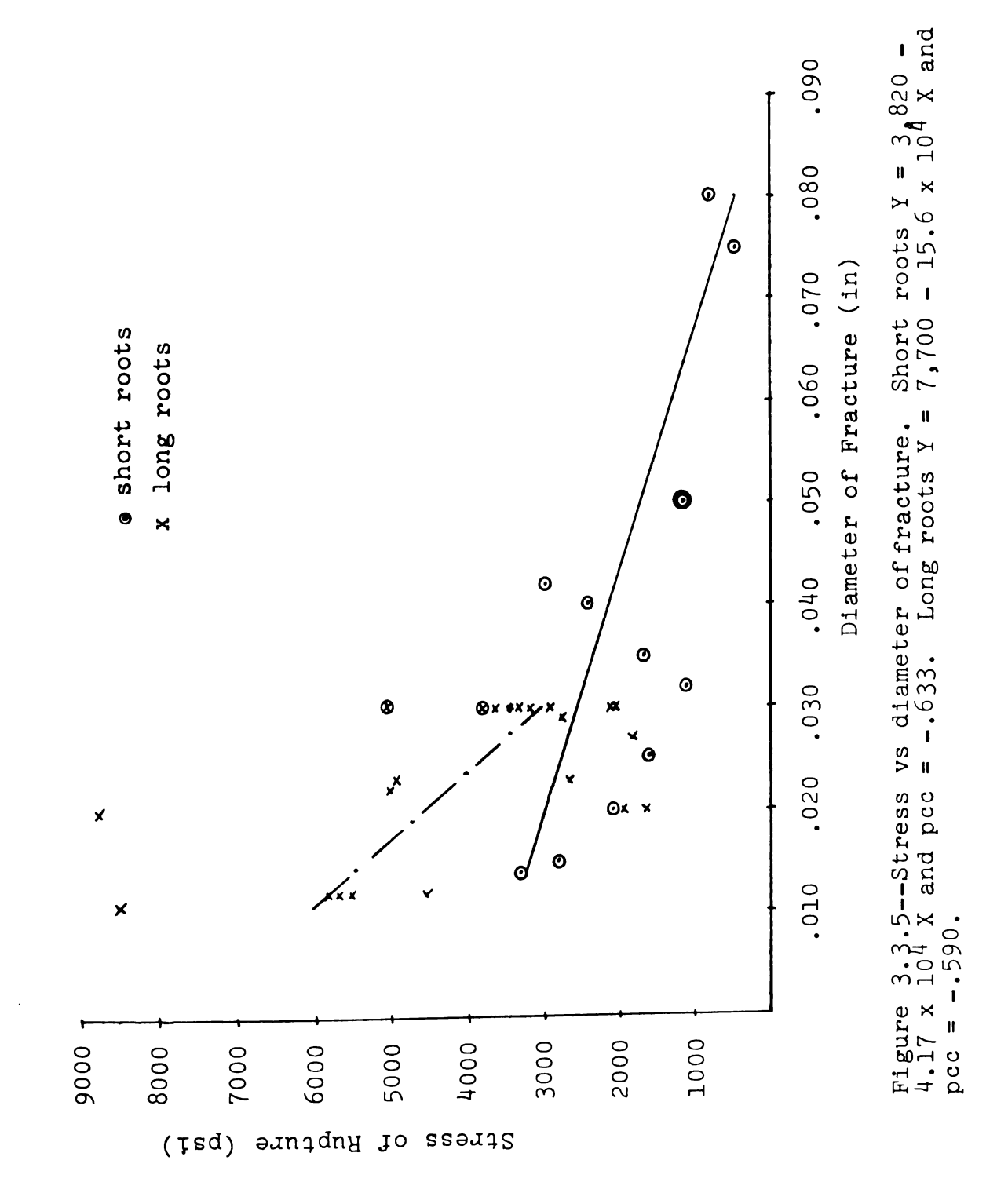
A plot of force vs. diameter of short and long roots, seen in Figure 3.3.4 shows that for both cases the trend was for an increase in force as the diameter of rupture increases. The regression equations and partial correlation coefficients (pcc) were: $Y = .63 + 37.5 \times 10^{-5} \times 10^{-$

Figure 3.3.5 shows a plot of failure stress vs. diameter. As might be expected, the stress decreased with an increase in diameter. It decreased at a greater rate for long roots. The respective regression equations and partial correlation coefficients for short and long roots were: $Y = 3,820 - 4.17 \times 10^4 \times$

The circumference was chosen as a linear dimension of the cross section due to consideration of the

From now on, in this chapter, whenever it is referred to, force, diameter, stress, strain, modulus and strength, correspond to parameters taken at the rupture point, unless otherwise stated.





biological nature of the root (Esau, 1966). Figures 3.3.6 and 3.3.7 show plots of "surface strength" $F/\pi d$ vs. diameter for short and long roots. The regression equation and partial correlation coefficients for short and long roots were, respectively:

$$Y = 18.5 - 28 X$$
; pcc = -.060 and

$$Y = 13.1 + 360 X$$
; pcc = .309.

The low value of pcc = - .060 for short roots indicated that there was a negligible correlation between $F/\pi d$ and diameter. Therefore, it might be assumed that the slope of the regression line was zero for short roots. Thus,

$$F_s = C_1 \pi d$$

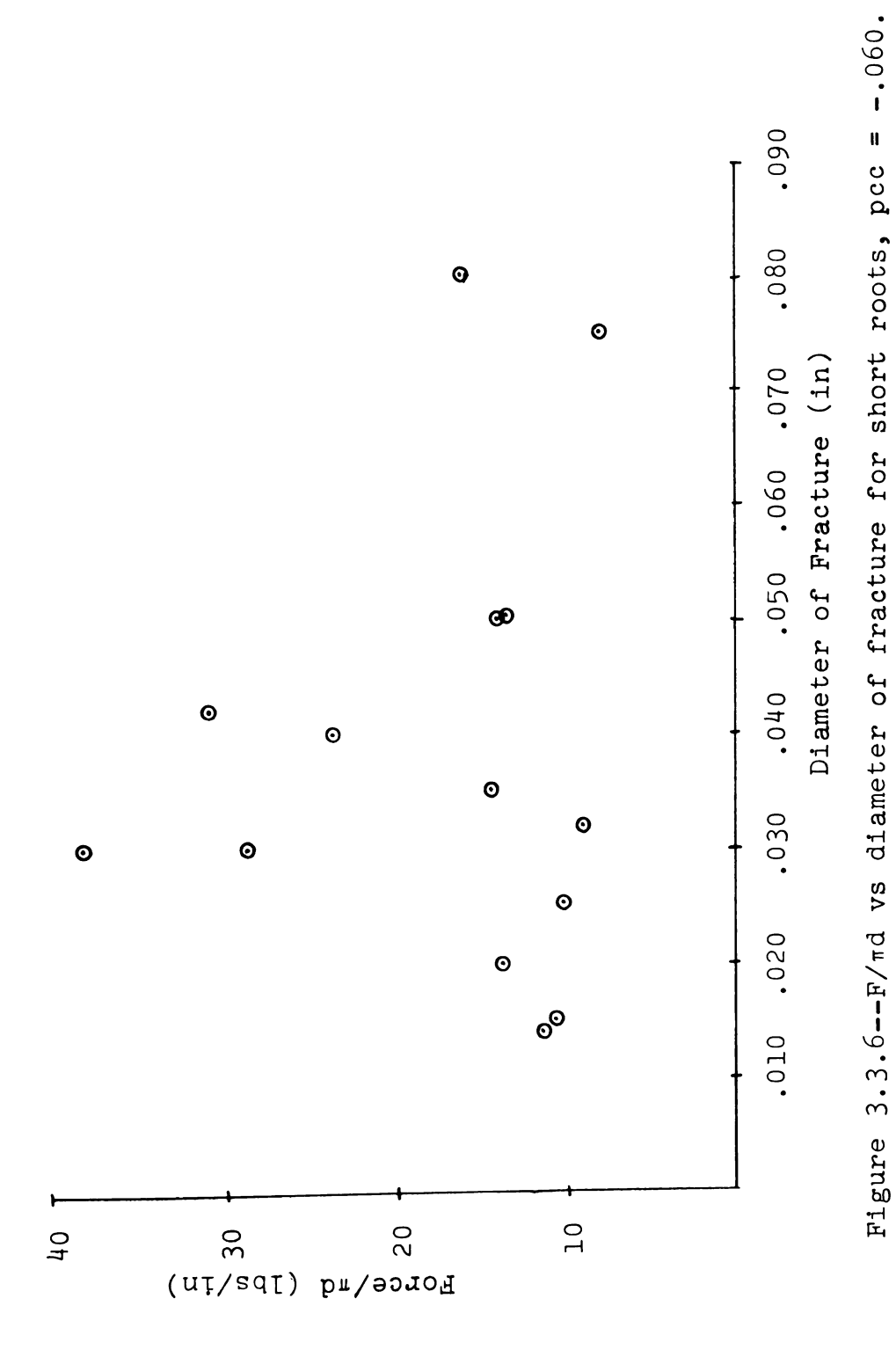
where

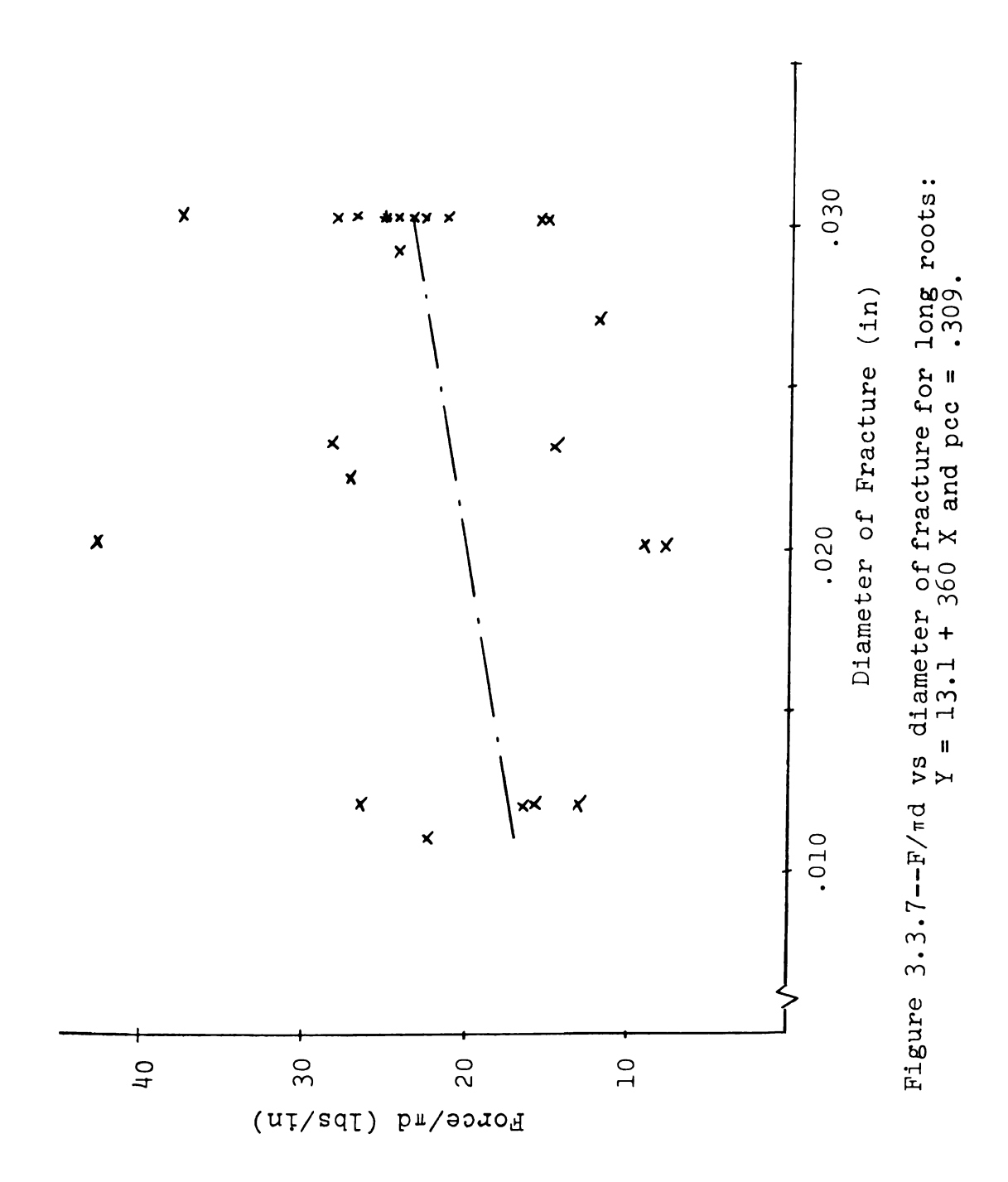
 F_s = rupture force for short roots, lbs;

 $C_1 = 17.4 \text{ lbs};$

d = rupture diameter, inch.

In the case of long roots, a t-test was used to verify whether the slope equals zero. The hypotheses were: H_0 : slope = 0 and H_a : slope \neq 0. The values obtained for t calculated and critical were: |t| = 4.82 and t (.05, 22) = 2.074, respectively, which indicates that there is evidence to reject the null hypothesis. Therefore, in





the case of long roots the effect of the area can not be neglected, and the relationship between force and diameter can be written as:

$$F_{L} = C_{3}\pi d + C_{4}\pi d^{2}/4$$

where

 F_L = rupture force for long roots, lbs.

 $C_3 = 13.1 lbs/in$

 $C_{\mu} = 1440 \text{ lbs/in}^2$

d = diameter of fractured section of the root, inch.

So far it has been seen that from a strength standpoint there were at least two types of roots, short and
long, and their average diameter and standard deviation
were calculated and given above. The tests indicated
that the force of rupture for short roots was mainly
related to the perimeter rather than the area which
might be due to their biological constitution. This
was not the case for long roots, for which it was seen
that the force of rupture was also related to a square
dimension of the cross section.

It was earlier shown that diameter and root length were used to identify two groups of roots and that there were different relationships between rupture force and diameter for these two groups. These observations

ثن

should be reflected in a comparison of force and root length. A plot of surface strength $F/\pi d$ versus root original length is shown in Figure 3.3.8. For this plot the corresponding values were taken from Table 3.1 and from the first specimen of Table 3.2. The values were arranged in Table 3.3 for easier comparison. The average values of $F/\pi d$ and of standard deviations for short and long roots were, respectively:

	Short Roots (lb/in)	Long Roots (lb/in)
Surface Strength	17.4	30.1
Standard Deviation	9.3	9.8

From the plot it could be seen that all long roots had an $F/\pi d$ value higher than the majority of the short roots. Despite the large values of the standard deviations, this confirmed that different rupture strength values should be considered for short and long roots.

Figure 3.3.9 shows a plot of modulus versus root original length. Average values of modulus and standard deviations for short and long roots were, respectively:

	Short Roots (psi)	Long Roots (psi)
Modulus	13,000	24,000
Standard Deviation	5 , 800	12,800

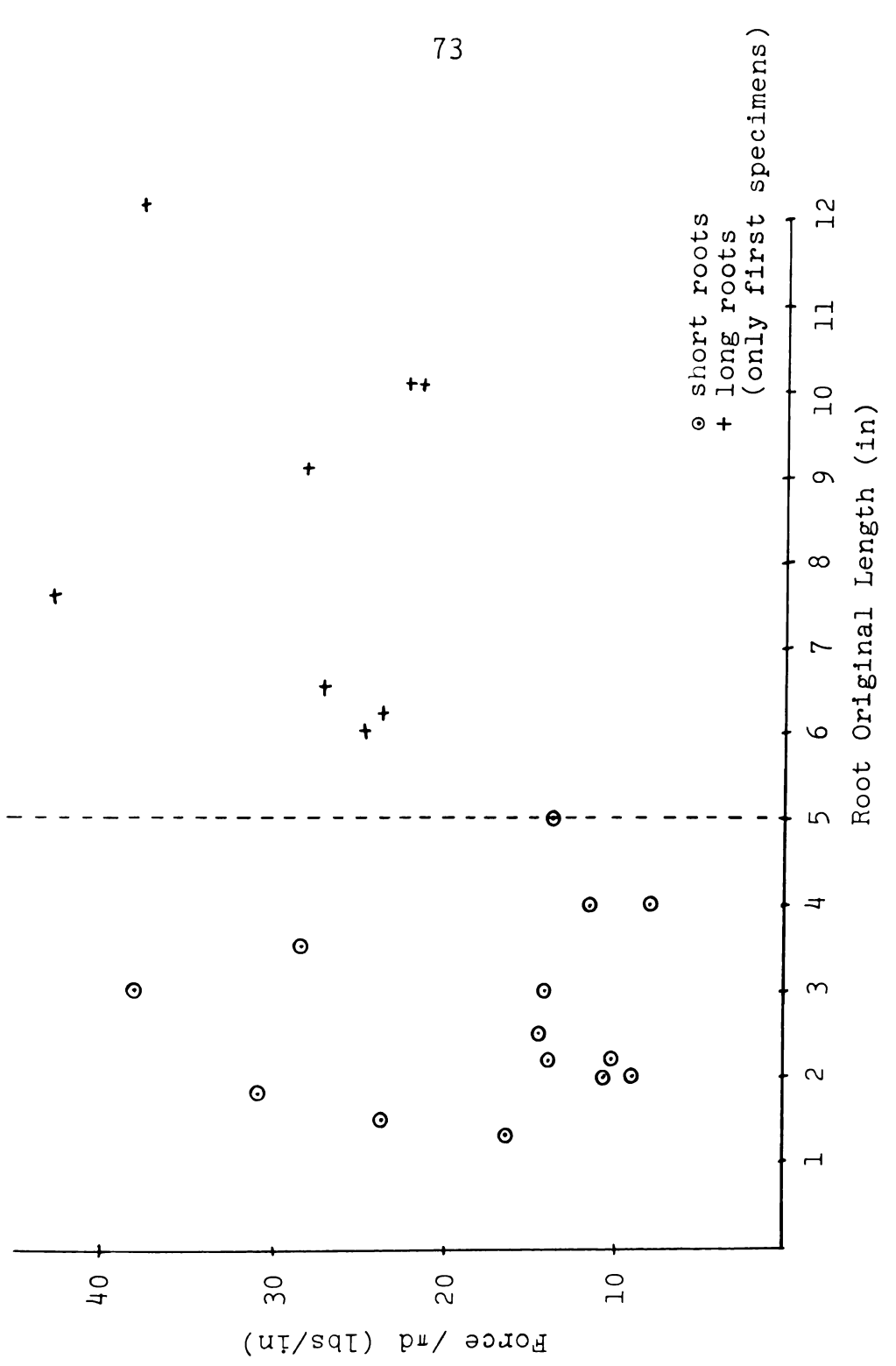


Figure 3.3.8--F/md vs root original length.

TABLE 3.3--Rupture strength parameter $F/\pi d$ in pounds per inch.

Short		Long roots (F/Nd)				
roots (F/Nd)	lst specimen	2nd specimen	3rd specimen	4th specimen		
14.2	27.5	28.9	12.2	15.5		
16.3	25.0	19.8	13.1	7.9		
9.0	43.2	27.7	25.6	_		
31.1	21.9	15.8	16.6	_		
13.8	22.6	16.8	_	_		
11.4	24.0	15.0	-	_		
38.3	28.7	22.4	_	_		
28.7	38.3	25.8	-	_		
14.0	9.2*	16.0	-	_		
8.0	-	_	-	_		
14.5	-	-	-	_		
23.8	-	_	-	_		
10.2	_	_	-	_		
10.6	-	-	-	-		
₹(averag	ge)					
17.4	28.9	21.0	16.9	11.7		
S(standa deviati	ard on)					
9.3	7.8	5.5	6.1	-		

^{*}This value was not considered in the analysis.

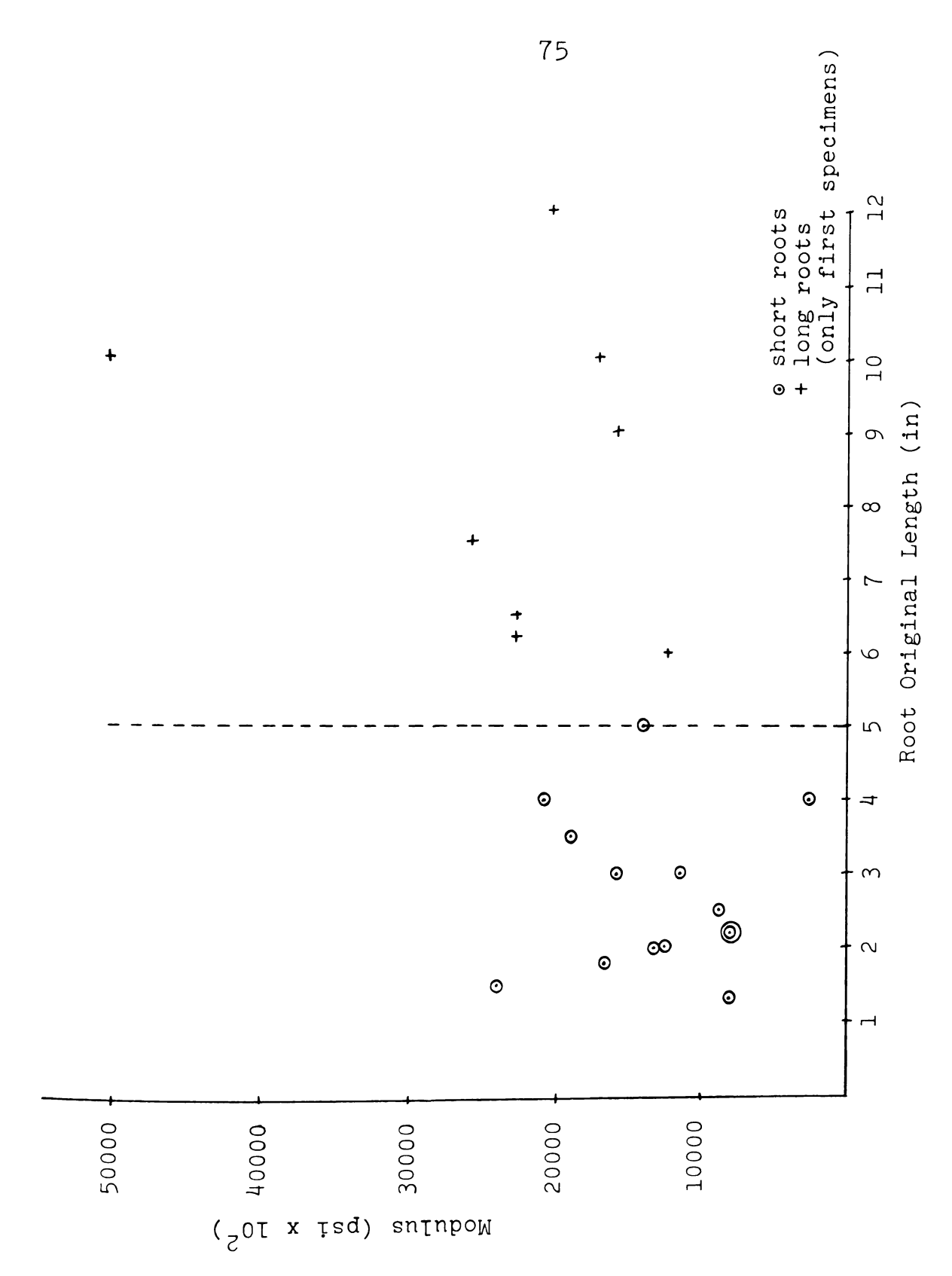


Figure 3.3.9 -- Modulus vs root original length.

Here, again, high values of the standard deviations were found, but there does appear to be differences between short and long roots, the longer roots being less elastic. A modulus based on the perimeter of the root might have been more representative of its elasticity than a modulus based on the area as it was defined.

Referring to the geometrical variations occurring along a root, it is seen from a plot of diameter vs. dipoint, Figure 3.3.10, that there may have been a slight decrease in diameter as the dipoint increased. However, the regression analysis showed that this influence was not significant.

A plot of force vs. dipoint (Figure 3.3.11) showed that the force decreased as the dipoint increased. The regression equation and partial correlation coefficient obtained were Y = 2.49 - .18 X and pcc = -.488. The t test showed that the correlation was significantly different from zero for all tests of long roots where the absolute value of the partial correlation coefficient was equal or greater than 0.440. For this case there was a significant change in force with dipoint which could be caused either by the conical shape or by a change in strength of the root with dipoint, or both.

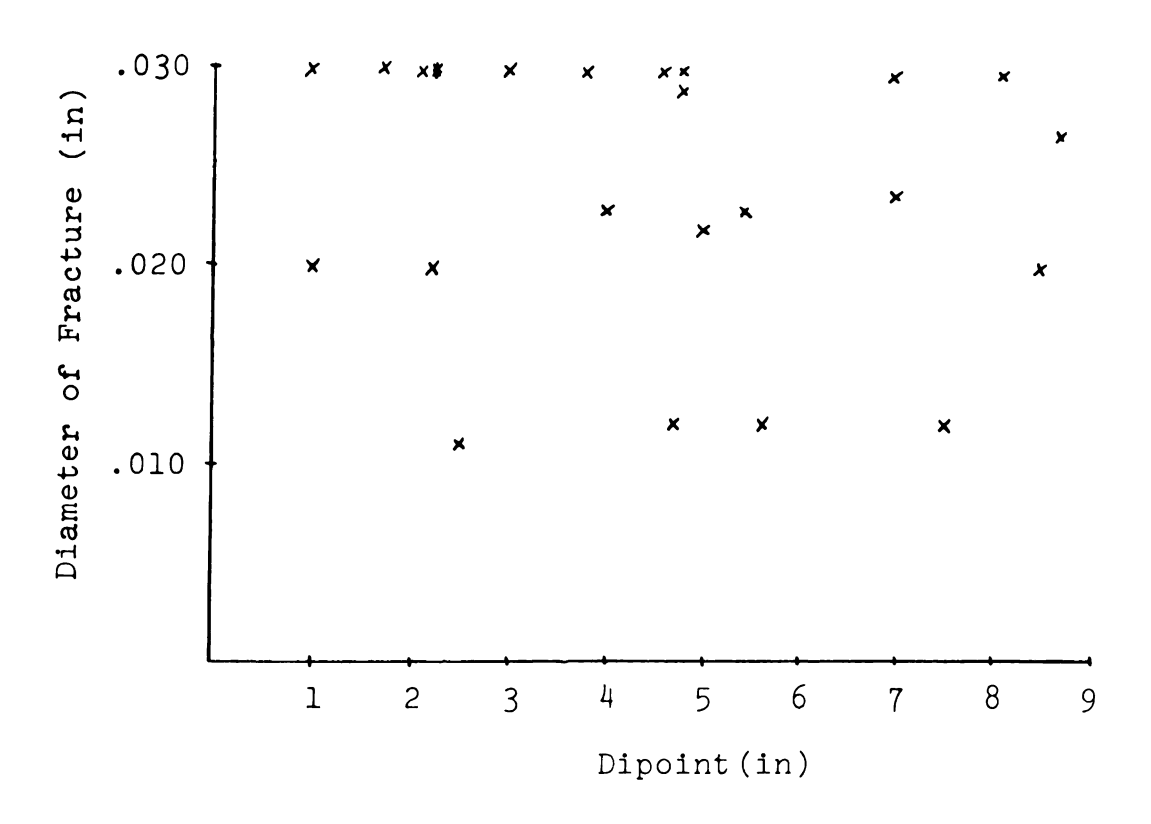
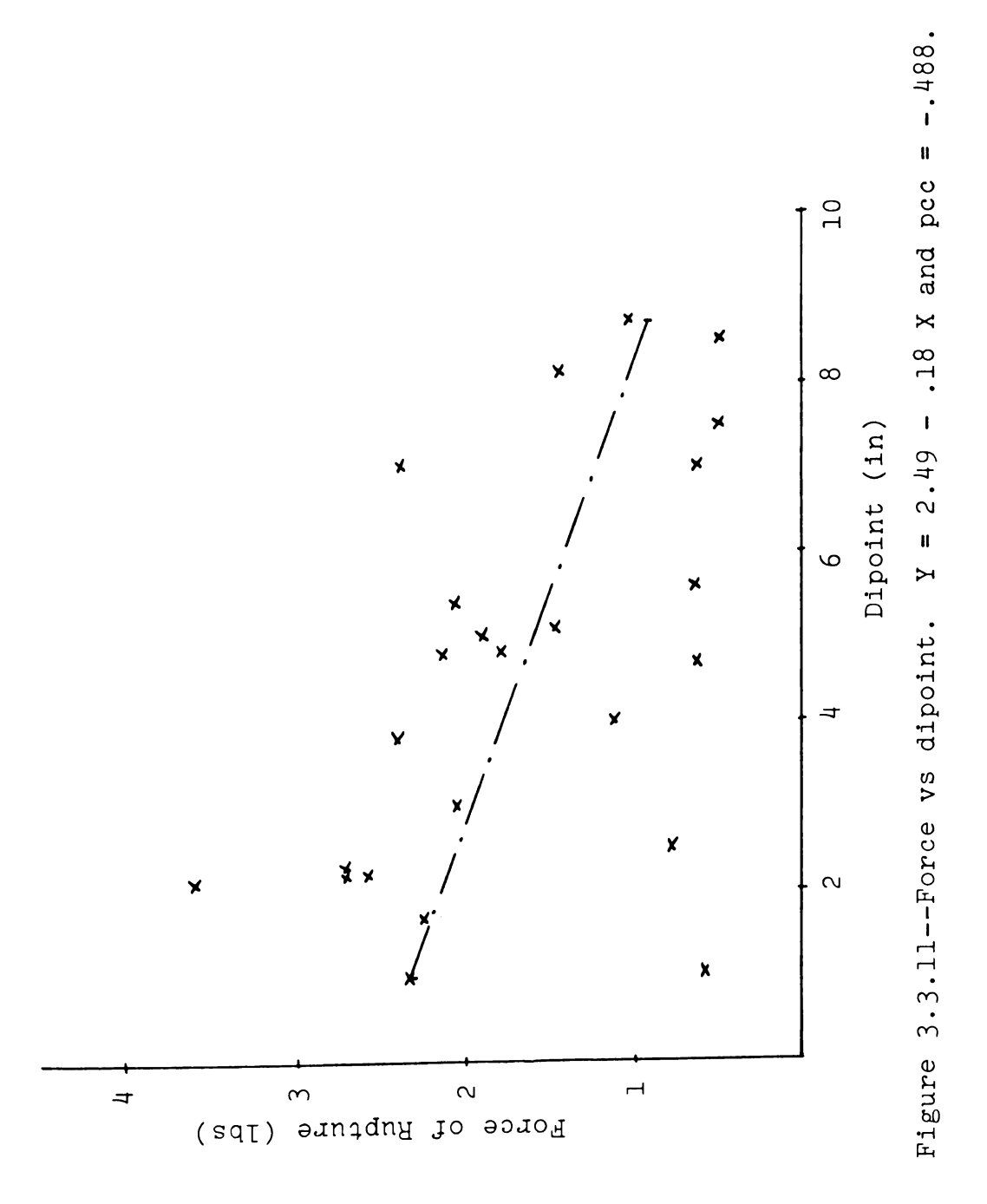


Figure 3.3.10--Diameter of fracture vs dipoint.



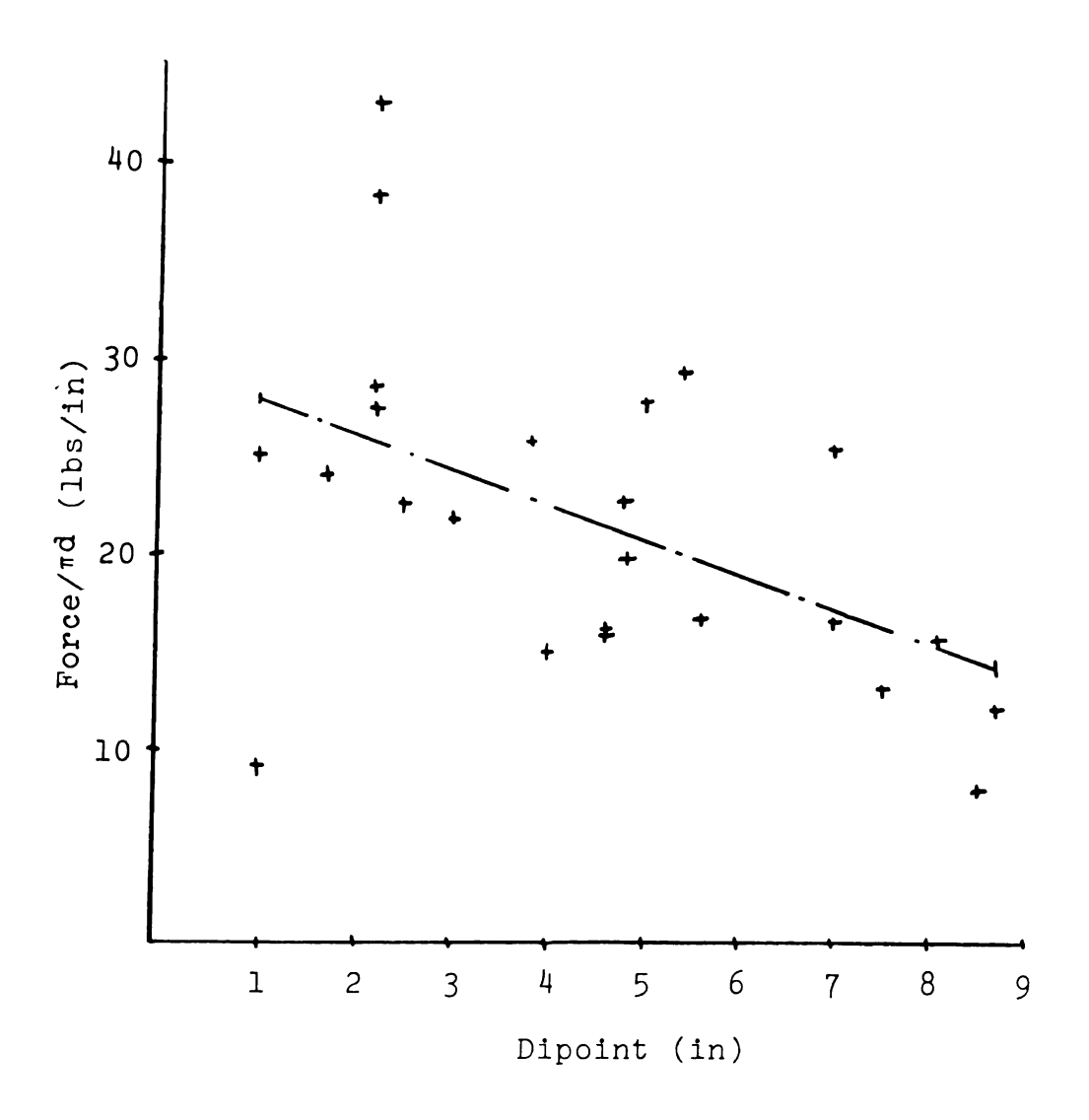


Figure 3.3.12--F/ π d vs dipoint. Y = 29.80 - 1.8 X and pcc = -.509.

Since an increase in dipoint caused a significant decrease in value of $F/\pi d$, which was considered the most important strength parameter of rupture, it may be stated that the root strength decreased as we departed from the attaching point toward the root tip.

4. STRESS DISTRIBUTION

4.1 Introduction

In this chapter a theoretical approach will be presented which describes the uprooting force applied to a root-soil composite. For this study several approaches were considered as to their feasibility, advantages and disadvantages.

Kaul (1965) reports that the inclusion of roots was found to increase the shear, tensile and compressive strength of soil. At first it was thought that the problem might be regarded as a reinforced medium, similar to reinforced concrete. The qualitative nature of the strength of concrete could be compared with that of the soil, but objections might be given to regarding the roots as similar to steel bars. A preliminary study of the research done on reinforced concrete indicated that little attention had been given to configurations of reinforcement similar to the root system. This approach was therefore abandoned.

Rosen (1964) studying the mechanics of composite strengthening states that when a fracture criterion is desired, an understanding of the average stress-strain response is no longer sufficient, and consideration must be given to internal irregularities in the state of stress. He presents a solution to these problems for failure of a

fibrous composite under uniaxial compressive and tensile load. The study is based upon consideration of the phenomena that occur subsequent to an initial internal fracture and when the strength of brittle fibers are defined by a statistical distribution function. Despite the different geometry between the root system and that of the reinforcing fibers, the solution could probably be applied to the mechanics of the root system later on when its statistical distribution function is better known. Rosen, in his work, defines the effective length of a fiber embedded in a matrix and presents a solution for the interface shear stress.

Maclaughlin (1966) working with matrices of fiberreinforced material models was able to obtain photoelastic
values for maximum shear stresses developed in the surrounding of the embedded fibers subjected to tensile forces.
The models were made by casting a birefringent epoxy resin
around variously arranged steel strips. The peak stresses
resulting from a gradually tapered fiber was found to be
slightly higher than that from a square-ended fiber. A
round-ended fiber produced a peak stress which was slightly
lower than that of the square-ended fibers. Peak stresses
resulting from two square-ended fibers butted closely
together were considerably higher and decreased with increasing gap. It made little difference whether the gap
was open, simulating a void resulting from a broken fiber,
or filled with matrix material.

The use of a photoelastic approach for the study of the root system was considered, since it was learned in a work reported by Richards Jr. and Mark (1966) that Moreno et al., in Spain, had used gelatin models to study reinforced concrete, using rubber bands as the reinforcing element. A complete review of literature was made of the use of gelatin models for photoelastic analysis. study included proportioning of gelatin mixes, moulding process, and calibration methods for testing for quantitative results. Several trials were made in cooperation with the Botany and Physiology Department of Michigan State University, in an attempt to germinate sorghum seeds in an Agar gelatin medium. The seedlings were able to germinate and it was noticed that the growth of roots was affected by the proportions of the gelatin mix. Difficulties were encountered in obtaining a translucency of the medium which permitted a good view in the polariscope. The necessity soon became apparent of controlling certain critical factors whose effects might invalidate the results completely. These factors were: friction between gelatin mix and the wall of the model; a minimum thickness of the model to transparency and plain strain state; and the calibration of the model root-gelatin.

It is known that one of the approaches used in the determination of the soil bearing capacity and for stability calculations of the soil-foundation system, is

based on studies of failure conditions. This method requires knowledge of how the failure in the foundation-supporting soil takes place. It was therefore decided to observe the cracks taking place underground and at the surface of a root-soil composite subjected to a pulling force. These observations proved valuable in the description of the failure surface. Therefore the phenomena were filmed and the results will be reported in the following sections of this chapter.

4.2 Theory of the Mechanics of the Root-Soil System

The root-soil system may be considered as being a reinforced composite with the following specific characteristics:

- a. the roots are mainly distributed in a conical pattern;
- b. this distribution is non-uniform both with regard to the apex angle of this cone and also circumferentially;
- c. the roots present geometrical and histological variations;
- d. there is a transition zone encompassing the attaching point with a high density of reinforcement (roots);
- e. the soil is an anisotropic medium with low tensile strength;

f. the bonding between root and soil is altered by the soil moisture content.

Forces applied to a plant are counteracted by two principal factors, the weight of the soil, plant and roots, and the forces due to the strength of the composite. It was seen that the value of the maximum force that could be applied to the plant was by far greater than the weight of the plant plus the root-soil bulb and also greater than the weight of the weight of the soil in the crater.

Therefore, this indicates that the root-soil composite presents a certain tensile strength. The soil itself presents a low tensile strength and it shall be considered mainly as a bonding matrix. The roots, compared to the soil, have a rather high tensile strength and in this analysis they will be regarded as if they were the main resisting element. The test results seemed to indicate that the material may be assumed to be Hookean up to about one half of the value of the maximum force.

The theory for a simplified root-soil system can be attempted upon the assumptions that:

- a. the center of the root distribution cone is the intersection of the vertical centerline of the plant and the soil surface line;
- b. the root system has rotational symmetry around the vertical plant axis. The distribution is defined as a function of the cone apex angle;

- c. the roots are cylindrical in shape but their strength decreases as the distance from the attaching point increases;
- d. the transition zone close to the center of the plant base is a hemisphere;
- e. only the portion of the pulling force created by the composite strength will be considered.The influence of soil weight will be neglected;
- f. the composite behaves as a Hookean body, up to a proportional limit or "yield strength" of the composite;
- g. the changes occurring in soil moisture are assumed small and the friction and adhesion between root and soil are constant;
- h. the actual behavior properties of the roots are assumed to follow the assumptions of the theory of elasticity.

Other assumptions will be specified at the appropriate time in the analysis of the root-soil system.

4.2.1 The Bond Between Main Roots and Soil Composite

An uprooting force applied to a plant reaches the main root through their attaching point. From the main root this force is transferred to the surrounding composite made up of soil, branch roots and root hairs, by bond or shear forces along the main roots.

The free body diagram of Figure 4.2.1 shows a segment of root embedded in the soil. The radial coordinate ρ_e defines that point of the root beyond which it remains stationary when subjected to a force F_t . The root segment from the origin (o) to ρ_o defines a central zone within which the physical phenomena are considered undetermined, and where it is assumed that the root-soil system behaves as a solid body.

From the free body diagram it can be written

$$0 = dF_s + dF_r (4.4)$$

or

$$-\int_{\rho_{O}}^{\rho} dF_{r} = \int_{\rho_{O}}^{\rho} dF_{s}$$
 (4.5)

Also,

$$F_{t} - F_{r} = \int_{\rho_{c}}^{\rho} dF_{s}$$
 (4.6)

where

 F_t = total force applied to the attaching point of the root $[F_t = (F_r)_{\rho=\rho_0}];$

F_r = residual force experienced by the root at
 a section under consideration;

 F_s = total tangential force in the axial direction at the root-soil interface.

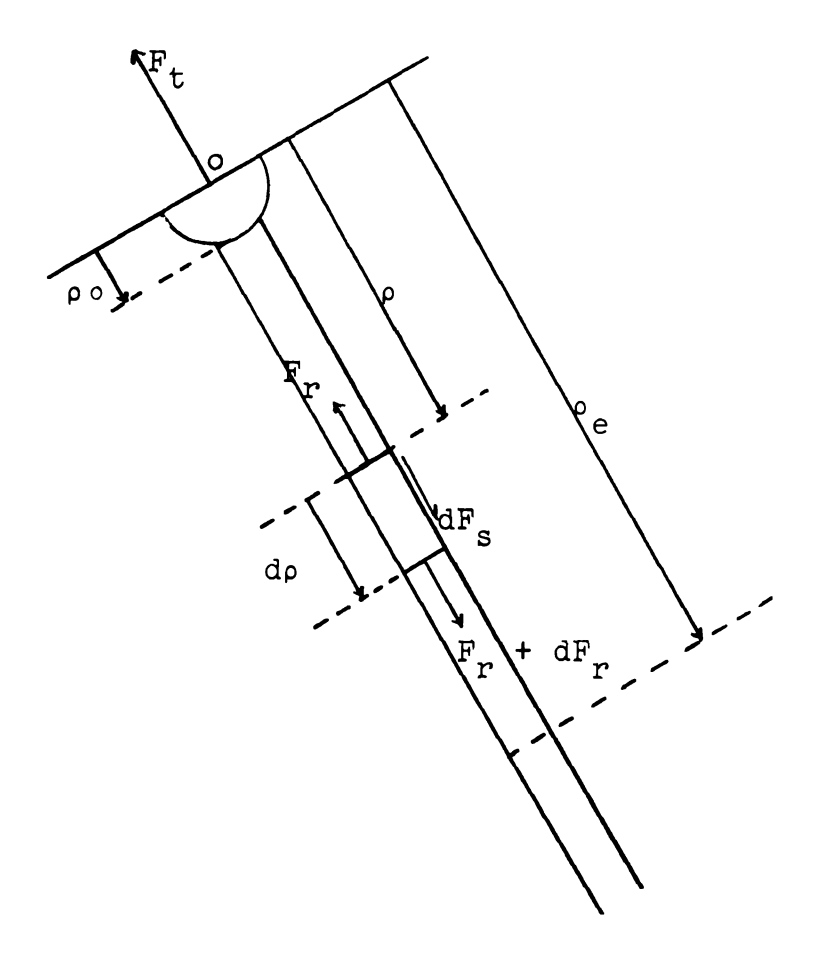


Figure 4.2.1--Free body diagram of root embedded in the soil.

The factors influencing the root soil bond are: adhesion, root-soil friction and pressures exerted on the roots from the outside. A possible interaction among these factors is to be considered. The presence of branch roots and root hairs alters this behavior further, due to an increase in bonding area and a shearing of these elements during the relative displacement between root and soil. The attracting force of adhesion is determined by two factors: the actual strength of attraction of a unit area of bonding and the actual area of the attracting bonds. Outside pressures applied to the root surface influence both of these quantities, so that evaluation of these results is difficult (Gill and Vanden Berg, 1966). Therefore, it is assumed here that the tangential stress (τ) acting in the axial direction of the root encompasses the influence of all the factors contributing to the transfer of forces between root and soil.

Thus, the elementary axial tangential force (dF_{s}) developed at the root-soil interface is given by

$$dF_{s} = 2\pi r \tau d\rho \tag{4.7}$$

where

r = root radius;

τ = axial tangential stress on the periphery of the root;

p = radial coordinate of the root element.

Therefore, the axial tangential force can be expressed as

$$F_{s} = 2\pi \int_{\rho_{O}}^{\rho} r\tau \, d\rho \tag{4.8}$$

and from equation (4.6) the residual force is given by

$$F_{r} = F_{t} - 2\pi \int_{\rho_{O}}^{\rho} r\tau \, d\rho \qquad (4.9)$$

The conditions under which an axial tangential stress τ exists are dictated by the factors discussed above, and also by the relative displacement (j) between root and soil. Thus, τ can be expressed in a general form as

$$\tau = f (j) \tag{4.10}$$

When subjecting the root to a force, different displacements of a given point at the interface will be experienced by the soil and the root due to differences in imposed stresses and in "elastic" properties. Thus, there will be a relative displacement (j) at the point of the root-soil interface which may be expressed as

$$j = s_r - s_s \tag{4.11}$$

where

 $s_r = root displacement, and$

 $s_s = soil displacement.$

Consider the diagram of Figure 4.2.1. The elongation of an elementary section do in terms of the property of the material may be expressed as

$$\delta \rho = \frac{F_r}{2\pi \ r \ E_r} \quad d\rho \tag{4.12}$$

where

 $\delta \rho$ = elongation of the elementary section dp;

 E_r = surface modulus of elasticity of the root with dimensions force/length.

If the displacement $s_{\bf r}$ is assumed to be zero at radius ρ_e the displacement of any root segment in the negative direction of ρ could be written as

$$s_r = \int_{\rho}^{\rho e} \delta \rho \tag{4.13}$$

Substituting the value of $\delta \rho$ found in equation (4.12) into equation (4.13) it becomes

$$s_{r} = \frac{1}{2\pi} \int_{\rho}^{\rho_{e}} \frac{F_{r}}{r E_{r}} d\rho \qquad (4.14)$$

If it is now assumed that the displacement of the soil is negligible as compared with that of the root, then equation (4.11) can be written as

$$j = s_r = \frac{1}{2\pi} \int_{\rho}^{\rho_e} \frac{F_r}{r E_r} d\rho$$
 (4.15)

The earlier definition of the radius $\rho_{\mbox{\footnotesize e}}$ now implies that for

$$\rho \geq \rho_e$$
; $j = 0$ and $\tau = 0$

From equation (4.9)

$$(F_r) \rho = \rho_e = 0$$
 (4.16)

It is proper at this point to define the effective length of a root as the radius $\rho_{\rm e}$ because from this radius outward the root does not experience any residual force.

The definition of the effective radius ρ_e could be expanded to mean the radius beyond which $s_r = s_s$.

Thus, from equations (4.6) and (4.9) it can be written that

$$F_{r} = 2\pi \int_{\rho}^{\rho_{e}} r\tau \, d\rho. \qquad (4.17)$$

It should be made clear that the shear stress function $\tau = f(j)$, given by equation (4.10), has to be

determined experimentally. A typical shear stressdisplacement diagram obtained from a direct shear apparatus for highly cemented and dried soils or hard, clean sands is given in Figure 4.2.2, curve 1. The reinforcement effect of the roots in the soil may be of the nature of curve 2. A higher value of τ_{max} for the composite curve may be justified by the fact that the penetrating action of the roots and their diametral growth cause a higher degree of compaction at the root-soil interface. From shear tests of soils it is also known that the shear strength increases during shear for confined specimens. If the movement of the root takes place under small changes in volume it is likely that this also imposes a "confinement" onto the process, and the shear stress is increased. The value of τ_{max} for soil alone takes place over a shorter displacement change, whereas that for the root-soil system is thought to persist for a greater change in displacement (j). This may be justified by considering that before the majority of branch roots and or root hairs have failed, longer displacements are to be expected as compared to the displacements for soil alone. At high values of the displacement (j) the value of the axial tangential stress would be reduced to root-soil friction.

Based on equations (4.9), (4.10), (4.15) and curve 2 of Figure 4.2.2, a theoretical attempt can be made to describe the general nature of variables such as the

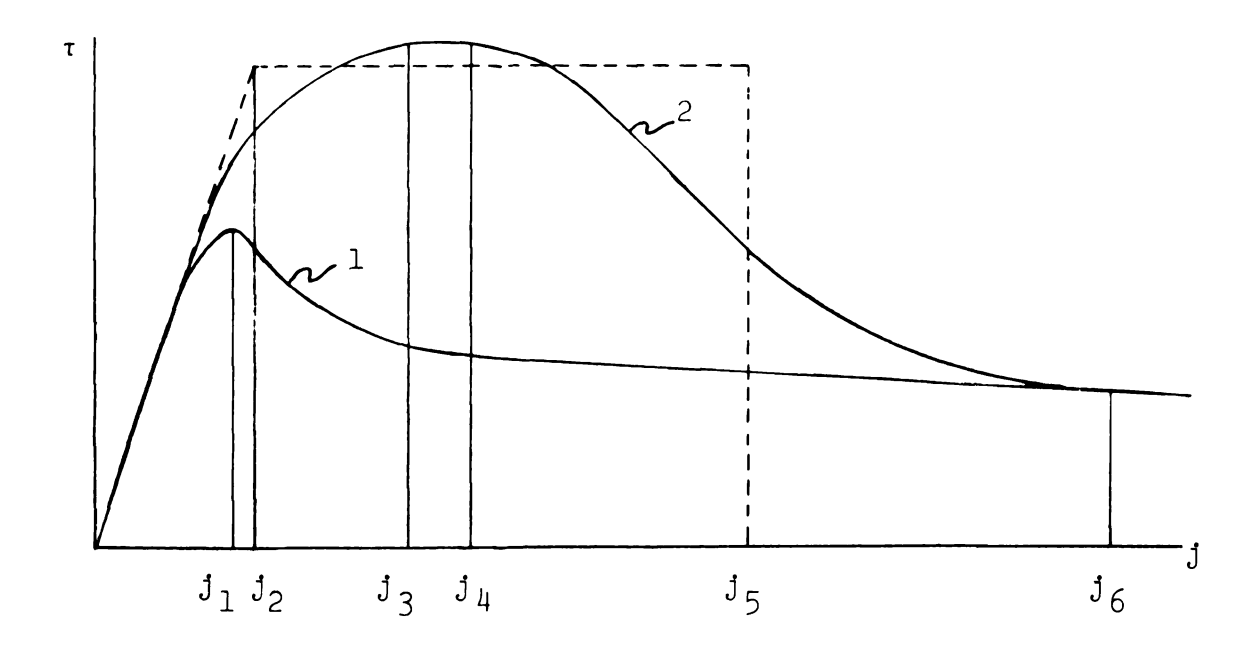


Figure 4.2.2--Axial tangential stress (τ) versus displacement (j). Curve 1 is a typical curve for soil. Curve 2 may represent the reinforcement effect of roots. The broken line represents the assumed linear model.

residual force F_r), the axial tangential stress (τ) and the relative displacement (j) as functions of the radial coordinate (ρ) of the root element (Figure 4.2.3).

Since it has been found that $(F_r)_{\rho=\rho_{\rho}} = 0$, there are two values known for F_r , namely: $(F_r)_{\rho_n} = F_t$ and $(F_r)_{\rho_e} = 0$. The displacement j equals zero at $\rho = \rho_e$ and has its maximum at $\rho = \rho_0$. Consider equation (4.9). If (τ) is assumed positive a decreasing tendency is to be expected for $\boldsymbol{F}_{_{\boldsymbol{\mathcal{P}}}}$ with increasing $\boldsymbol{\rho}_{\boldsymbol{\cdot}}$. For small values of $\boldsymbol{\rho}_{\boldsymbol{\cdot}}$ high values for j can further be expected. From curve 2 of Figure 4.2.2 it is seen that at high values of j, the axial tangential stress (τ) is constant but small. Thus, the curve of F_n in Figure 4.2.3 is expected to present a slightly negative slope for points between ρ_{o} and $\rho_{1}.$ For points beyond ρ_1 , the j values are assumed to be less than j_6 in Figure 4.2.2. This means that the τ values are higher and therefore the decrease in F_{p} is faster. From ρ_1 to ρ_2 the value of F_r will decrease until it becomes zero at ρ_a .

If the assumed values for F_r are introduced in equation (4.15), it shows that the basic assumptions regarding the displacement j are reasonably correct.

A mathematical derivation can be found for the curves of Figure 4.2.3 by considering equations (4.9), (4.10) and (4.15).

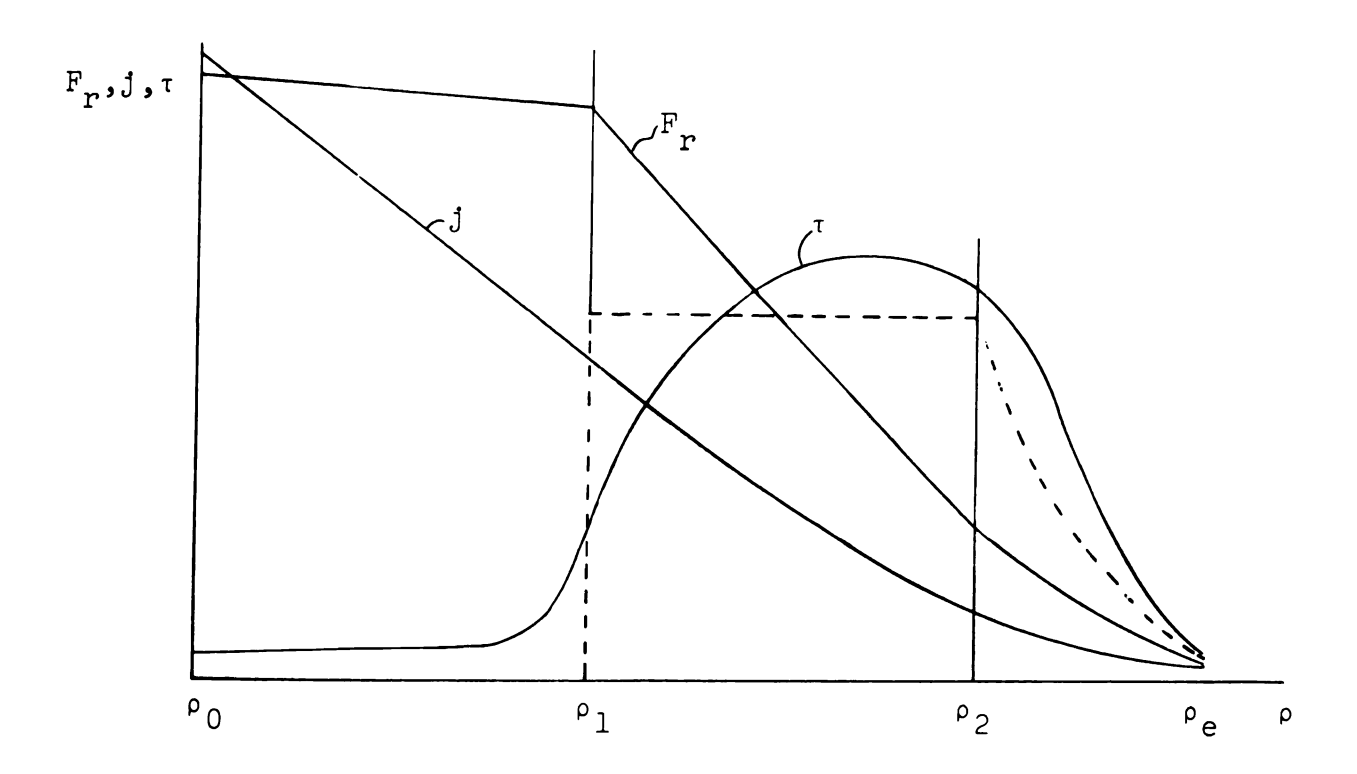


Figure 4.2.3--Residual force (F), displacement (j) and the axial tangential stress (τ) as functions of the radial coordinate (ρ). The broken line represents the values of τ as given by the assumed linear model.

$$F_{r} = F_{t} - \int_{\rho_{o}}^{\rho} 2\pi r \tau d\rho \qquad (4.9)$$

$$\tau = f (j) \tag{4.10}$$

$$j = \frac{1}{2\pi} \int_{\rho}^{\rho_e} \frac{F_r}{r E_r} d\rho \qquad (4.15)$$

Taking derivatives of equations (4.9) and (4.15) with respect to ρ gives

$$\frac{\mathrm{d}F_{\mathbf{r}}}{\mathrm{d}_{\mathbf{p}}} = -2\pi\mathbf{r}\tau\tag{4.18}$$

and

$$\frac{dj}{do} = - \frac{F_r}{2\pi r E_r} \tag{4.19}$$

The negative sign in equation (4.19) is due to the order of the limits of integration that are used. The second derivative of j is then

$$\frac{d^2j}{d\rho^2} = -\frac{1}{2\pi r E_r} \frac{dF_r}{d\rho}$$
 (4.20)

Substituting the value of $dF_{\rm r}/d\rho$ from equation (4.18) into equation (4.20), gives

$$\frac{d^2j}{d\rho^2} = \frac{\tau}{E_r} \tag{4.21}$$

and the general equation can be written as

$$\frac{d^2j}{d\rho^2} - \frac{f(j)}{E_r} = 0 (4.22)$$

In order to solve equation (4.22), f (j) must be known. Assume τ = f (j) to be represented by the simplified model given by the broken lines shown in Figure 4.2.2. For reasons mentioned earlier, it is assumed that the values for j and τ given below will apply in the regions of ρ in Figure 4.2.3, as follows:

The solution will be made considering the three regions for ρ indicated above separately.

For the portion ρ_0 to ρ_1 , equation (4.22) becomes

$$\frac{\mathrm{d}^2 \mathbf{j}}{\mathrm{d} \sigma^2} = 0 \tag{4.23}$$

Integrating gives

$$\frac{\mathrm{d}j}{\mathrm{d}\rho} = C_1 \tag{4.24}$$

and

$$j = c_1 \rho + c_2$$
 (4.25)

Using equation (4.19) and (4.24) gives

$$-\frac{F_r}{2\pi r E_r} = C_1 = -\frac{F_t}{2\pi r E_r}$$

because at $\rho = \rho_0$

$$F_r = F_t \tag{4.26}$$

and

$$j = -\frac{F_{t}}{2\pi r E_{r}} \rho + C_{2}$$
 (4.27)

From Figures 4.2.2 and 4.2.3 it can be seen that when $j=j_5$, $\rho=\rho_1$ and equation (4.27) can be written

$$c_2 = j_5 + \frac{F_t}{2\pi r E_r} \rho_1$$
 (4.28)

and therefore

$$j = j_5 + \frac{F_t}{2\pi r E_p} (\rho_1 - \rho)$$
 (4.29)

4.

Also when $\rho = \rho_0$, $j = (j)_{\rho_0}$; and from equation (4.29)

$$(j)_{\rho_0} = j_5 + \frac{F_t}{2\pi r E_r} (\rho_1 - \rho_0)$$
 (4.30)

For the portion ρ_1 to ρ_2 equation (4.22) becomes

$$\frac{d^2j}{d\rho^2} = \frac{K}{E_r} \tag{4.31}$$

Integration gives

$$\frac{df}{d\rho} = \frac{K}{E_p} \rho + C_4 \tag{4.32}$$

and

$$j = \frac{K}{2E} \rho^2 + C_4 \rho + C_5 \tag{4.33}$$

From equations (4.19) and (4.32)

$$-\frac{F_r}{2 r E_r} = \frac{K}{E_r} \rho + C_4 \tag{4.34}$$

and

$$F_r = -2\pi r K \rho - 2\pi r E_r C_4$$
 (4.35)

But when $\rho = \rho_1$, $F_r = F_t$ and from equation (4.35)

$$C_4 = -\frac{1}{E_r} \left(\frac{F_t}{2\pi r} + K_{\rho_1} \right)$$
 (4.36)

Thus, equation (4.35) can be written as

$$F_r = F_t - 2\pi K r (\rho - \rho_1)$$
 (4.37)

Combining equations (4.36) and (4.33)

$$j = \frac{K}{2 E_r} \rho^2 - (\frac{F_t}{2\pi r E_r} + \frac{K\rho_1}{E_r}) \rho + C_5$$
 (4.38)

By applying the boundary conditions

$$j = j_2$$
 at $\rho = \rho_2$; and $j = j_5$ at $\rho = \rho_1$,

equation (4.38) becomes

$$j_2 = \frac{K}{2 E_r} \rho_2^2 - (\frac{F_t}{2\pi r E_r} + \frac{K\rho_1}{E_r}) \rho_2 + C_5 (4.39)$$

and

$$j_5 = \frac{K\rho_1^2}{2E_r} - \frac{F_t}{2\pi r E_r} \rho_1 + C_5$$
 (4.40)

Equations (4.39) and (4.40) can be combined to

$$j_5 - j_2 = \left[\frac{-K}{2 E_r} (\rho_1 - \rho_2) - \frac{F_t}{2\pi r E_r}\right] (\rho_1 - \rho_2)$$
(4.41)

For the portion ρ_2 to ρ_e equation (4.22) becomes

$$\frac{\mathrm{d}^2 \mathbf{j}}{\mathrm{d}\rho^2} - \frac{\mathbf{a}\mathbf{j}}{\mathrm{E}_r} = 0 \tag{4.42}$$

Let $a/E_r = A^2$. A solution of equation (4.42) is

$$j = C_7 e^{C_8 \rho}$$
 (4.43)

therefore,

$$\frac{\mathrm{d}\mathbf{j}}{\mathrm{d}\rho} = c_7 c_8 e^{C_8} \rho \tag{4.44}$$

and

$$\frac{d^2j}{d\rho^2} = c_7 c_8^2 e^{c_8} \rho$$
 (4.45)

Substituting the values of equations (4.45) and (4.43) into equation (4.42) results in

$$C_8 = \pm A \tag{4.46}$$

The general solution can now be written

$$j = C_9 e^{A\rho} + C_{10} e^{-A\rho}$$
 (4.47)

When $\rho = \infty$, j = 0, and $C_{10} e^{-A\rho} = 0$. Therefore, $C_9 = 0$ and equation (4.47) is

$$j = c_{10} e^{-A\rho}$$
 (4.48)

When $\rho = \rho_2$, $j = j_2$, and

$$C_{10} = j_2 e^{A\rho_2}$$
 (4.49)

Thus equation (4.48) can be written as

$$j = j_2 e^{-A} (\rho - \rho_2)$$
 (4.50)

Then,

$$\frac{dj}{d\rho} = -Aj_2 e^{-A(\rho - \rho_2)}$$

and using equation (4.19)

$$F_r = 2\pi r E_r A j_2 e^{-A(\rho - \rho_2)}$$
 (4.51)

From equation (4.37) F_r is found to be at $\rho = \rho_2$

$$(F_r)_{\rho_2} = F_t - 2\pi K r (\rho_2 - \rho_1)$$

and from equation (4.51)

$$(F_r)_{\rho_2} = 2\pi r E_r A j_2$$

which gives

$$F_t = 2\pi r [K (\rho_2 - \rho_1) + E_r A J_2]$$
 (4.52)

In summary, the following equations apply:

for $\frac{\rho_0 \leq \rho \leq \rho_1}{j = j_5 + \frac{F_t}{2 r E_r}} \qquad (\rho_1 - \rho)$ (4.29)

 ρ_1 can be found from equations (4.30) and (4.52)

$$F_{r} = F_{t} \tag{4.26}$$

For $\rho_1 \leq \rho \leq \rho_2$

$$j = \frac{K}{2 E_r} \rho^2 - (\frac{F_t}{2\pi r E_r} + \frac{K \rho_1}{E_r}) \rho + C_5$$
 (4.38)

 C_5 can be derived from equation (4.41)

$$F_r = F_t - 2\pi r K (\rho - \rho_1)$$
 (4.37)

for

$$\frac{\rho_2 \leq \rho \leq \infty}{j = j_2 e^{-A} (\rho - \rho_2)}$$
(4.50)

 ρ_2 is found from equation (4.53)

$$A^2 = a/E_r$$

$$F_r = 2\pi r E_r A j_2 e^{-A (\rho - \rho_2)}$$
 (4.51)

For the solution the following equations are available:

$$F_t = 2\pi r [K (\rho_2 - \rho_1) + E_r A j_2]$$
 (4.52)

$$j_{5} - j_{2} = \left[\frac{K (\rho_{2} - \rho_{1})}{2 E_{r}} + \frac{A j_{2}}{2 \pi r}\right] (\rho_{2} - \rho_{1})$$
(4.53)

$$(j)_{\rho_0} = j_5 + \left[\frac{K}{E_r} (\rho_2 - \rho_1) + A j_2\right] (\rho_1 - \rho_0)$$

$$(4.54)$$

These equations contain only three unknowns (F_t , ρ_1 and ρ_2) and can therefore be solved. It can be seen that under the assumptions made for these calculations F_t will have a fixed value determined by $\rho_2 - \rho_1$ which in its turn is a function of the soil and root properties. ρ_1 will be a function of (j) ρ_0 . An increase in (j) ρ_0 will mean an increase in ρ_1 and therefore in ρ_e but no change in F_t , unless the soil properties change with ρ . If the applied force is less than F_t as determined by equation (4.52), (j) ρ_0 will be less than j_5 and the solution has to be changed correspondingly.

Based on these equations, the curves for F_r and j in Figure 4.2.3 can be derived.

4.2.2 The Displacement of the Attaching Point

An analysis of the displacement of the attaching point of the root may be attempted on the assumption that the root is affected by the displacement only between the plant and ρ_e , and that it remains basically straight over this length.

From Figure 4.2.3 it can be shown that the displacement of the sttaching point of the root is given by

$$\Delta L = \sqrt{(L + d \cos \theta)^2 + (d \sin \theta)^2} - L (4.55)$$

where

ΔL = elongation of a root at the attaching point;

L = root length between ρ_0 and ρ_e ;

d = vertical displacement at the base of
 plant (or of the attaching point);

θ = angle that a root makes with the vertical
axis of the plant.

By assuming $\Delta L/L$ a small number and neglecting the second order term in $\Delta L/L$, equation (4.55) becomes

$$\Delta L = \frac{d^2}{2L} + d \cos \theta \tag{4.56}$$

Equation (4.56) shows that ΔL is a linear function of cos 0. If the ratio d/L is assumed to have a low

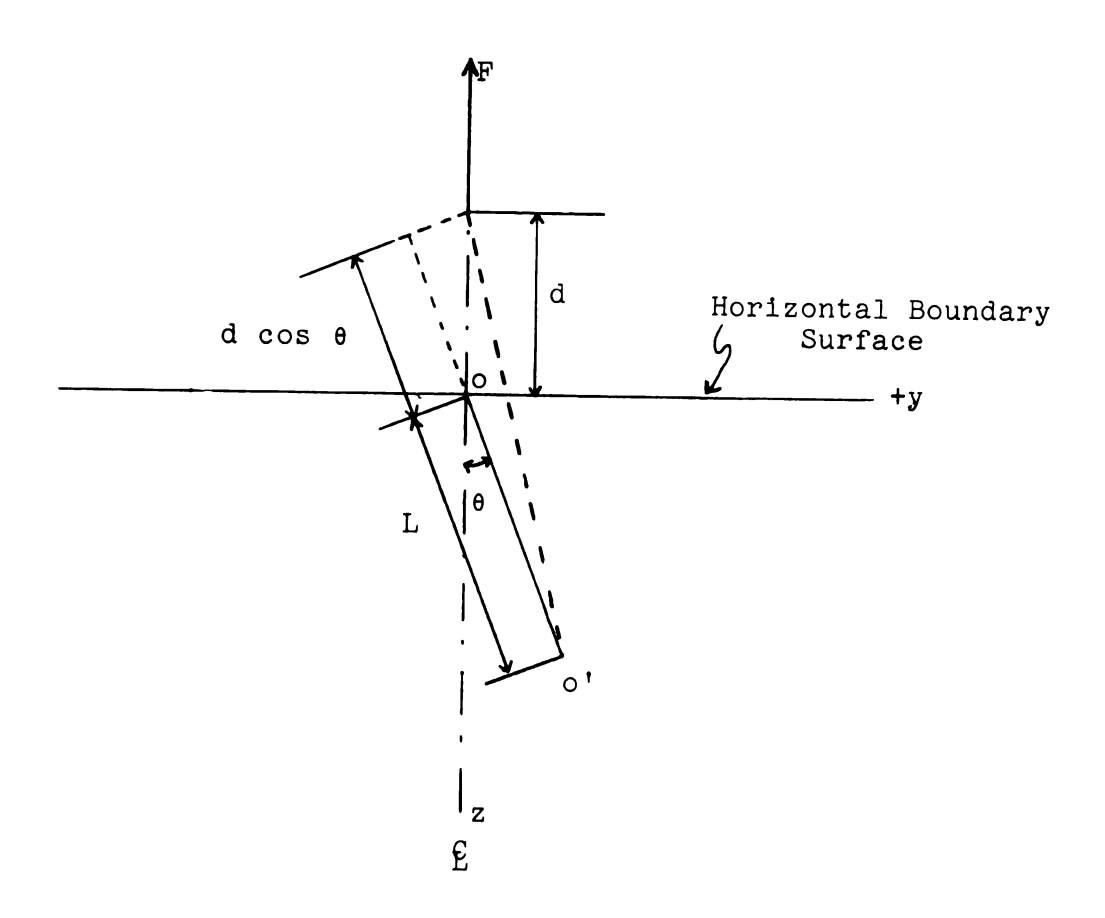


Figure 4.2.4-- The displacement at failure surface is maximum for θ = 0, and minimum for θ = $\pi/2$.

value and $\Theta < \pi/2$, then

 $\Delta L = d \cos \theta \tag{4.57}$

From equation (4.55) it can be shown that the elongation of a root at the attaching point is maximum at $\theta = 0$ and minimum at $\theta = \pi/2$.

4.2.3 Stress Distribution in the Soil Composite

The soil composite is regarded in this discussion is composed of soil, branch roots and root hairs excluding the main roots. Then, the reinforcing action of the root elements of the composite can be assumed to be of such a nature and order that the displacements of the root elements and the pure soil will be the same.

From the analysis of Section 4.2.2 it was seen that the transfer of forces from root to soil acquires significant magnitudes for a radius equal or larger than ρ_1 . Thus, it may be inferred that for the analysis of stress distribution in the soil the values of radius ρ of main interest are those from ρ_1 to ρ_e and beyond. Furthermore, ρ_1 and ρ_e define points which may be assumed to be relatively close as compared with the whole length of the root.

An assumption which has been proposed by Boussinesq (1885) and used by Jumikis (1962) and which is qualitatively

in agreement with the Boussinesq stress distribution is that the displacement of a point in the soil is given by

$$s \propto \frac{1}{\rho} \tag{4.58}$$

The displacement (s) is assumed to apply equally for reinforcing roots and surrounding soil; \underline{s} may further be assumed to be proportional to the displacement (ΔL) of the attaching point.

From equations (4.57) and (4.58) the displacement (s) of a point N (ρ , θ) in Figure 4.2.5 can be expressed as

$$s = \frac{C d \cos \theta}{\rho} \tag{4.59}$$

where

C = constant of proportionality, with dimensions
 of length.

Now compare the point N in Figure 4.2.5 with a point M (ρ + d ρ , θ) in the same direction of ρ . The displacement at point M is given by equation (4.59) as

$$s_1 = \frac{C \, d \, \cos \, \theta}{\rho + d\rho} \tag{4.60}$$

The strain of the composite element of the length $\ensuremath{\text{d}\rho}$ is

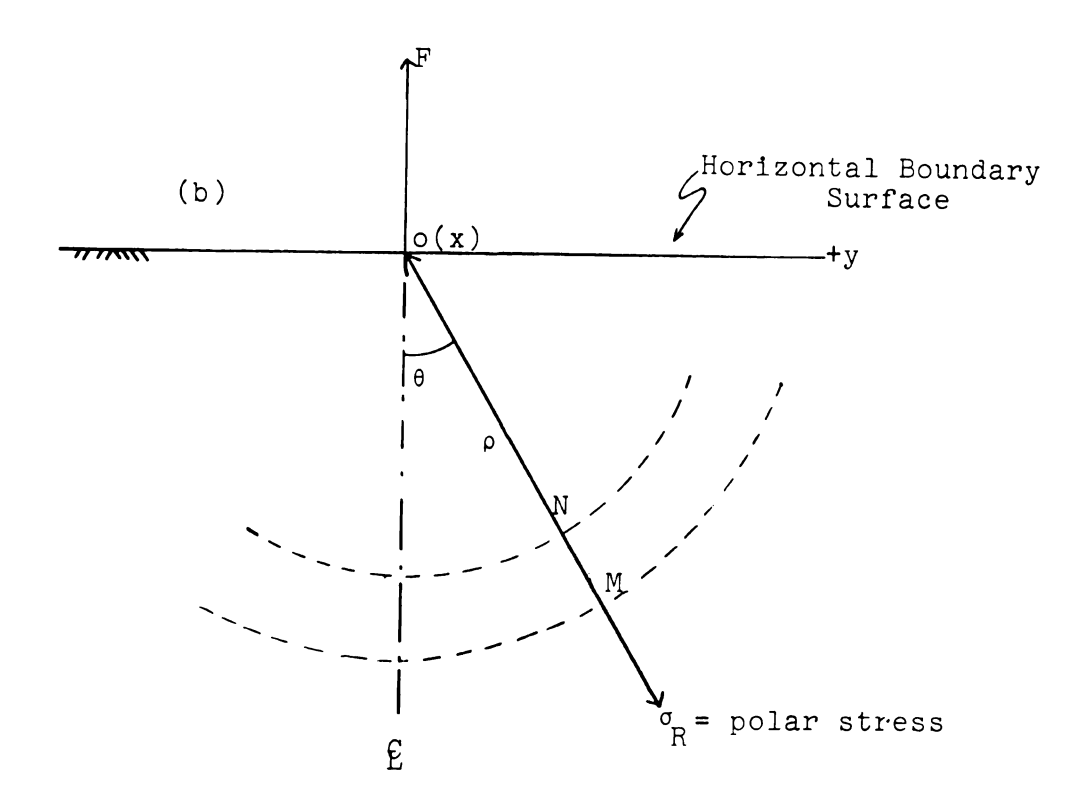


Figure 4.2.5—The static system of the soil composite.

$$\varepsilon = \frac{s - s_1}{d\rho} = \frac{C d \cos \theta}{\rho^2 + \rho d\rho}$$
 (4.61)

Considering that $d\rho$ is small compared to ρ ,

$$\varepsilon = \frac{C \, d \, \cos \, \theta}{\rho^2} \tag{4.62}$$

At this point an average stress σ_R may be defined on the basis of the total force in the radial direction and the cross-sectional area of the composite element, including both roots and soil. Based on previous assumptions of linear stress-strain relationship it might be written that

$$\sigma_{R} = B \epsilon = \frac{B C d \cos \theta}{\rho^{2}}$$
 (4.63)

where

 σ_R = polar tensile stress in the root-soil composite;

B = constant of proportionality, with dimensions force per unit area. \underline{B} is normally a function of θ and ρ .

From the equilibrium diagram of Figure 4.2.6, the forces acting in the z-direction are given by

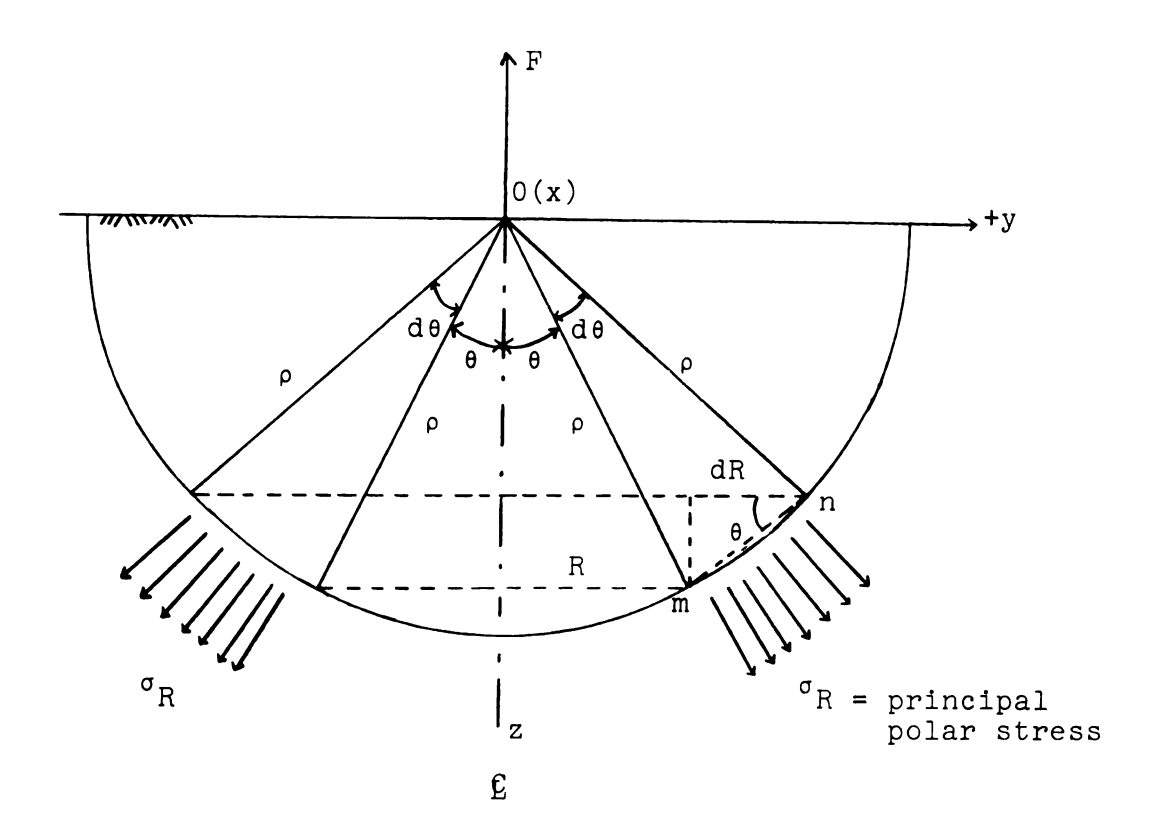


Figure 4.2.6--Equilibrium diagram: $\Sigma F_z = 0$.

$$F = \int_{-\infty}^{A} \sigma_{R} \cos \theta \, dA \qquad (4.64)$$

where

$$dA = 2\pi R$$
 $\rho d\theta$, but $R = \rho \sin \theta$, so $dA = 2\pi \rho^2 \sin \theta d\theta$

Thus, equation (4.64) can be written as

$$F = 2\pi \int_0^{\theta_0} \sigma_R \rho^2 \sin \theta \cos \theta d\theta \qquad (4.65)$$

where θ_o is the limit for force transmitting elements,

$$\Theta_0 \leq \pi/2$$

Substituting the value of σ_R from equation (4.63) into equation (4.65) and assuming B and C constant for $\theta \leq \theta_0$,

$$F = 2\pi B C d \int_{0}^{\theta_{0}} \sin \theta \cos^{2}\theta d\theta \qquad (4.66)$$

or after integration, as

$$\int_0^{\theta_0} \sin \theta \cos^2 \theta d\theta = -\frac{1}{3} \Big|_0^{\theta_0} \cos^3 \theta = \frac{1}{3} (1 - \cos^3 \theta_0)$$

B C d =
$$\frac{3}{2}$$
 $\frac{F}{(1 - \cos^3 \theta_0)}$ (4.67)

Substituting the value of equation (4.67) into equation (4.63),

$$\sigma_{R} = \frac{3 F \cos \theta}{2\pi \rho^{2} \left(1 - \cos^{3} \theta_{0}\right)} \tag{4.68}$$

Figure 4.2.7 illustrates equation (4.68).

Summarizing, it can be said that the transfer of forces from roots to the soil is characterized by distinct values of the radial coordinate $\rho.$ For values from ρ_0 to ρ_1 the force transfer is not significant, and the stresses are taken up by the root. From ρ_1 to ρ_e the transfer of force to the soil is effective and the stresses are then shared by root and soil. The region ρ_1 to ρ_e may be considered as a probable region of failure. The strength of the composite in this region will be influenced by the imperfections that the root-soil composite might present. Thus, it would be difficult to characterize exactly how the composite fails because of the dependence of the strain distribution between its elements. From ρ_e to ∞ the stresses are taken up entirely by the reinforced soil and decrease.

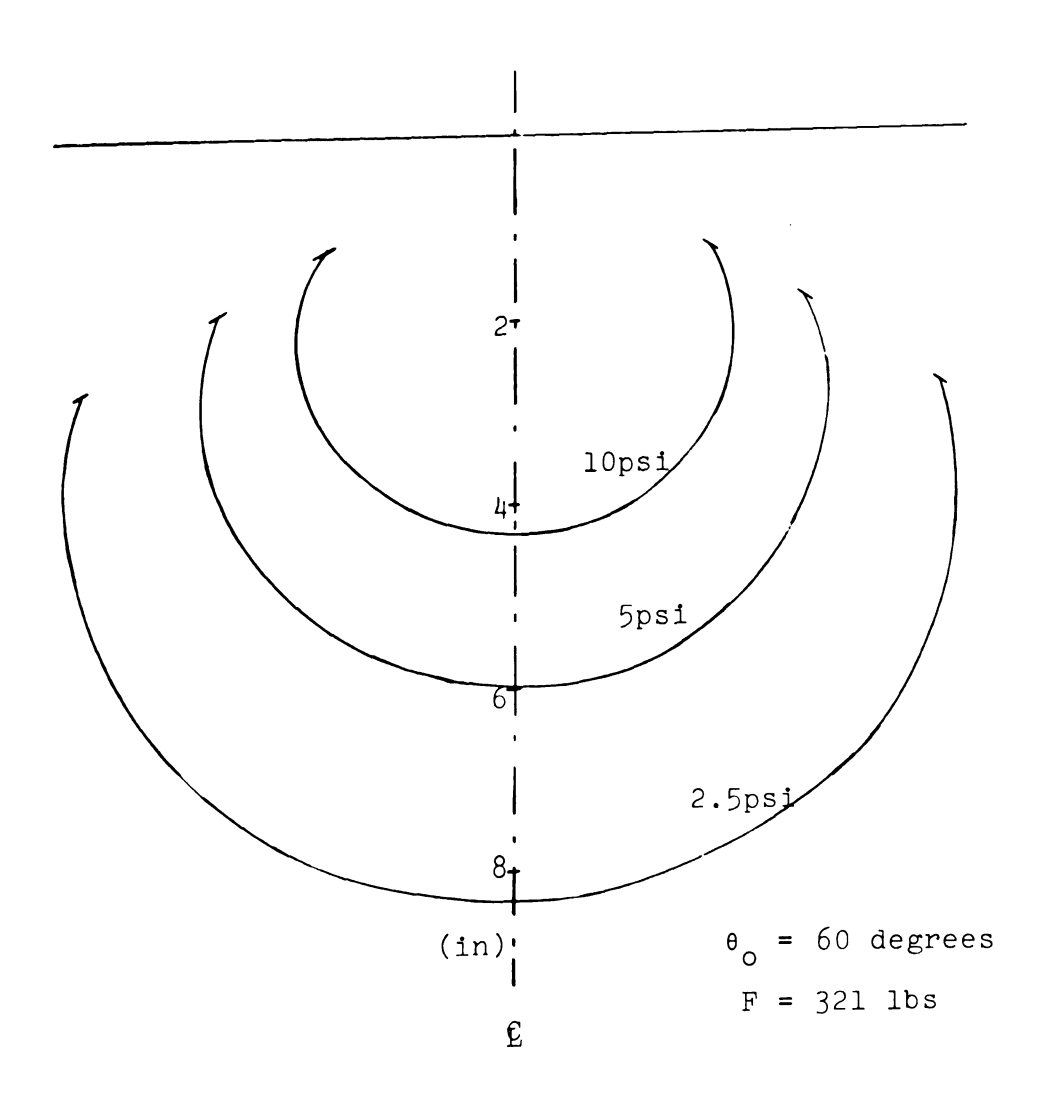


Figure 4.2.7--Isostrength curves σ_R = constant.

4.2.4 The Failure Strength of the Root-Soil Composite

The observations made of the underground failure and those presented in Section 2.3.2 provide elements for estimating the strengthening effect of the roots on the soil.

The strength of the composite is given by that of the soil plus a reinforcing effect introduced by the roots. This additional strength can be described by a reinforcing factor, which depends upon the distribution of the roots with the radial coordinate ρ and the angle θ .

It was seen from the direct tracing experiment of roots and from the plot of Figure 3.3.2 that the greatest number of main roots were found at an angle (α) from the soil surface between 60 and 80 degrees. Also, for values of (α) less than 30 degrees, the number of roots declines to practically zero. The branch roots and root hairs may be assumed to be distributed in approximately the same manner as the main roots. From the profiles of craters given in Figure 2.3.3 (A), (B) and (C), it can be seen that the "flat" bottom portion of the crater is involved by an angle (θ) of about 50 degrees. For values of θ of 50 degrees and above, the failure surface attains a typical Rankine pattern, due to reasons which will be discussed later in this chapter.

Therefore, the reinforcement effect of the root upon the soil as reflected by the actual failure surface, will be considered for values $0 \le 0 \le 50$ degrees.

In Figure 4.2.8, the isostrength curve σ_R = const., from equation (4.68), would represent the surface of incipient failure of the non-reinforced soil. The shape of the actual failure surface of the composite is taken from the tests (Figure 2.3.2 (C) N-S profile of experiment 25). It is assumed that this surface represents the locus of points of equal strength of the composite, neglecting the fact that the failure surface develops gradually with decreasing force and decreasing active area. Since the length of roots near the centerline are rather short, it will be assumed that the strength of the composite is equal to that of the not reinforced soil at θ = 0. Thus, in Figure 4.2.8 the isostrength curves should coincide at the point (A) where they intersect the centerline of the plant.

The strengthening effect is assumed to be expressed by the factor

$$K = \frac{\sigma_{12}}{\sigma_{11}} = \frac{F_2}{F_1} \tag{4.69}$$

Where

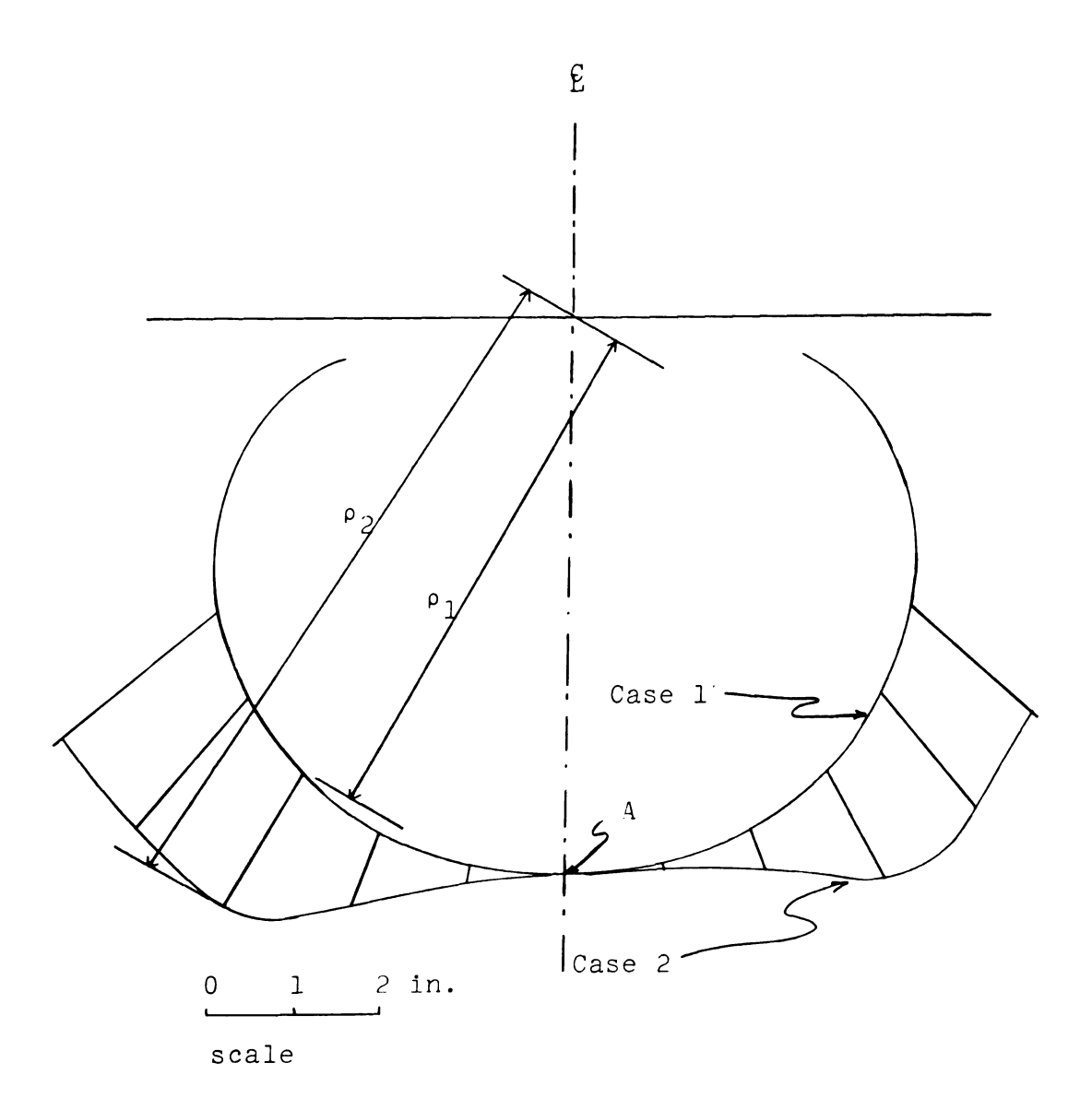


Figure 4.2.8—The strengthening effect of roots on failure surface; case 1 is the surface failure of soil along; case 2 is the failure surface of the composite [N-S profile of exp. 25, Figure 2.3.3 (C)].

K = strengthening factor of roots on soil;

 σ_{l_2} = stress at radius 1 for composite caused by F_2 ;

 σ_{l_1} = stress at radius 1 for soil alone caused by F_{l_1} ;

 σ_{2_2} = stress at radius 2 for composite caused by F_2 ;

F₂ = force necessary to cause failure of composite;

F₁ = force necessary to cause failure of nonreinforced soil.

Thus, from equation (4.68) it can be written that for a constant $\boldsymbol{\theta}$

$$F_2 = C_1 \sigma_{1_2} \rho_1^2 = C_1 \sigma_{2_2} \rho_2^2$$

and

$$F_1 = C_1 \sigma_{1_1} \rho_1^2$$

where

 ρ_1 and ρ_2 = radii of points on the failure surface of the composite and soil alone, respectively, for a given direction θ

For both F_1 in case 1 and F_2 in case 2 the stresses reach the critical value S_R in point A. S_R is the rupture strength of the composite independent of the angle θ and the radius ρ . S_R applies outside the failure surface. The same stress applies for all points on the curve of case 1, for the pure soil, and for all points on curve of case 2 for the reinforced soil, respectively. Thus,

$$\sigma_{1_1} = \sigma_{2_2} = S_R$$

and

$$K = \frac{\rho_2^2}{\rho_1^2} \tag{4.70}$$

If values of K versus θ (for $0 \le \theta \le 50$) were plotted, the overall effect of root strengthening can be estimated.

4.3 Observed Failures

As mentioned earlier in Sections 2.2 and 4.1, a film was made of the underground and top surface cracks, in order to learn more about the failure pattern. For the underground failure the sectors were opened as described in Section 2.3. The photographs to be presented were selected from a 200 foot film, and were considered to be most representative of the respective phenomena.

Reservations should be made as to the use of the word "surface" in the descriptions of the underground and the top surface cracks that will follow. Actually what was observed in the underground and in the soil surface represent failure surface traces in a vertical and in a horizontal plane, respectively.

4.3.1 Underground Failure

The filming was made on October 1, and the pictures from 4.3.1 to 4.3.12 represent one specimen.

Figure 4.3.1 shows the sectioned wall at zero load. The print of the squares in the photograph correspond to a square of 0.75 inch actual size. The centerline of the plant is on the left of the reader. At a point 8 squares to the right and 12 squares below the surface (8, 12) on the sectioned wall a discolored region is seen which represents a nonhomogeneity of the composite. Its effect on the failure surface will be noted later.

When the maximum pulling force is reached, a crack appears immediately below the point of application of the force (plant centerline) at a depth of about 7 inches (0, 9), (Figure 4.3.2). It indicates the region where the failure of the composite begins. This fact may be explained with reference to the stress distribution discussed in Section 4.2.3 where it can be seen that for a given distance from the center of the plant the stress will have a maximum at $\theta = 0$. The depth where it will

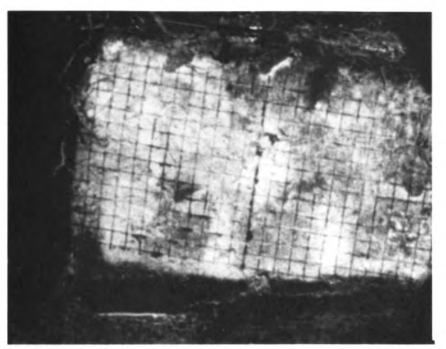


Figure 4.3.1--Sectioned wall at zero load. Centerline of plant on the reader's left, at the end of grid. Grid lines are .75 inch apart.

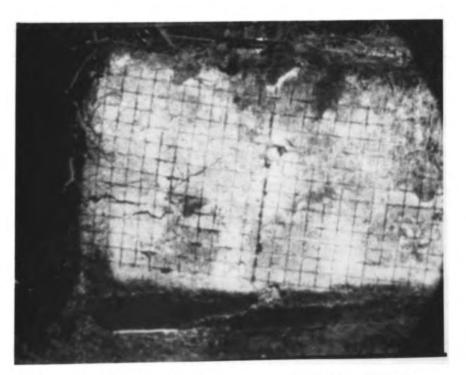


Figure 4.3.2--Failure occurred first at the centerline.

take place depends on the size and of the length of the roots.

As the pulling continues, the cracks extend toward the right and upwards, as can be seen in Figure 4.3.3. Here it is visible that the master crack is already outlined and normally characterized by larger displacements. However, secondary cracks appear above the master crack and within what will later be the fractured bulb. This is quite evident in Figure 4.3.4. In this figure the effects of the nonhomogeneity of the composite are noticed by the deviations experienced by the master crack. As stated earlier, this effect and that of the hard pan layer can affect considerably the shape of the bottom of the crater. Notice that the secondary cracks are quite evident and so is the deflection of the composite, as indicated by the deflection of the grid lines.

Figure 4.3.4 also shows a tension crack outlined at a point (5,0) at the soil surface. The forming of the tension cracks is due to less reinforcement at the soil surface, and the fact that the soil is characterized by a low tensile strength. The tension cracks play an obvious role in the disruption of the soil bulb as will be seen later.

Figure 4.3.5 shows the tension and secondary cracks now quite evident. The forming of the latter is related to the effective length of the roots. Effective length has earlier been defined as the radius (ρ_e) where the main

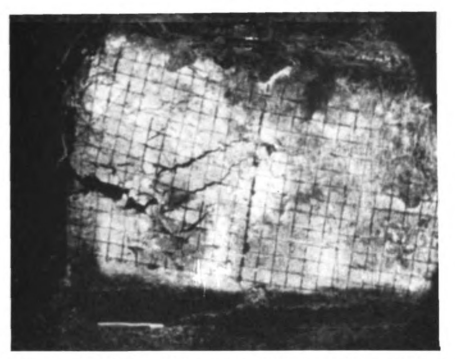


Figure 4.3.3--Rankine pattern is well outlined here. Note the master and the secondary cracks.

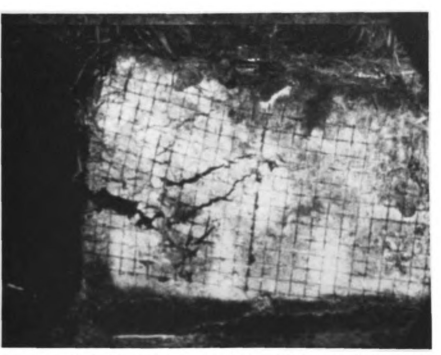


Figure 4.3.4--Tertiary crack and tension crack at soil surface are outlined.

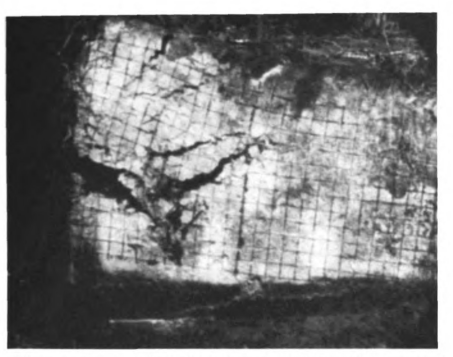


Figure 4.3.5--Tension crack and tertiary crack at soil surface is now quite visible. Note effect of non homogeneity on failure surface.



Figure 4.3.6--Observe the compression zone and an unfractured root which did not attain the effective length.

part of the pulling force has been transferred to the soil. Beyond the effective length the root serves only as reinforcement of the soil and is normally subjected to a small fraction of its strength. The master crack indicates the average effective length of the root system at a particular point when stress at this point has reached rupture values. The secondary cracks appear below and above the master crack, due to variations in effective length of individual roots.

Referring back to Figure 4.3.3 note that the master crack makes an angle of about 45 degrees with the horizontal in its outer part. Note, also, that the secondary cracks follow the same pattern, and that a tertiary crack appears at about 3 inches above the secondary and behaves likewise. This pattern may indicate slip lines representing shear failure in the material. If the development of this pattern is followed through the sequences of Figures 4.3.1 to 4.3.6 and 4.3.8, it may be concluded that as the composite deflects upwards a compression takes place out to the right from a hypothetical nearly vertical plane located about 4 to 5 inches from the centerline, at the height of the first crack. To the right of this plane it appears that a pressure is built up which is responsible for this pattern of slip lines (Rankine passive failure). The occurrence of this compression zone may be attributed to a wedging caused by the pulling force and the upward movement of the composite, as shown in Figure 4.3.7. In this diagram P

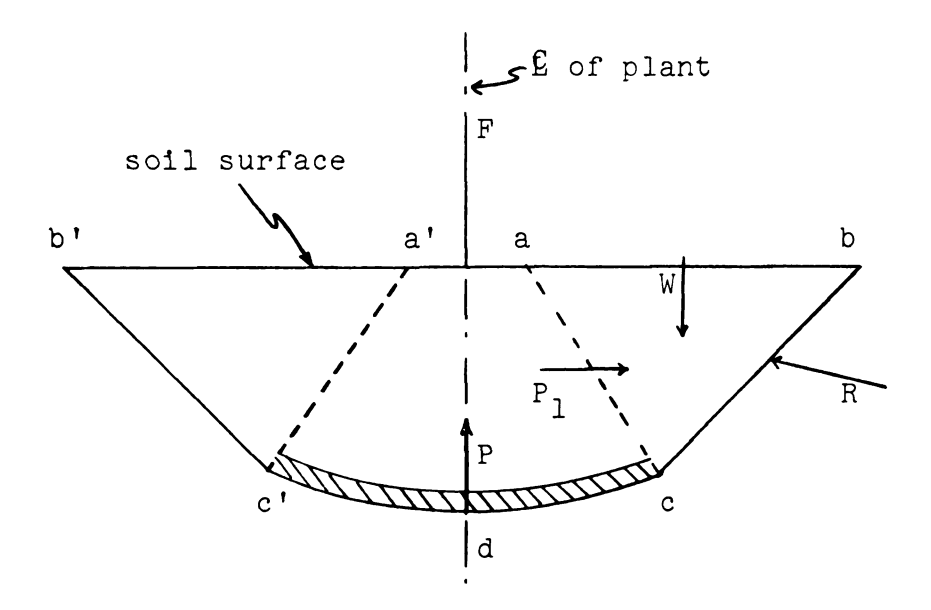


Figure 4.3.7--Forces acting on the root-soil bulb.

....

represents the part of the pulling force F that has been transmitted by the root to the force transfer zone cdc', at the bottom of the future disturbed soil. F minus P equals the weight of the material above cdc'. P creates stresses in the boundry ca which have the horizontal component P_1 . The action of P_1 may be considered a passive pressure on the element acb because the weight of the soil is of small magnitude compared with P_1 . Bond forces acting in the direction of the surface represented on the trace \underline{bc} counteract P_1 and their action originates a compression zone which becomes salient at the corner b, as shown in the extreme right of Figure 4.3.8 and in the close-up of Figure 4.3.9. In the sectioned tests, the soil in that region, at a certain stress, would flake off from the vertical wall. This is not shown in this sequence of pictures, but was consistently observed and registered in other sectioned tests as in Figure 4.3.19. In later stages of the pulling, the soil in the bulb is subjected to bending due to the weight of the soil and the strength of the bond along the edge of the future crater. This bending causes tension cracks at the soil surface closer to the plant and accentuates the compression in the area of the future crater rim, as mentioned earlier. The tension crack will determine the size of the future rootsoil bulb, as is apparent in Figure 4.3.10.

Referring back to Figure 4.3.6, 4.3.8, and the closeup of Figure 4.3.11, it is seen that there is a root which



Figure 4.3.8--The disruption in the bulb is outlined based on surface tension crack.

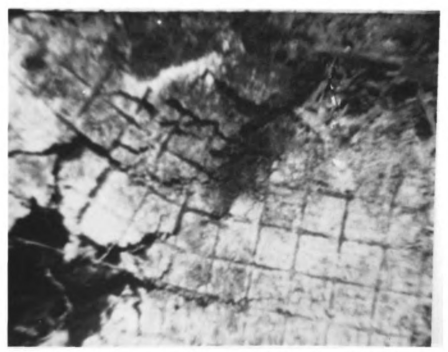


Figure 4.3.9--A close up of the compression zone.



Figure 4.3.10--Final stage of rupture prior to bulb disruption.

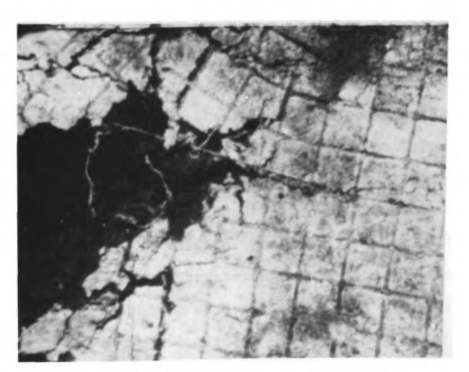


Figure 4.3.11--A close up of root in the process of reaching the effective length.

did not experience rupture and is still being stretched, despite the large relative displacement at that point. This may be used as a typical example of what was meant by effective length. This particular root due to its positioning in the composite (and maybe partly due to the sectioning of the composite) did not attain an effective length until the master crack had opened wider than for the majority of roots, and therefore did not contribute with its strength in the failure process. Note, however, in Figure 4.3.12 that in the open crack of the failure, there are practically no root ends projecting beyond the fractured bulb. This indicates that they fractured with the composite as a unit. The only root ends which appear are those related to the non-homogeneity of the composite and to a region of smaller displacement where some of the local roots were not stretched enough to be effective.

In order to relate the magnitude of the pulling force to the underground failure pattern, a test was filmed with the x-y recorder in the field of view. The sequence of figures from 4.3.13 to 17 shows the development of the cracks related to the value of the pulling force. It is recognized here how inaccurate this relation might be if based only on the photographs given. But it was possible to reproduce this relation to a reasonable degree of accuracy by comparing the projection of the film and the curve which is given in Figure 4.3.18. Figure 4.3.18 shows

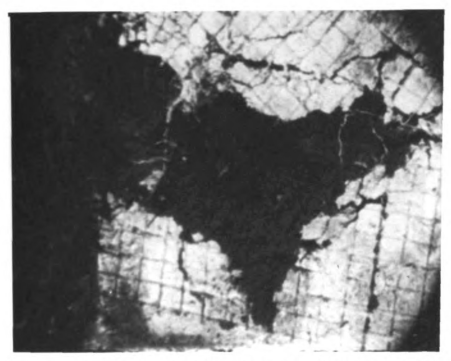


Figure 4.3.12--Observe that the roots are all fractured at the failure surface.

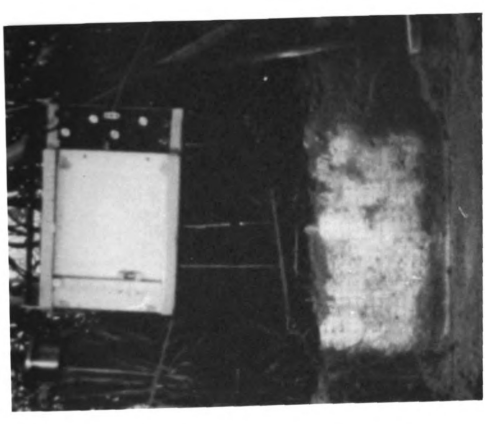


Figure 4.3.14--x-y recorder in the field of filming; recording pen has moved.



Figure 4.3.13--Underground failure with x-y recorder in the field of filming, at zero load.

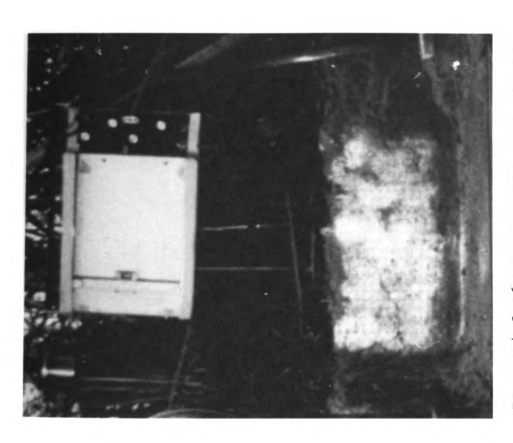


Figure 4.3.16--Crack pattern at .97 of $^{\rm F}$ max.



Figure 4.3.15--Crack appeared at .85 of F max (Fmax = 247 lbs).

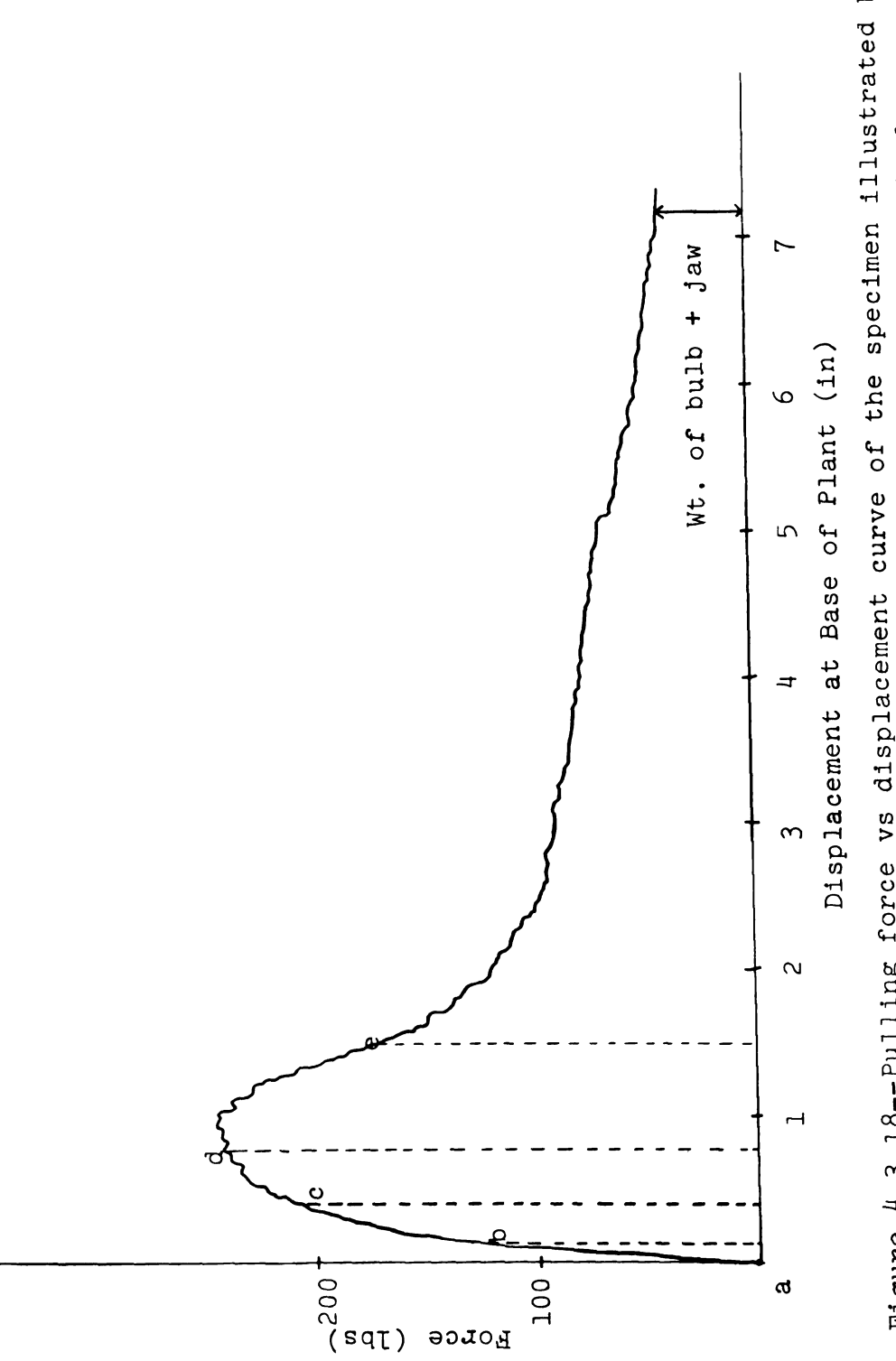


Figure 4.3.18--Pulling force vs displacement curve of the specimen illustrated by figures 4.2.13 to 17 and 19. Points from a to e correspond, respectively to figures 4.2.13 to 17.



Figure 4.3.19 -- Note bulb disruption about the compression plane, in final stage of rupture.



Figure 4.3.17--Crack pattern when force had declined to .70 $\rm F_{max}\textsc{\cdot}$

the points a, b, c, d and e which correspond respectively to pictures 4.3.13 to 17. This experiment was listed as number 7 in Table 2.2. Figure 4.3.13 shows the system at zero load and 4.3.14 is right after the recording pen had moved. In Figure 4.3.15 the value of the force was about .85 of the maximum value when the cracks were first detected, indicating that failure had started taking place. Figure 4.3.16 shows the pattern at about maximum force [.97 of F max. (F max = 247 lbs)]. In Figure 4.2.17 the force had already declined to about .70 of F max.

Figure 4.3.19 shows the final stage of the rupture. The separation of the outer part from the bulb is now quite clear, and so is the Rankine pattern portion of the failure surface. Note, also, that the white grid has disappeared at the compression zone, from which the soil broke loose due to that stress.

Two tests were made in order to verify if the underground failure would occur symmetrically in the composite. A relatively high degree of symmetry was found present up to the final stages of the rupture process, as can be seen in Figures 4.3.20 and 4.3.21. However, this was changed in the final stages of the process, as indicated by Figures 4.3.22 and 4.3.23.

4.3.2 Soil Surface Cracks

The sequences of photographs 4.3.23(a) to (d) show the pattern of surface cracks, recorded on October 14.



Figure 4.3.20--Shows the symmetry of the cracks in the initial stage of rupture.



Figure 4.3.21--Shows that symmetry persisted until the final stage of rupture.

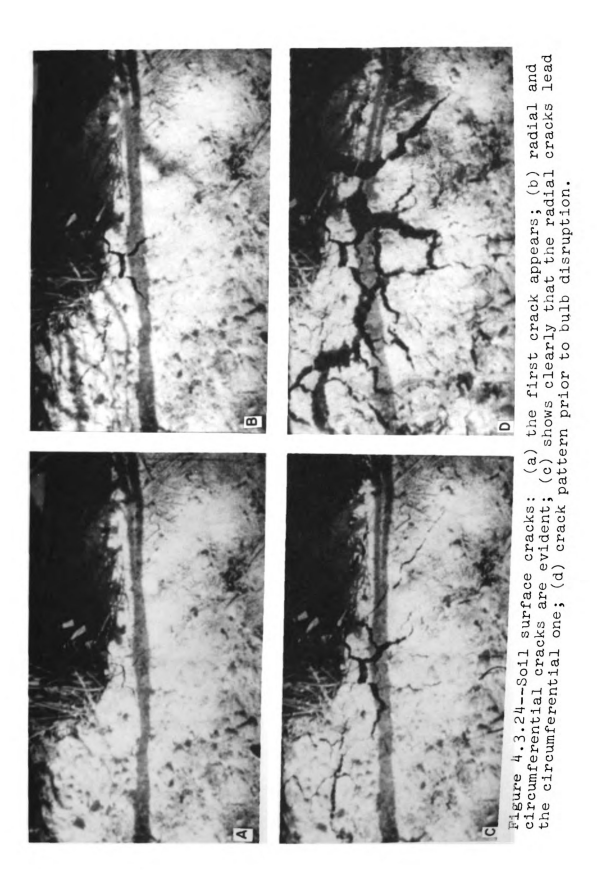
+



Figure 4.3.22--The disruption of the bulb leads to an assymmetric appearance.



Figure 4.3.23--No symmetry can be visualized by observing the pulled out bulb.



,		1
		!
		I .
		!
		1

Figure 4.3.24 (a) and (b) show, respectively, the system when the first crack appeared in the field of filming and a more advanced stage, where the radial cracks are leading. From the latter photographs one cannot precisely tell whether the radial or the circumferential crack appeared first. However, from observations during the tests and by considering Figures 4.3.24(a) and (d), it may be concluded that the radial cracks appeared first. appearance of the radial crack first may be attributed as an effect of the geometry of the root system. When the radial cracks appeared, they indicated that the strength of the composite perpendicular to their direction had been exceeded. Actually, the "umbrella" nature of the root-geometry, suggested that the strength of the composite in a direction perpendicular to the radial cracks was expected to be of a relatively low magnitude.

The pictures of Figure 4.3.24(a) to (d) show a chronological sequence of the surface cracks leading to a final stage of the disruption process. From observations made in other tests, it was noticed that these cracks were significantly visible only after the maximum pulling force had passed its peak.

The circumferential crack corresponded to the tension cracks that appeared for the underground observations. The fact that they appeared later can be explained also by the rather "anisotropic" nature of the composite,

having a "polar" root geometry. By "polar" root-geometry is meant the fact that the root radiated from the attaching point not necessarily radially, but polarly. This geometry of the reinforcement characterized the composite as a typically "polar" resistant medium, i.e., the greatest strength was in the direction of the roots. However, the ascertainment of an overall "anisotropic" behavior of the root-soil composite requires other techniques in the experiments.

5. RECOMMENDATIONS FOR FURTHER WORK

Based on the observations and results obtained in this study, the following future investigations are recommended:

- 1. A series of experiments with single roots in the soil, to determine the force and the displacement distribution between the root and the soil for an increasing load, and to verify the derivations made in Section 4.2.1. This should be studied at different soil conditions such as different moisture content and different degree of compaction, considering the influence both (a) at the time of the testing and (b) during the growth period up to the time of testing.
- 2. The distribution in space of roots with regard to length, number, diameter, and strength properties.
- 3. Changes of the distribution of roots in space with plant growth.
- 4. Studies of possible time dependent effects with regard to roots and the composite (visco-elastic behavior).
- 5. To investigate other measures for the plant size and the root system size, as for instance the dry weight of the roots in the root-soil bulb.
- 6. An attempt should be made to utilize a photoelastic approach by use of gelatin models.

- 7. A mechanics for the root-soil system should be further developed, as to determine the desirable root distribution from a strength standpoint and how it can be achieved by controlling nutrients, moisture, and the degree of compaction of the soil.
- 8. Further studies of the failure process including film techniques.
- 9. Verify the results also for plants presenting pronounced tap roots.

6. SUMMARY OF RESULTS

The results obtained from the field tests of uprooting force show that the penetrometer reading did not correlate or affect significantly the maximum pulling force or the respective displacement at the base of the plant. The soil characteristics which may influence the maximum pulling force and the respective displacement at base of the plant were the soil moisture content and the bulk density. The bulk density may have affected the plant development. The plant characteristic best correlated to the variation of the maximum pulling force and the respective displacement at the base of the plant was the diameter of the stem bundle at the plant base. The weight of the root-soil bulb which may be considered as a root-soil characteristic also was correlated to the maximum pulling force. The crater volume and the weight of the root-soil bulb were related and they may represent two comparable measures of root system size.

Under the pulling force the root-soil composite seems to behave as a Hookean body up to value of the displacements at the base of plant which corresponded to about 0.5 of the recorded maximum pulling force. This behavior was altered for sectioned tests, and a more non linear behavior was noticed at lower values of the displacements at the base of plant and maximum pulling force.

From the studies of the root system it was seen that there were two types of roots, namely: short roots, with a larger diameter and lower strength, and long roots with smaller diameter and higher strength. Also, the strength for short roots is mainly related to a linear dimension (circumference) of the cross-section, whereas that for long roots was also related to a square of that dimension (area). For long roots the strength decreased slightly from the attaching point toward the root tip. The tapering of long roots seemed to be negligible.

The observations of the underground failure indicated that it started at the plant centerline and propagaged outwards until a Rankine failure pattern was noticed from the bottom failure to the soil surface. The initial failure took place at a value of the pulling force slightly below the maximum pulling force and then developed under a symmetrical pattern, which may be altered by nonhomogeneity of the composite.

The top surface cracks seem to indicate that the highest strength of the composite is in a direction along the roots. The radial cracks leading the circumferential ones are indicative of the existence of a plane of least strength. This plane is vertical and contains the plant centerline.

REFERENCES

- Bertrand, A. R. and H. Kohnke. (1957). Subsoil conditions and their effects on oxygen supply and the growth of roots. Soil Science Society of America Proceedings. 21:135-140.
- Boussinesq, J. V. (1885). Application des Potentiels a L'Etude de L'Equilibre et de Mouvement des Solides Elastiques. Paris: Gauthier-Villars. 721 pp.
- Dillewijn, C. Van. (1952). Botany of Sugar Cane. The Chronica Botanica Co., Waltham, Mass., USA. 371 pp.
- Esau, K. (1966). Anatomy of Seed Plants. John Wiley and Sons, Inc., New York, USA. 376 pp.
- Gill, W. R. and G. H. Bolt. (1955). Pfeffer's studies of the root growth pressures exerted by plants. Agronomy Journal. 47:166-168.
- Gill, W. R. and R. D. Miller. (1956). A method for study of influence of mechanical impedance and aeration on the growth of seedling roots. Soil Science Society of America Proceedings. 20:154-157.
- Gill, W. R. and G. E. Vanden Berg. (1966). Soil Dynamics in Tillage and Traction. United States Department of Agricultrue, Agricultural Research Service, Agriculture Handbook No. 316. 511 pp.
- Hall, D. M. (1934). The relationship between certain morphological characters and lodging in corn.
 Minn. Agr. Expt. Sta. Tech. Bul. 103. 31 pp.
- Holbert, R. Jr., and B. Koehler. (1924). Anchorage and extent of corn root systems. Journal of Agricultural Research 27:71-78.
- Jumikis, Alfreds R. (1962). Soil Mechanics. D. Van Nostrand Co., Inc., Princeton, New Jersey, USA. 791 pp.
- Kaul, R. N. (1965). The influence of certain mechanical properties of an uncompacted soil. Unpublished Ph.D. Thesis, North Carolina State University, Raleigh.

		1
•	•	
		į

- Letey, J., O. R. Lunt, L. H. Stoltzy, and T. E. Szuszkiew. (1961). Plant growth, water use and nutritional response to rhizosphere differentials of oxygen concentration. Soil Science Society of America Proceedings. 25:183-189.
- MacLaughlin, T. F. (1966). Effect of fiber geometry in fiber-reinforced composite materials. Experimental Mechanics 6:481-492.
- Michigan Agricultural Experiment Station (1967). STAT Series Description. Michigan State University, Computer Laboratory Library, No. 5 and 7.
- Miller, E. C. (1916). Comparative study of the root systems and leaf areas of corn and sorghums.

 Journal of Agricultural Research 6:311-332.
- Nelson, C. E. (1958). Lodging of field corn as affected by cultivation, plant population, nitrogen fertilizer and irrigation treatment. Production Research Report No. 16, ARS, USDA, 16 pp.
- Newman, J. E., S. R. Miles and P. L. Crane. (1952).

 Performance of private and open-pedigree corn
 hybrids in Indiana. Indiana Agricultural Experiment Station, Circular 380, 23 pp.
- Pavlychenko, T. K. (1937). The soil-block washing method in quantitative root study. Canadian Journal of Research Sec. C, 15:33-57.
- Richards, R. Jr., and R. Mark. (1966). Gelatin models for photoelastic analysis of gravity structures. Experimental Mechanics 6:30-38.
- Roo, H. C. (1966). Root training by plastic tubes III: Soil aeration appraised by tube-grown plants.

 Agronomy Journal 58:483-492.
- Rosen, B. W. (1964). Mechanics of Composite Strengthening. Chapter 3, pp. 37-75, in Fiber Composite Materials. American Society for Metals, Metals Park, Ohio, USA. 245 pp.
- Scott, T. W. and A. E. Erickson. (1964). Effect of aeration and mechanical impedance on the root development of alfalfa, sugar beets and tomatoes. Agronomy Journal 56:575-576.

- Spencer, J. T. (1940). A comparative study of the seasonal root development of some inbred lines and hybrids of maize. Journal of Agricultural Research 61:521-538.
- Stoltzy, L. H., J. Letey, T. E. Szuszkiewicz and O. R. Lunt. (1961). Root growth and diffusion rates as functions of oxygen concentration. Soil Science Society of America Proceedings 25:463-467.
- Tackett, J. L. and R. W. Pearson. (1964). Oxygen requirements of cotton seedlings roots for penetration of compacted soil cores. Soil Science Society of America Proceedings 28:600-605.
- Weaver, John E. (1926). Root Development of Field Crop. McGraw-Hill Book Co., Inc., New York, USA. 291 pp.
- Wiersum, L. K. (1957). The relationship of the size and structural rigidity of pores to their penetration by roots. Plant and Soil 9:75-85.
- Williamson, R. E. (1964). The effect of root aeration on plant growth. Soil Science Society of America Proceedings 28:86-90.
- Wilson, H. K. (1930). Plant characters as indices in relation to the ability of corn strains to with-stand lodging. Journal of American Society of Agronomy. 22:453-458.

